UiT The Arctic University of Norway

Faculty of Science and Technology

Roll motion on small traditional Norwegian fishing vessels

How smaller fishing vessels respond to roll motion and roll damping with and without bilge keel.

Gøran Kristiansen

Master's thesis in Technology and Safety in the High North – TEK 3901 – August 2021

Preface

This Master's thesis is the final work of my master's degree in Technology and Safety in the High North at UiT – The Arctic University of Norway, Tromsø with an in-depth study of stability on vessels regarding the Nautical aspect. The work in this thesis was carried out at the Department of Technology and Safety in the spring, - and beginning of autumn semester of 2021, due to combination of working at sea while taking my master degree. The thesis is built up by research from similar previous work, theme literature, pre-projects by author and experiments conducted at UiT. This Master's thesis contains 20100 words, 39 Figures and 7 tables.

Acknowledgements

Working on the master's thesis has been challenging and due to precisely this, the knowledge and interest regarding the topic has also increased. The challenges encountered could not have been solved, and the improved knowledge that I have acquired could not have been achieved without all the guidance, recommendations and positive feedback given during this assignment.

I want to thank Associated Professor Karl Gunnar Aarsæther for all the help, guidance and education ever since the bachelor thesis, during the master's program, and not least, the master's thesis. I also want to extend my gratitude to the Nautical team at UiT for all the positive feedback and recommendations they have contributed.

Thanks to UiT – Narvik for a great job with 3D printing of the model quickly, efficiently, and precisely according to the submitted design, and to Frantz Esaiassen for the finishing touches regarding sanding-, priming and coating of the model.

Furthermore, I want to thank my office colleagues and fellow students: Martine Maria Pedersen, who has studied with me through bachelor and master's studies. Sushmit Dhar, who has studied with me during my master's thesis. It would have been challenging to complete this master's thesis without the good and positive atmosphere in office 1.041 and the moral support they have contributed with, relevant and irrelevant problem solving, and the provided motivation.

Finally, I must thank my friends and family who have supported and helped me during all the years of my studies.

Gøran Kristiansen

Faculty of Science and Technology
UiT – The Arctic University in Norway
August, 2021

Abstract

Prediction of vessel motion in a seaway is considered one of the triumphs of research in ship hydrodynamics. Engineers can predict heave and pitch movements with remarkable accuracy from a small amount of information about the vessel characteristic and sea state. Furthermore, prediction of sway and yaw is also possible to predict with reasonable accuracy.

Roll motion is one of the six degrees of freedom and is the most difficult to predict, as roll motion is extremely sensitive to the viscous effect and induced flow separation. Roll motion problem has increased ever since vessels used sails as propulsion and was replaced with steam machines and iron plates replaced wood, leading to design modifications in the vessels affecting transversal stability, increasing the vessel's roll motion.

The fishing vessels fleet commonly operates in almost all weather conditions. The safety of fishers depends on the vessel's characteristic to resist and maintain stability in high seas that can lead to large-amplitude motion with a combination of wave-induced ship motions.

Roll motion can be a problem for vessels without any appendages that reduce the roll motion, e.g. bilge keels - stabilizers with no moving parts, form the most straightforward and cheapest element that can help decrease this motion.

Through the last four decades, studies and investigation of roll motion use the approach developed by Ikeda et al. in the '70s and is the foundation to the guidelines presented by (ITTC, 2017).

This thesis uses the procedures and guidelines from (ITTC, 2017) and compares the effects of bilge keel between model experiments and the numerical result.

Abbreviations

ITTC	International Towing Tank Conference
MRU	Motion Reference Unit
CoG	Center of Gravity
UiT	The arctic University of Norway
CDTM	Component Discrete Type Method
NEMOH	Hull modelling software
DELFTship	Hull modelling software
PO	Percentage Overshoot
Engauge Digitizer	Hull modelling software
CVS	Comma-separated values
MOB	Man Over Board
NSIA	The Norwegian Safety Investigation Authority
NMA	Norwegian Maritime Authority
Ro-Ro	Roll on - Roll off vessel
LCG	Londitudal Center of Gravity
VCG	Vertical Center of Gravity
GM	Distance from CoG to Metacentre
JRCC	The Joint Rescue Coordination Centre
NBS	Nordic Boat Standard
FRP	Fiberglass Reinforced Polyester
dof	degrees of freedom
F_N	Froude number
nm	Nautical Mile
R_e	Reynold's number
BEM	Boundary Element Method
b/d	half width-draught ratio
A_c	area coefficient
ODE	Ordinary Differencial Equation
CSD	Compute Section Data
CFD	Computational Fluid Dynamics
RKF45	Runge-Kutta-Fehlberg method
STL	STereoLithography - file format created by 3D systems CAD software

Nomenclature

ω	roll angle velocity	
a	Length of pressure distribution	[m]
a	Gravity acceleration	[m/s^2]
A_M	Area of midship section	[m^2]
A_w	Area under water	[m^2]
A_{wR}	wetted surface in roll	[m^2]
B	Breadth	[m]
b_{BK}	Width of bilge keel	
C	Damping coeffisient	
C_f	Frictional coeffisient	
C_M	Midship section coefficient	[-]
C_p	Pressure coefficients	
C_R	Hull disctiption factor	
D	Draught	[m]
D	Depth	[m]
F	Force	[Nm]
F_N	Froude's Number	[-]
g	Gravity	[m/s^2]
H	Hight	[m]
H_0	Width/draught ratio	
H_t	Thickness of material	[m]
I_{xx}	Rotational inertial	
k	radius of gyration, related to bilge keel	
K	Restoring force coeffisient	
K_N	Factor lift force	[-]
L	Length	[m]
l_0	Leverage arm	[m]
lR	Leverage arm	[m]
L_{rxbk}	Length from roll axes to tip of bilge keel	
M	Metacenter	[m]
m	mass	[kg]
M	mass	
ωn	vessel own frequency	[deegres/rad]
nm	Nautical Mile	[nm]
OG	Distance from waterline to CoG	[m]
ϕ	Represent angle of roll	
R_e	Reynold's Number	[-]
R_f	value of the 3D vessel hull form	
r_{max}	Dist from CoG (roll axis) hull surface	
S	Length of pressure distribution	[m]

S_f	value of the 3D vessel hull form	
T	Draught	[m]
U	Forward velocity	[m/s]
V	Speed	[m/s]
ν	Viscosity	[kg/ms]
γ	Lewis-form parameter factor	
λ	Geometrical similarity requirement	[-]
ξ	damping factor	[-]
ρ	Density of liquid	[kg/m^3]
σ	Area coeffisient	
$\dot{\varphi}$	Roll velocity	[]
ϕ_a	Wave ampliude	[m]
ξ	damping ratio	[-]
$\dot{\phi}$	Velocity in roll	
$\ddot{\phi}$	Acceleration in roll	

Table of Contents

List of Tables

List of Figures

1 Introduction

The Norwegian fisheries fleet consists of about 4-4500 vessels, making it the largest fleet sector in Norway. Traditionally the fisheries fleet is separated between larger ocean-going vessels and smaller coastal vessels. Until 2013, the technical inspection for vessels from 8 to 15 [m] has been based on the original type certification issued to the boat builder and with no type certificate for vessels under 8 [m]. The type certificate for these vessel classes covers everything from hull strength, electrical system and stability calculations.

There have been many accidents involving smaller fishing vessels (0 < 15 meter) in Norway. From 1981 until 2019, 67 reported and investigated accidents, 14 accidents with vessel length < 10,67 meter and 53 with vessel length 10,67 < 15 meter, regarding capsizing due to increasing, wind, sea and waves (Norwegian Maritime Authority, 2020). This may come from waves have risen above the vessel's rail and together with vessel motion, led to water ingress into some, or all, rooms in the vessel through unsecured openings or progressively worsening stability properties by water not cleared from the deck.

There are many dangers when working on vessels, both small and large, - fishing or commercial, even in good weather. The risk of accidents increases in bad weather; fall on deck, getting hooked in fishing gear, Man Over Board (MOB), waves rising above the rails leading to; green water[1], water ingress in rooms, and capsizing due to the increase of roll motion. The chances of survival regarding MOB are small in Northern Norway due to the remote and large areas, with the cold arctic water. Furthermore, the risk of capsizing smaller vessels is significant due to rapidly changing weather, the high number of these vessels, and their small size, and sometimes tragic outcomes. For people in general, the changing weather does not have to be of great importance, or may not seem so bad, but for those who work at sea or maritime related professions and especially those who work on smaller fishing vessels, knows and understand the dangers of change and increase in the weather. Investigation reports done by the Norwegian Safety Investigation Authority (NSIA) shows that weather, sea and waves addition to relatively heavy loads and rapidly shifting of cargo on smaller vessels are reasons for capsizing and sometimes with a tragic outcome, such as:

1. *Capsizing of fishing vessel Andreas, east of Nord-Fugløya* (Havarikommisjon, 2020).

[1] Green water is a term used by seafarers when there is much sea on deck, the water looks green.

2. *The sinking of fishing vessel Lill-Anne, Vestfjorden* (Havarikommisjonen, 2010).

Andreas was fishing outside a small island in Northern Norway with larger gill nets than usual to cover larger areas and deeper in the ocean for a better catch. During the day, the weather increased to a strong breeze, 12 [m/s] from south-southeast. There is no exact wave measurement in this area. However, the Department of Meteorology's computer model estimated a significant wave height between 1.2 – 1.7 [m] in this area and wave swell with a period from 8 – 10 [s]. It is assumed that the increasing weather, catch and the extra weight of longer and more gill nets made *Andreas* capsize due to waves on deck leading to water ingress to the vessel. The fisherman on *Andreas* drowned as a result of the capsizing. *Lobo,* - a similar fishing vessel that capsized in the same area at the same time due to waves rising above the railing on the vessel. Water filled *Lobo* which lead to a capsizing almost simultaneously as the emergency alarm from *Andreas* was received at The Joint Rescue Coordination Centre (JRCC) Northern Norway. The fisherman on Lobo survived and the conclusion of what happened to *Andreas* is supported by this testimony. This twin accident highlights risk associated with these smaller vessels.

Lill-Anne was sailing from Mausund, Trøndelag, along with two collages on another vessel, *Adrian*, which is slightly longer and build in steel in 1980, to participate in the winter fishing for cod in Lofoten, Nordland. To reach Lofoten, *Lill-Anne* and *Adrian* had to cross Vestfjorden, known for the rapid change of wind, sea and weather. The Department of Meteorology predicted a strong breeze of 12 [m/s] and up to 2 [m] waves the evening of the accident. Both vessels navigators concluded it would be safe to cross as the wind would come from behind. *Adrian* sailed 0.7 [nm] behind *Lill-Anne* with the same heading and speed with radar and visibility. However, the navigator on *Adrian* states that waves sometime interfered with *Lill-Anne's* visibility for seconds. A sudden wave made tools onboard *Adrian* fall on the floor. The time it took the navigator to pick up the tools and return to the navigation position was estimated to be under 1 minute (by the navigator). By then, *Lill-Anne* was not seen on either radar or visually. NSIA concludes upon weather forecast, weather forecast simulation and stability calculations of *Lill-Anne* that simultaneous waves of 5 [s] intervals had raised over the rails and flooded the vessel, resulting in a quick capsizing and sinking. The navigator's statement onboard *Adrian* strengths the theory of rapid capsizing regarding the time estimate.

There are two essential topics to consider when dealing with vessel response in a seaway; static stability and dynamic response. Hydrostatical stability is about the equilibrium between external forces and the resulting righting moment. The righting moment depends on the vessel's shape and location of the center of gravity. All calculations regarding static equilibrium are time-independent, which means that the vessel settles in a given position which it attains after an external force influence after an unknown, but presumably long, time period.
Hydrodynamic response means how the vessel will behave in a seaway when influenced by time-varying waves, wind and other environmental forces, meaning how the vessel will respond regarding motions in response to a varying heeling moment with restoring forces over a time period. When studying stability phenomena such as; roll motion and parametric roll, understanding of the vessels dynamics is essential. Roll motion is an underdamped degree of freedom and also where the vessel is easiest to set in motion. It is easier to set the vessel in motion in roll vs pitch or heave, and this degree of freedom is easily excited by wave forces.

Stability calculations refer to the hydrostatic stability calculation, although the dynamic stability is just as important, if not more, for smaller vessels in a seaway. The dynamic stability measures the ship's ability to absorb the energy from varying forces of waves and gusting winds. The roll motion is a vital motion to study since it is one of the most challenging motion for fishers, sea workers in general, and the risk of accidents associated with motions in roll. Additionally, one may experience motion sickness, difficulties standing upraised, and even challenging to rest and sleep as a result of rapid or large roll motions. Roll motions on a vessel is under-damped and it is common to mount accessories on the hull under the waterline in the form of bilge keels or an extended bottom keel to reduce motions on vessels. Determining the effect of such accessories is important in order to design such accessories to dampen the roll motion which in turn increase the safety and comfort for sea workers. From an engineering point of view, quantifying the effect of the accessories allows the settling time from the initial heel movement to the hydrostatic equilibrium to be determined together with the history of roll movements until the motion comes to a rest.

Research on roll motion and roll damping has been ongoing for decades, mostly on merchant vessels like; Ro-Ro, - cruise, - and container vessels due to their size, the value of ships and cargo being much larger than fisheries fleet worldwide. Container vessels with a flat transom

stern, broad mid-section, and significant bow flare are also at high risk of the parametric roll phenomenon, resulting in high stress on the hull and the risk of losing containers at sea.

Ro-Ro vessels have large external doors close to the waterline and open vehicle decks with few internal bulkheads and has a reputation for being a high-risk design were an improperly secured loading door can cause a ship to take on water and sink.
Modern cruise ships tend to have less hull strength, speed, and agility than other commercial vessels. The reason for having a slight roll motion as possible will be for hull strength and the comfort of passengers and associated facilities such as shops, restaurants and swimming pools.

The shape of merchant vessels and fishing vessels is significant different from merchant vessels regarding length, width and depth. The main reason for the size difference is the vessels' use, the merchant fleet is designed to cross oceans as fast as possible with maximum comfort and maximum cargo capacity. Smaller fisheries vessels on the other hand are designed to exploit coastal resources and to conform to size regulations that determine access to fisheries resources. Figure 1 shows the different between the old traditional vessels and the modern vessels, the design and construction of today's modern fishing vessels are short, broad, and high to keep within fleet groups regulated by over-all length while loading as much cargo; fish, gills net, water/ice and bunker as possible. Other drivers for fishing vessel designs are, - access to fish in small fjords on a day-to-day basis, and to adapt to the requirement for crew certificates above certain thresholds. There have been accidents with these "paragraph" vessels lesser than 15 [m], and concerns about the stability of these vessels has emerged, such as fishing vessel *Fay* (Havarikommisjon, 2021).

a) *Older traditional Norwegian fishing vessel (Havarikommisjonen, 2010).*

b) *Modern fishing vessel (Marin Design, 2016).*

Figure 1: Older vs. newer fishing vessels.

Both traditional and modern fisheries vessels are fitted with appendixes to reduce motions, and it is important to study the function of these appendages on the hull shapes found on fisheries vessels. Bilge keel size and placement determine their effectiveness; they should be attached at the bottom edge at the broadest part of the vessel. Fisheries vessels may have deep keels and shallow distance between the 'edge' of the ship hull and the surface. Bilge keels should not be placed to shallow such that there is a risk of slamming when the bilge keel leaves and reenters the water surface. Bilge keels may also be in danger of hitting other objects, i.e. quay, or fishing nets can snag at the edges of the bilge keel during hauling. Such practical considerations may lead to the placement of bilge keels in suboptimal areas.

Another contribution to damping on fisheries vessels is the 'skeg'. The skeg is a deep bottom keel integrated in the hull in the aft part and often used to house the propeller shaft. Skeg is very common on smaller vessels, the purpose is providing course stability and to prevent drift-off when in engage in fishing operations. The skeg also contribute to damping of roll motions, although less effective than bilge keels, due to size of area and of lever arms. Smaller fisheries vessels mostly feature a skeg, but may also have bilge keels installed.

The smaller fishing vessels of length 11 [m] and down have a long service life. The traditional vessels are still popular among fishermen. The typical vessel is cast in Fiberglass Reinforced Polyester, making a hull that is resistant to corrosion and wear and leads to reduced maintenance costs versus a vessel constructed in aluminum, steel or wood. This durability leads to a service life of about 40 years for a small traditional vessel. The vessels below 11 [m] is the most numerous class of fishing vessels in Norway and *Andreas, Lobo* and *Lill-Anne* are all from this group. These smaller vessels are more exposed to wind and waves, and

experience more motions in seaway due to their small size. It is therefore important to know how both the static stability and dynamic response of these vessels influence the motions of these vessels.

This thesis will investigate upon the estimation of roll damping for smaller vessels and how the established theory developed for merchant ships performs on predictions targeting smaller fisheries vessels. This will be investigated by

- Digitizing and converting a classic hull from a traditional lines plan to a 3D computer model
- Obtain a physical model of the classic hull based on the 3D model with removable bilge keels.
- Use model experiments to estimate the roll damping characteristics of the hull with and without bilge keels
- Calculating the roll damping characteristics for the hull from established theory and reproduce the experiments
- Compare the results of physical and numerical tests

2 Theory

The study of vessel motion, damaged vessels and the loss of stability due to water ingress are essential topics; since this thesis focus on vessel movement in roll, it is important to mention studies and research that contributes to knowledge regarding the stability and the response that follows. The dynamic response to a vessel is vital regarding damage stability in the transient phase from when load shift, or the loss of buoyancy occurs, until quasi-static behavior dominates with slow changes to the vessel floating position. Through decades many procedures and computer programs have been developed to analyze and build knowledge about transverse stability phenomena on ships. Computer simulation is the common aid to study vessel response from water ingress or motions in a seaway.

2.1 Background

Damaged vessels and stability: Water ingress in damaged vessels can be a slow process, especially if doors are closed and watertight leading to a quasi-static situation. However, closed but non-watertight doors cannot contain the water indefinitely as the water seeps slowly through the doors. When the doors give in, either by the pressure from the water or other failure, the water flow increases considerably, and sudden changes in weight distribution and compromised compartments results in quick changes in floating position before the vessel slowly finds a new floating position. This process may continue for several iterations when the vessel slowly heel more and more as water still seeps into the newly flooded room. Cases like this are evident in previous studies on progressive flooding (Veer, 2000), (Ruponen, Kurvinen, Saisto, & Harras, 2010) and can be compared to a load suddenly shifts on the vessel.

Such complicated damage cases where the sequence of compartments being flooded interact with vessel motions is often studied in the time-domain. There are several time-domain flooding simulation tools, and these methods use Bernoulli's equation to calculate the water flow through the openings. The general approach is to simulate these cases in time by placing weights that illustrates water volume and study the vessel movement as progressive water ingress. (Ruponen P. , 2014), (Ruponen, Kurvinen, Saisto, & Harras, 2010) and (Rodrigues & Soares , 2015) have used numeric simulation for investigating progressive water ingress. Progressive flooding simulations may also be solved with Computational Fluid Dynamics (CFD), but it is worth mentioning that CFD is computationally expensive and requires special

knowledge to use. This thesis focus on transverse movements (roll motion) and will apply classical mechanics and available empirical models to study the response of vessels in roll.

Vessel motion: Studies of vessel roll motion by physical tests and numerical calculations should follow established methods or standards, e.g. published by the ITTC, to maintain a common procedure between organizations, and if necessary, be validated by others if any doubt or uncertainty in the results. Established procedures are important in theoretical calculations, but more important when the phenomena is covered by empirical formulas. This is the case with roll motions of vessels and it is important to have specific methods and documented formulas when applying the empirical equations, which bases on vessel geometric shape, characteristics and main dimensions.

Roll motions on vessels is a complex phenomenon made up of external forces, the counteracting forces from buoyancy, friction, flow separation, vortexes and radiation of waves. Prediction of roll damping on vessels comes from extensive research and testing. This work has resulted in empirical equations that mainly use vessels' main dimensions and hull shape for calculations. Today the equations, which describes the damping in roll, have been verified for traditional vessel hull design; such as; RoRo (Roll on-Roll of vessel), container vessel and oil tanker. However, some of the empirical coefficients included in the equations may not be accurate for all types of vessels since the geometry of the vessel hull is used recreate results from experiments based on a limited set of hull forms. This may results in an over or underestimation of a vessel's predicted motion since the vessels hull may differ considerably from the hulls used to establish the empirical relationships.

Even though the norm is to study the larger vessel due to the vessel's cost, production of model and testing, and their hull size and shape, it is essential not to forget the numerous smaller vessels. Studies on smaller vessels can describe how viscous forces affect hulls with a hull shape and fitted appendixes that differ from the larger merchant fleet. Studies may further change and modify expressions in existing equations or suggest new equations for identified physical effects. Improved equations may results in hull design changes through increased understanding of the physical phenomena of roll damping.

Yoshiho Ikeda and Yoji Himeno have contributed considerably in the late '70s to research on vessel motion, especially on roll motion on vessels, and have largely defined the components that constitute the damping forces and how to estimate the damping term in the second-order

differential equation describing the roll motion. (Ikeda , Komatsu, Himeno, & Tanaka, 1976), (Ikeda, Himeno, & Tanaka , 1977), (Ikeda, Himeno, & Tanaka, 1977) and (Ikeda , Himeno, & Tanaka, 1978). Together they carried out experiments and research upon roll motion on fishing vessels, commercial, single and multihulls, and done studies on the roll characteristics of small fishing vessels and research on estimating the bilge keel component of roll damping. Ikeda has also contributed with research on roll motion with water intrusion and stability for damaged vessels. (Himeno, 1981) summarized the, then current, state of art and the method for the numeric prediction of roll damping together with the original computer code. The body of abovementioned work is often referred to as the «Ikeda method» (ITTC, 2017). These formulas have been systematically collected in a guideline by the ITTC for the prediction of roll motion. The Ikeda method is the most established empirical formulation for roll damping estimation of vessels and is often implemented in commercial computer programs that study vessel movement.

Although Ikeda and Himeno have studied, contribute to research and experiments regarding stability and vessel motion through decades, there are still uncertainties regarding the empiric formulas used, even for the commercial fleet, which has been extensively studied.

A study by (Söder, Rosén, & Huss, 2017) of Ikeda's roll damping prediction method and its applicability to modern Ro-Ro carriers found deviations related to changes in vessel shape in the bow and stern. The authors conclude an underestimation of the speed dependence of the bilge keels damping with the original method. The explanation of the conclusion can partially be by underestimating the contribution of bilge keels' lift force in Ikeda's analytical expressions.

(Aarsæther, Kristiansen, Su, & Lugni, 2015) Compared prediction results, with experiments for a medium sized Norwegian fishing vessel to study the roll damping effect for a fishing vessel with forwarding speed, and found estimating under prediction of the damping effect's prediction skeg keel with zero speed. However, the dominating bilge keel effect masks the skeg keels' effect.

Ikeda has studied his previous papers regarding the terms used in the prediction of roll damping. Ikeda concluded some of the terms might not be suitable for all ships, especially modern ships; for example, large passenger ships with flat hull shape and a high position of

the centre of gravity or long natural roll, without correcting the terms (Kawahara, Maekawa, & Ikeda, 2012).

Although all these studies, and others, have found inaccuracies for different hull forms regarding the damping term or other terms, it is essential to remember that the studies made by Ikea et al. in the late '70s and early '80s is the foundation for studies to this day. Also, it is not the old versus new studies with newer technology that makes the discrepancies found during research and testing, but the design changes of the hull shape.

2.2 Prediction of vessel motion

Prediction of dynamic motions such as ship response in a seaway or during roll motions can be seen as an application of Newton's second law for a rigid body in a vacuum.

$$F = ma \tag{2.1}$$

This fundamental equation is the starting point, and the effect of waves, damping forces and restoring forces can be introduced through the force term. The equation can be generalized to account for 1, 2 or 3 dimensional axes of motion and rotation. Equation (2.1) can be expanded to a linear differential equation of second order with linear velocity dependent damping and position depended stiffness. This is shown in Equation (2.2) where M is mass, C and K are coefficients giving magnitude to the damping and restoring force. ϕ is used as the independent variable since it is commonly used to represent the angle in roll for vessels.

$$M\ddot{\phi} + C\dot{\phi} + K\phi = 0 \tag{2.2}$$

This linear differential equation is often expanded with frequency dependent hydrodynamic forces such as added mass and damping, and the damping may not be strictly linear. The general form for the response of a second order differential equation with frequency dependent terms for added mass and damping for roll movement can be written as:

$$\big(I_{xx} + A(\omega)\big)\ddot{\phi} + C(\omega, \dot{\phi}) + K\phi = 0 \tag{2.3}$$

$\omega = anglular\ freqency\ of\ motion\ in\ roll$

I_{xx} is the rotational inertial for the vessel, $A(\omega)$ is the frequency dependent added mass. Added mass is not a physical mass but a contribution of the hydrodynamic force, in phase with accelerations, due to motion of the vessel that creates a fluid pressure on the vessel hull. The damping coefficient $C(\omega, \dot{\phi})$ is written as a function of both frequency and roll velocity. This function can consist of several components which make up the total damping moment, for roll damping this is typically divided into components such as wave, - eddy, - skeg, - bilge, - lift, - and friction damping. The restoring force is in this case kept linear for simplicity

with a constant coefficient K as in Equation (2.2). Equation (2.3) is an ordinary differential equation with constant coefficients for a single frequency, such as the frequency of roll motion. This equation can be solved, numerically in time if the coefficients, dependence on roll velocity or magnitude of the coefficients are known. Some of the coefficients such as linear restoring force and frequency dependent added mass and damping can be fund from mathematical calculations and established empirical formulas, while others might require model test in order to predict the magnitude of the effects empirically.

2.2.1 Prediction from experiments

Experiments, or model tests, is carried out with a scaled down model of the physical vessel. All model tests start from the design drawing of the hull. This drawing is the foundation of hull models and fabricated with a specific scaling ratio compared to real-sized vessels. In order to decide the correct scaling ratio, it is important to take three fundamental demands into account;

Geometric similarity: Model and actual size vessel are geometric correct, although different scale.
Kinematic similarity: All effects-, sizes and direction must be equal in specific areas on both model and actual size vessels.
Dynamic similarity: When the inertia forces for specific parts of the model hull and the actual size vessel are proportional to scale, along with the geometric and kinematic similarity is fulfilled, the dynamic similarity is complete.

Physical model testing occurs in large water tanks, as more extensive facilities allow larger model scales, leading to reduced errors when scaling results between model and full scale. Larger model tanks also reduce the interference between the model test and the boundaries of the tank, leading to reduced noise in the results. When performing experiments of vessel motions, it is important to limit waves generated from the experiment returning after being reflected at the tank walls and influencing the results. Reduction of reflected waves can be achieved by wave dampers or by a sufficiently large tank and ending the experiments before the reflected waves arrive at the model. Several methods are available to reduce wave interference, and the type of each wave damping equipment is limited to physical limitations regarding the tank and type of experiment. There are two main categories regarding wave absorbers: active and passive wave absorbers. However, active absorbers can be related to the wave-making machine itself, which is programmed to absorb the reflected wave and consist of, e.g. a paddle. The paddle movement to absorb waves is opposite to the movement of the paddle generating the waves.

For passive absorbers, the beach of constant slope reaching the bottom using sand, gravel, or stones seems to be the most popular arrangement. However, other materials such as transversal bars, horsehair, and wire screen are also used (Ouellet & Datta, 1986).

Some tanks are over 200 [m] long, 50 [m] wide and 5 [m] deep, example of water tank size is shown in Table 1 page 14. The type of water tank often decided what experiment and the model size is to be used. E.g., if the experiment is to investigate how a vessel behaves in the head-on sea, a longer towing tank is to prefer. If the experiment investigates roll motion, then the use of a shorter and deeper water tank may be practical. In either case when performing water tank experiments, it is essential to be able to:

1) Have controlled conditions and environment - depending on the experiment; have control of reflected waves
2) Be able to repeat the same test or experiment several times. To show that the experiment is repeatable and the results don't change. Furthermore, to provide multiple data series to establish how much impact noise and uncontrolled random variations have on the result.
3) Have accurate sensors. As noise and variation in sensor readings may be influenced by the speed and the magnitude of motion from the model during the experiment.

Table 1: Water tanks at NTNU, Trondheim – Norway (Minsaas, Baarholm, & Steen , 2010).

Examples of water tank	**L , B , D [m]**
Ocean pool **(modeling waves from 2 directions, wind and current)**	80 [m], 5 [m], 10 [m]
Towing TANK **(Modeling of waves. Two carriers, so that two separate experiments can be performed simultaneously)**	260 [m], 80 [m], 5 [m]

Several types of instrumentation and experiment equipment can be used and depends on which physical effect is studied.

When investigating ship resistance, the model is attached to a carrier that can drag or push the model along the tank through the water with a specific speed, usually without waves, while measuring the experienced resistance. An illustration of a full scale ship and a model scale resistance test is seen in Figure 2, page 15.

a) *Illustration of "Havila Kysrtuten", one out of four identical vessels (Sintef, 2020).*

b) *Model scale test of «Havila Kystruten» connected to instruments for test in tank (Sintef, 2020).*

Figure 2: Model testing, actual vessel size is L x B x d: 124.1 x 22 x 4.6 [m].

Repetition of this procedure is necessary to gather data for a range of velocities for later analysis and to get results that reduce the effect of noise and uncontrolled conditions. For performance in waves, tanks with wave generators at model test centers can generate specific waves for the vessel in the wanted direction, speed, amplitude, and frequency to investigate specific motion. Due to physical environmental effects, any test will take a longer time to implement as water must settle between each sequence which can be a time consuming procedure depending on the effectiveness of wave damping in the tank.

Results from experiments at a smaller scale are not directly applicable to full scale, particularly when considering interactions between structures, vessels and water. Therefore results are scaled according to scaling laws between model scale and full scale. The scaling laws are derived from non-dimensional numbers describing similarity of flow phenomena.

Froude number (F_N) and Reynold's number (R_E) is methods used for scaling of result from model testing to real size vessel. Froude number consist of speed (U), length (L) and gravity (g), and should be used when Froude number is less than ≈ 0.4 (Faltinsen, 1990).

$$Froude\ number, F_N = \frac{U}{\sqrt{Lg}} \tag{2.4}$$

Equality in F_N in model and full scale will ensure that gravity forces are correctly scaled. Moreover, surface waves are gravity-driven, so equality in F_N will provide that wave resistance and other wave forces are correctly scaled. It is therefore possible to find wave resistance coefficient for wave-making directly from model testing as long as the Froude number for both model and actual size vessel is the same (Haugslett, 2015).

Reynold's number consist of density of water (ρ), Speed (V), Length (L) and kinematic viscosity (ν), and equality in R_E will ensure that viscous forces are correctly scaled.

$$Reynold's\ number, R_E = \frac{\rho V L}{\nu} \tag{2.5}$$

It is important to remember that the result after scaling may not be exact due to the viscous effects and it is not possible to find the viscous friction coefficient directly by model testing, although there is possible to find a form factor (k) which applies to all Reynold's number and by using empiric formulas the viscos friction coefficient can be found for both model and real size vessel. Reynold scaling result in unreal velocities for model scale vs actual vessel since Reynold scaling doesn't change the viscose effect in the water.

$$Reynold\ scaling = \frac{\rho_V V_V L_V}{\nu_V} = \frac{\rho_M V_M L_M}{\nu_M} \tag{2.6}$$

$$V_M = \frac{V_V L_V}{L_M} \tag{2.7}$$

As seen in Equation (2.7), if the vessel has a speed (V_V) of 10 [m/s], length (L_V) of 200 [m], and the model scale is 1:10, the speed to model (V_M) is equal to 200 [m/s]. Even if there is a slight change in density or viscosity, the speed is unfeasible to achieve in a model test.

Therefore, Froude dominates regarding experiments with vessels, and the scaling between model and full scale comes from requiring similarity between the Froude numbers, as shown in Equation (2.8). Equation (2.9) how the scaling between speed for vessel and speed for the model is.

$$Froude\ scaling = \frac{V_M}{(gL_M)^{1/2}} = \frac{V_V}{(gL_V)^{1/2}} \tag{2.8}$$

$$V_V = V_M \sqrt{\frac{L_V}{L_M}} = V_M \sqrt{\lambda} \tag{2.9}$$

λ is the geometrical similarity requirement: $\lambda = \frac{L_V}{L_M}$. The other scaling relations can be derived from physical units of mass, length and time. Table 2 shows the scaling factors between model and full scale using Froude scaling.

Table 2: Froude Scaling Conversion Factors (Heller, 2012).

Parameter	*Dimension*	*Froude scale ratio*
Geometric similarity		
Length	L	λ
Area	L^2	λ^2
Volume	L^3	λ^3
Rotation	–	1
Kinematic similarity		
Time	T	$\lambda^{1/2}$
Velocity	LT^{-1}	$\lambda^{1/2}$
Acceleration	LT^{-2}	1
Discharge	L^3T^{-1}	$\lambda^{5/2}$
Dynamic similarity		
Mass	M	λ^3
Force	MLT^{-2}	λ^3
Pressure and stress	$ML^{-1}T^{-2}$	λ
Young's modulus	$ML^{-1}T^{-2}$	λ
Energy and work	ML^2L^{-2}	λ^4
Power	ML^2T^{-3}	$\lambda^{7/2}$

Froude similarity considers, besides inertia, the gravity force dominant in most free surface flows, especially if friction effect is negligible or for highly turbulent phenomena such as wave breaking. The Froude similarity requires identical Froude numbers between the model and its prototype for each selected experiment. Other forces, defined by the non-dimensional Reynolds and Weber number, are not similar between model and prototype when Froude scaling is applied. The effects they describe may be significantly different between model and full scale (Heller, 2012).

2.2.2 Numerical calculations

The movement of a vessel can be predicted by numeric calculations based on theoretical models of the forces in Equation (2.1). As long as the mass is known, and the calculated forces are correct, the result of solving the equations for the response should give the response of the vessel. It is however not straight forward to develop theoretical models which is solvable for the hydrodynamic forces on a general ship hull. Theoretical calculations require a model for the geometry, while physical tests require an actual scale model, theoretical models require a numeric description.

The equation and numerical calculation can help predict how the vessel will respond theoretically in a seaway, e.g. motions in pitch or roll. Some effects, especially viscous flow effects, can be difficult to calculate or predict theoretically for a general shape in arbitrary motions. By doing systematic model testing with and without appendages on the hull and comparing analyzing the results, it is possible to separate viscous force effects and study its contribution. This establishes numeric, or empirical models that can be used to predict vessel motions. . e.g. can the result from empiric models show that the skeg keel effect is more significant than first assumed on the hull, or from the physical test, that the bilge keel may contribute lesser than expected with the given placement. This method provides the possibility to change or modify the vessel design.

Theoretical calculation of flow problems around a vessel hull, is often carried out by using computer programs which uses potential theory in the form of 2D strip theory or 3D panel theory. These computer programs effectively solve wave forces and damping contribute from wave radiation, although they neglect the viscous effects. Theoretical calculation of vessel response is dependent on three inputs:

1. Problem definition – i.e. which motions will be solved and physical effects shall be included.
2. Governing equations – for potential flow it will be the equations that define the flow potential. For this thesis it will be the second order differential equation based on Newtons second law.
3. Domain - Which consists of boundary conditions and the floating objects geometry, in this study, the hull geometry.

A problem can, e.g. be a vessel motion and in the case of this thesis the motion of the vessel in roll. A starting point for this problem is analyzing the problem with a potential theory code. A computer program can generate specific wave radiation for the vessel in the wanted direction, speed, amplitude, and frequency to investigate specific motion. The radiation potential gives the added mass and damping when rotation of the hull in roll radiate waves away from the vessel.

Radiation of waves is only a part of the damping in roll. Potential theory calculations establish the wave radiation damping and frequency-dependent added mass. However, since these calculations neglect the viscous effect, ITTC presents empirical equations for the Ikeda Method in order to calculate the viscous roll damping. According to the International Towing Tank Conference (ITTC, 2017), all contributions to the second-order differential equation (Equation (2.3)) must be found. The viscous damping term in the equation is the most complex as it involves several empiric parameters and hull dependent variables used to calculate;

- Lift damping
- Friction damping
- Eddy damping
- Appendix damping; Bilge keel, skeg keel and rudder

Governing equation

The second order equation in Equation (2.3) can be classified as either under-, critically- or over damped depending on the relationship between the inertia, stiffness and damping terms. When considering roll damping, Equation (2.3) can be written as:

$$\left(I_{xx} + A(\omega)\right)\ddot{\phi} + 2\xi\omega_n\dot{\phi} + \omega_n\phi = 0 \qquad (2.10)$$

As seen in equation (2.10) Inertia has been separated into rigid body inertia and added mass. The damping term is decomposed with damping (ξ) and vessels natural frequency (ω_n) in order to find the coefficient for damping.

Vessels natural frequency

$$\omega_n = \sqrt{\frac{k}{m}} \tag{2.11}$$

Damping ratio can be expressed as;

$$\xi = \frac{C}{C_c} \tag{2.12}$$

$C = actual\ damping$

$C_c = Critical\ damping$

Where critical damping is equal to;

$$C_c = 2\sqrt{km} \tag{2.13}$$

By inserting equation (2.13) in equation (2.12), the ζ can be written as;

$$\xi = \frac{C}{2\sqrt{km}} \tag{2.14}$$

The damping ratio (ξ) is a critical coefficient for predicting roll motion, such as parametric rolling. A correct value for the damping ratio is important as it determines the characteristics of the system response to an external disturbance. Figure 3 illustrates different damping scenarios.

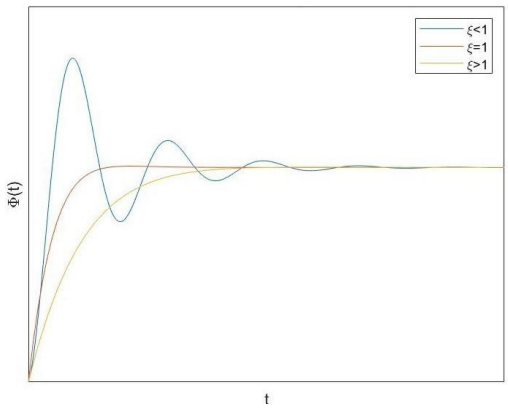

Figure 3: Illustrating a vessel being over, - critical, - or under damped, Picture: Own archive.

As seen in Figure 3 page 20; the blue line indicates under damped vessel, red is critical damped and yellow is over damped. However, the heel angle is the same for all three conditions at the end, and this can refer to the equilibrium angle in hydrostatic stability. Additionally, for the underdamped vessel, $\xi < 1$, there is an overshoot, and the vessel will move back and forth against the equilibrium state. As mentioned, all three situations will end up equally from a static view; the dynamic and damping give information of what happens from the vessel is set in motion till the state of equilibrium. Furthermore, if the overshoot is too significant, water entry with progressive filling is possible, especially in the first roll motion where the response reaches a maximum.

$$PO = 100e^{-\left(\frac{\xi\pi}{\sqrt{1-\xi^2}}\right)} \tag{2.15}$$

$PO = Percantage\ Overshoot$

However, a critical damped vessel would have the best motion in roll, which goes relatively quickly to a state of equilibrium with no overshoot. Although, how will the physical values in Equation (2.14) have to be modified in order to reach critical damping? It requires knowledge about the magnitude of the stiffness and mass to illustrate critical damping.

The k from equations above can be compared with the stiffness to the vessel and will be depending on the righting moment lever arm GZ and Δ, m is inertial mass and will be depending on I_{xx} as shown in Equation (2.16) and Equation (2.17).

$$k = GZ\Delta \tag{2.16}$$

$$I_{xx} = (0.35B)^2 \tag{2.17}$$

The Inertia (I_{xx}) in roll axes are based on experience for older vessels to be around 36 - 38 [%] of the vessel width (Aasjord & Enerhaug, 2013), although (Faltinsen, 1990) uses 35 [%].

The equation for damping ratio will be;

$$\xi = \frac{C}{2\sqrt{GZ\Delta(0.35B)^2\Delta}} \tag{2.18}$$

Simplified;

$$\xi = \frac{C}{2\Delta(0.35B)\sqrt{GZ}} \tag{2.19}$$

Critical damped means the damping ratio is equal to 1, and then the damping coefficient can be found using equation (2.19).

$$1 = \frac{C}{2\Delta(0.35B)\sqrt{GZ}} \tag{2.20}$$

$$2\Delta(0.35B)\sqrt{GZ} = C \tag{2.21}$$

The equations above show that critical damping can be estimated using known parameters for any vessel. It also shows that C is increasing primarily with regards to displacement, beam and GZ.

It is important to remember that equation (2.21) is not accurate enough to test or study vessel motion, although it illustrates the relationship between ship stability, mass and relative damping ratio. However, critical damping increases with high GZ, meaning a very steady vessel or larger displacement, indicating the vessel's size. Furthermore, a smaller fishing vessel, meant for open seas, has strict regulation regarding stability demands set by the government, and critically damped vessels may breach stability requirements, since roll motion is underdamped due to the small contribution from C in wave radiation, simultaneously as the stiffness is high. In all practical cases, the roll is an underdamped degree of freedom with an overshoot in the response, as seen in Figure 3 page 20.

2.2.2.1 Added mass and Damping by wave radiation

Damping by radiation of waves can count for up to 30 % for commercial cargo ships regarding roll damping. However, for ships with shallow draught and wide section this component can have a larger effect. A ship will make the most waves in heave and pitch, while roll motion itself does not make so much waves due to the amount of water the hull "pushes" away in pure rotation about the x-axis.

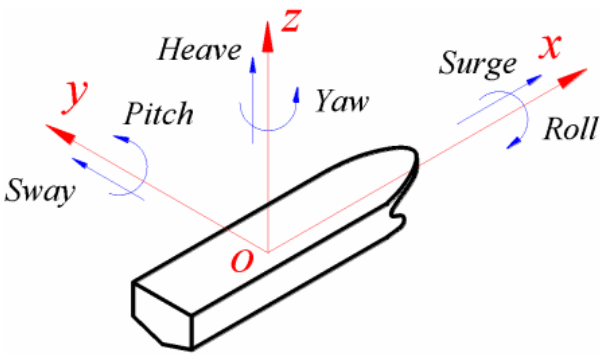

Figure 4: The six degrees of freedom which a ship can move (Winter, 2018).

Radiation forces are forces arising due to vessel motion. It is common to divide these forces into added-mass forces, proportional to body acceleration, and wave damping forces, proportionate to body velocity.

The added mass force may be considered an inertia force relating to the mass of water carried with the body motion. It is essential to realize that it is not a fixed amount of water — but the movement of a floating body influences the water. The added mass coefficient is equivalent to how large the fluid inertia force becomes when the body is accelerated. There is a relation between the radiation damping and excitation forces. Both are measures of how strongly linked the body is to the wave field at sea: A body that can reflect waves in one direction when moved will experience excitation when acted upon by incident waves coming from the same direction. The wave damping force is related to the average force exchanged between the sea and the body. This force arises due to outgoing waves generated from vessel motion. The wave damping coefficient estimate how large the radiated waves will be (Pecher & Kofoed, 2016).

A common procedure to estimate or calculate wave damping is using potential theory based on the vessel hull form. There are two popular methods to obtain this, either by 2D strip

theory computer programs such as; VERES[2] & PDSTRIP[3] or 3D panel code programs; WAMIT[4] & NEMOH[5]. Both methods calculate the hydrodynamic force on the vessel in motion but not the viscous effects. Furthermore, both methods solve frequencies depended, added mass and damping problems regarding roll motion.

[2] VERES (https://www.sintef.no/en/software/shipx/)

[3] PDSTRIP (https://sourceforge.net/projects/pdstrip/)

[4] WAMIT (https://www.wamit.com/)

[5] NEMOH (https://lheea.ec-nantes.fr/valorisation/logiciels-et-brevets/nemoh-presentation)

2.2.2.2 Viscous roll damping

Potential flow theory, which, e.g. NEMOH uses, does not include the viscose effect from the radiation of waves. Estimation of this effect can be conducted by following (ITTC, 2017), which bases on the study from (Ikeda , Himeno, & Tanaka, 1978), (Ikeda , Komatsu, Himeno, & Tanaka, 1976), (Ikeda, Himeno, & Tanaka , 1977), (Ikeda, Himeno, & Tanaka, 1977). Even though the damping is dominated by viscous forces and only a small part is radiation of waves in roll motion, the radiation effect will influence the result considerable if neglected.

The principal components of roll damping as defined by (ITTC, 2017) is summarized below. The composing of roll damping consists of two hull-depended parts; lift and friction damping, and one sectional part; eddy damping. Other devices, such as; bilge keel, skeg keel, and rudder that affect roll damping, must be defined and calculated separately. In (ITTC, 2017) the damping coefficients presented are expressed in linear form, while eddy, friction, bilge keel, and skeg keel coefficients in this thesis are quadratic. The damping coefficients presented in ITTC are expressed in linearized form. In this thesis both linear and non-linear (quadratic) coefficients are used, as the damping is assumed to be nonlinear. For this reason, a presentation of what components depends on and a description of the components themselves is given.

Lift damping

Lift damping comes from the roll velocity ($\dot{\varphi}$). The rolling velocity causes a circulation flow that generates low and high-pressure fields on the hull surfaces and gives the hull an angle of attack (α) against the forward speed U. This angle of attack is linearly increasing with the distance (l) from the centre of roll as illustrated in Figure 5 and, therefore, becomes particularly large for vessels with a high centre of gravity.

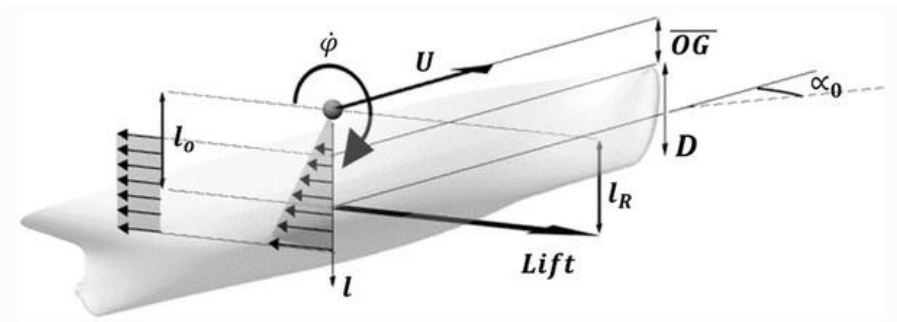

Figure 5: Illustrates how roll velocity effect lift damping (Söder, Rosén, & Huss, 2017).

Illustrating the forward velocity *(U)*, the draft (D), the roll velocity ($\dot{\varphi}$), the distance from the waterline level to the vertical centre of gravity $\overline{OG}$, the effective lever l_0 where the local angle of attack is α_0 and the effective lever for the lift force l_R (Söder, Rosén, & Huss, 2017).

The lift damping coefficient is proportional to the ship velocity and independent of the roll period.

$$Liftdaming = \frac{\rho}{2} VLdK_n l_0 l_R \left[1 - 1.4\frac{\overline{OG}}{l_R} + \frac{0.7\overline{OG}}{l_0 l_R}\right] \quad (2.22)$$

Where ρ are density, V is speed, L is the length of vessel, d is draught, K_n represent the lift slope often used in for ship maneuvering.

$$K_n = 2\pi\frac{d}{L} + k\left(4.1\frac{B}{L} - 0.045\right) \quad (2.23)$$

k is additionally dependent on a midship coefficient (C_m). Further on, l_0 is defined in such a way that the quantity $\frac{l_0\dot{\Phi}}{V}$ corresponds to the angle of attack of the lifting body, l_r denotes as the distance from the point O (the still water level) to the centre of lift force. Last, $\overline{OG}$ is the distance from still water to CoG.

Lift damping is one of the components that won't change regarding the hull geometry, as all values don't need or include a description of the hull and only rely on the shape of the midship section (C_m) for the vessel.

Friction

Viscous friction between fluids and hull can be explained as water hanging onto the hull. This component relies on Reynold's number or the scale effect between the model and the actual size vessel, and in roll motion, it is a pure friction component. The viscous friction component often is referred to as how a thin, flat and smooth plate will behave, which has the same submerged area as the actual size ship and the same velocity. Through experiments and research, an empirical formula to calculate the frictional component for full-scale ship(s) has been developed. The friction effect increases with forward speed.

$$Friction\ damping, dF = \frac{\rho}{2} S_f R_f^3 C_f \quad (2.24)$$

R_f and S_f is the value of the 3D vessel hull form, and C_f is defined as the frictional coefficient.

$$Friction\ damping, dF = \frac{\rho}{2} S_f R_f^3 C_f \left(1 + 4.1\left(\frac{V}{\omega L}\right)\right) \quad (2.25)$$

V is speed, L is length of vessel and ω is roll angle velocity. Furthermore, friction damping has most effect at low speed.

Eddy damping

Eddy damping consists of the change in pressure around the hull and the separation of vortexes. Unlike the lift force and friction force, the eddy damping depends on sectional hull form, which needs to be integrated along the vessel length, Figure 6 illustrates how separation of vortex is connected to the hull shape.

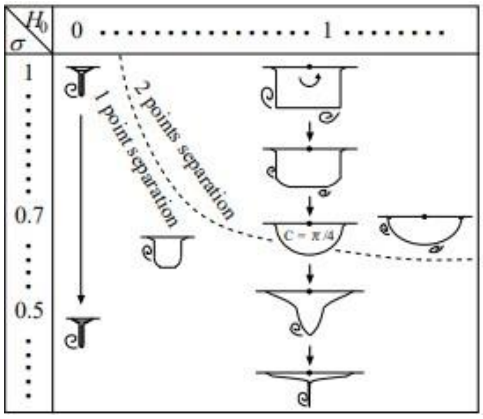

Figure 6: Illustrates how vortex shredding generates with regards to hull shape (ITTC, 2017).

The amount of eddies created is depending on two parameters relating to the hull shape. Since the shape of the vessel varies along its length, the hull is divided into sections. Each section has a shape with curvature, width and breadth and the eddy damping is assumed constant over each section. The eddy damping on in section is dependent on the half width-draught ratio (H_0) and the area coefficient (σ) of each section.

$$H_0 = \frac{B}{2T} \tag{2.26}$$

$$\sigma_c = \frac{A_w}{BT} \tag{2.27}$$

$H_0 = \frac{B}{2T}$Where B is the width of the section, T is the draught and A_w is the wetted surface area under water.

$$Eddydamping = \frac{\rho}{2} d^4 C_R \tag{2.28}$$

The equation (2.28) can seem to be very straightforward, as rho (ρ) and draught (d) are known. The difficulties is the C_R, which describes the hull form. C_R description consists of multiplication between estimated Lewis-form parameters for each section of the vessel and ratios between R/d, $\overline{OG}$/d, H0, and R/d. These need to be integrated over the vessel length.

Moreover, a function (γ) needs to be solved, dependent on Lewis-form parameters, which describes how fast the water runs underneath the vessel, resulting in pressure coefficients (C_P) and r_{max}/d relation, will be multiplied by C_R, r_{max} is the maximum distance from centre of gravity (roll axis) to hull surface.

Lewis-form parameters can approximate vessel-shaped sections when the vessel sections are symmetric about the centre plane, depending on the H0/σ definition.

In this investigation, some of the C_R values became negative and resulted in negative damping, making the simulation invalid. Since the C_R value cannot be negative, the solution became to set C_R-value never lesser than zero.

The reason for the negative C_R value is the hull geometry. The hull for these older traditionally Norwegian fishing vessels has a large width and small volume underneath the water, which leads to the value of H_0 and σ in C_R negative.

The solution to set $C_R \geq 0$ is supported by investigating a study by (Kawahara, Maekawa, & Ikeda, 2012). In their investigation, C_R was set identically zero for large portions of a ship where calculation of the C_R values based on the H_0 and σ values in the paper also gave

negative C_R values. In the case of a traditional fishing vessel, the vessel block coefficient (C_B) and midship coefficient (C_M) fell outside the valid range area for the Ikeda method.

Bilge keel

Steel rails that contribute to roll damping by the increase of viscous flow and eddies. Bilge keels should be mounted on the broadest part and perpendicular to the vessel's hull, and in such a matter that there is no chance for the bilge keel to leave the water surface.

Figure 7: Car carrier, Cougar Ace, green arrow marks the bilge keel (Bell, 2008).

As can be seen in Figure 7 even though this particular vessel is approximately 200 [m] it shows that the bilge keel is only mounted on the widest part of the vessel.

A bilge keel damping action is relatively small but very effective damping. Its exact position on the vessel has been studied to maximize the roll resistance. Several positions and dimensions are usually tried out during the model trials to optimize the bilge keel effect. The bilge keel is generally placed in the amidships section of the vessel hull, often perpendicularly at the turn of the bilge.

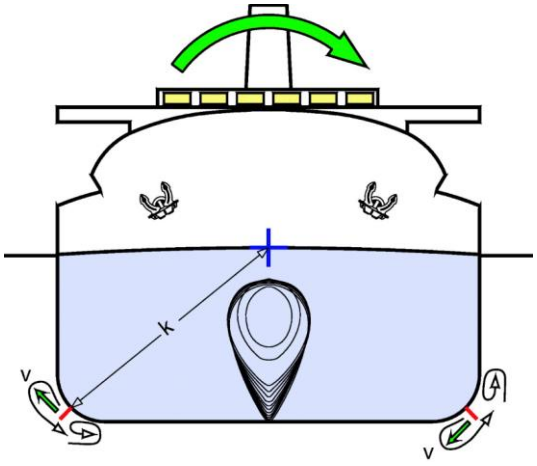

Figure 8: Importance of the lever arm k, and eddies created by bilge keel (Baniela, 2008).

Even from a smaller roll velocities, bilge keel is effective to damp roll motion, as the lever arm k in (Figure 8) generates very velocities of the bilge keel versus the water flow. At forward ship velocity the bilge keels acts as wings which dampen motion in the same manner as hull-lift damping when water flow moves over the forward end of the bilge keel with an angle of attack and generates a lift force, opposed to the roll motion. However, the main effect of bilge keels is due to the increase of eddies behind the bilge keel, which increases the roll damping. The friction and roll damping effect of bilge keels increases with speed (v) and the vessel roll velocity (Baniela, 2008).

> *"(…) In pure, simple harmonic motion, there is no friction, but naturally, when the roll motion occurs, the friction, which is always there, increases with the bilge keels."*

Studies show the bilge keel can reduce rolling motion on vessels up to 20 [%] in the rough sea with a wind speed of 24 [knots] (Putra, Iskandar, & Novita, 2018).
Furthermore, in more powerful seas with wind speed to 40 knots, the rolling motion reductions can be as high as 13 [%]. The placement and size of the bilge keel will determine its ability to reduce ship rolling movement. The use of a longer and broader bilge keel will make it more effective in reducing rolling movement. However, bilge keels in large dimensions may affect the ship's resistance and obstruct fishing operation during setting and hauling of fishing gear (Putra, Iskandar, & Novita, 2018).

The total bilge keel component consists of four segments; lift force, wave damping, hull pressure, the normal force (ITTC, 2017). Although lift force is speed-related and wave damping is such a small contribution, they are neglected in this study. The sectional linear coefficient for the normal force component of the bilge keel from the roll damping without forwarding speed, BK_{KN0}.

$$Bilge\ Keel\ damping, dBK_{KN0} = \frac{\rho}{2} L_{rxbk}^{3} f b_{BK} C_d \qquad (2.29)$$

L_{rxbk} is the length from roll axes to tip of bilge keel, f is a correction factor to take account of the increment of flow velocity at the bilge, b_{BK}width of bilge keel is, C_d is drag coefficient and rest is known from previous.

The sectional linear coefficient for the hull pressure of the bilge keel from roll damping without forwarding speed, BK_{KH0}.

$$Bilge\ Keel\ damping, dBK_{KH0} = \frac{\rho}{2} L_{rxbk}^2 f^2 \int_G C_p l_p\ dG \tag{2.30}$$

The integral can be written as

$$\int_G C_p l_p\ dG = d^2\left(A_0 C_p^- + B_0 C_p^+\right) \tag{2.31}$$

$C_p^{+/-}$is pressure coefficients**,** $A_0$and $B_0$is form factors.

Skeg component

It contributes to reducing the roll motion, although, normally it is not as effective as the bilge keel. Skeg keel has shown to be more effective to decrease drift off rather than roll motion.

$$Skeg\ Keel\ damping, dSK = \frac{\rho}{2} l^2 \left[(C_d L_{sk} l_1) - \left(\frac{C_p^+ a l_2}{2}\right) + \left(\frac{3 C_p^- S l_3}{4}\right)\right] \tag{2.32}$$

As seen in Figure 9, page 32, the creation of different pressure, over and under pressure, comes from the water flow direction, decided from roll direction. From Figure 9, page 32, there is a pressure sideways on the skeg keel, creating an over-pressure (C_p^+) on the left side, with a leverage arm (l_2). On the right side, an under-pressure (C_p^-), with a leverage arm (l_3). Both leverage arms are acting accordingly to the distance to CoG.

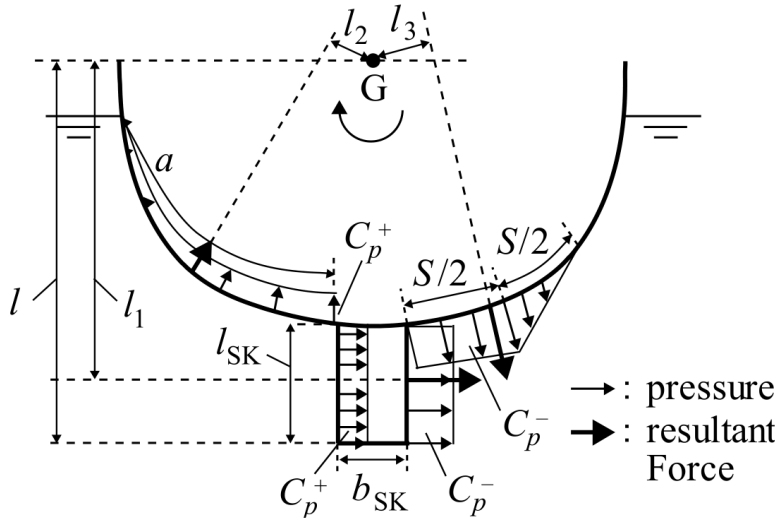

Figure 9: Illustration of pressure created by skeg keel (ITTC, 2017).

Each pressure coefficient has pressure profiles acting around the skeg, depending on width, height and length. Additionally, the pressure influences the hull, with a distance from the top of the skeg keel to the waterline. In Figure 9, the distance the pressure is impacting on the C_p^+ side is gradual decreasing over the length a, while C_p^-, the pressure is divided into two sections; one where the pressure is constant (S/2) and another where the pressure gradual decreases (S/2). As shown in figure 4, page 23 from ITTC, the pressure distribution and pressure profile are estimated, and the leverage arms affecting the length a and S are empirically determined. The pressure coefficients Cp depend on Keulegan–Carpenter number (Kc), a dimensionless value, and describes the dominating force between drag force and inertia forces for any objects in an oscillatory fluid flow. For small Keulegan–Carpenter number inertia dominates, while for large numbers, the drag forces dominate.

The pressure on both sides of the bilge keel and the bilge keel itself makes it necessary to calculate how the pressure act section-wise. The same way as the eddy and bilge keel and integrate the pressure over the defined length of the skeg keel, as the skeg keel does not extend over the vessel's entire length.

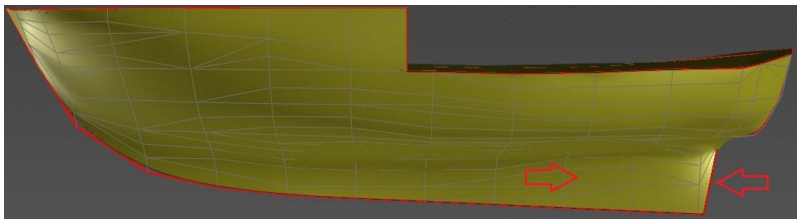

Figure 10: Illustrates skeg keels length extension, Picture: from DELFTShip.

Furthermore, by looking at Figure 11, it can be easy to understand the difficulties of describing where skeg keel ends with regards to height and length, as traditionally Norwegian fishing vessels are built streamlined with smooth transitions between the hull and skeg.

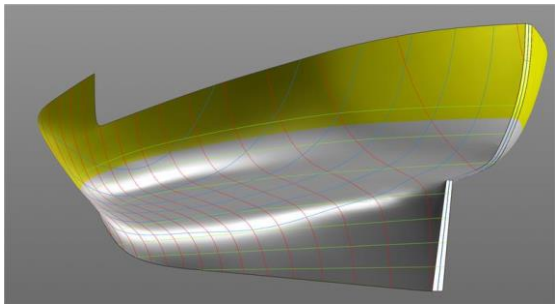

a) From aft, illustrating height of skeg keel.

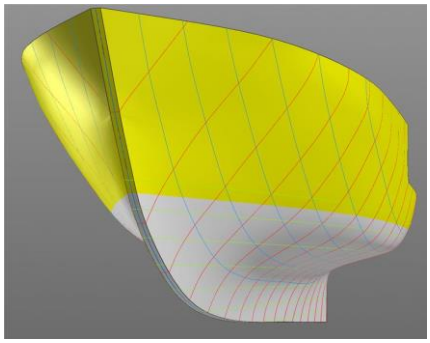

b) Illustrating length of skeg keel.

Figure 11: Shows underwater-hull, Picture: from DELFTShip.

3 Methodology and Material

3.1 Method

For all parties involved in a vessel, whether it is commercial or fishing, large or small, ship-owner or nautical engineer, it is of great interest to determine how a vessel will respond in a seaway, either during the vessel's design or before any modifications. For predicting vessel motion, a numerical and sometimes physical test is needed to verify vessels' motion and stability; furthermore, vessel motion prediction means knowledge based on experience, aka empirical knowledge. Empirical knowledge is a term that refers to information obtained from observations, experience or experiments, for this theme it will be from physical model experiment or validated computational theoretical models in, e.g. seaway or wave response.

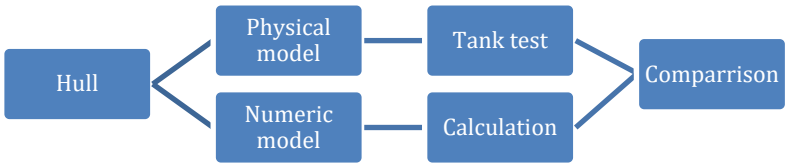

Figure 12: Basic illustration of two approaches for predicting vessel motions.

At the beginning of any vessel design, a fundamental question is; which motion will the vessel have in a seaway, although not knowing the effect of design choices without the possibility of acquiring knowledge through trial and error. The physical effects experienced by the vessel must be described by a model, physical or theoretical, to predict vessel motions. Both physically and theoretical models are aids to obtain knowledge about the physical effects influencing a vessel hull in a seaway, effect of changes to hull or the effects of appendixes mounted to the hull. Both physical and theoretic models support each other in obtaining knowledge of physical phenomena, see Figure 12.

Figure 12 illustrates how this study is built up; it is one physical model test and one numerical calculation. The numerical calculation in this case investigates how the Numerical Estimation of Roll Damping from (ITTC, 2017) fits an older traditional Norwegian fishing vessel. Furthermore, both methods investigate the effect of skeg keel, with and without bilge keel and the possible "misplaced" bilge keel as the bilge keel in the study is placed to limit interference with fisheries operations.

By defining physical effects and testing these by performing experiments; the same experiment with several repetitions in the same condition, and varying conditions, hull parameter, and or without appendixes; experience and knowledge is acquired.

All physical tests can be considered a model where any changes will enhance knowledge for the effect resulting from the change, even though physical model tests are on a smaller scale and the magnitude of the changes may not be the same in actual vessel sizes. The test results can be put together in an empirical model that can reproduce the tests' results. Furthermore, in the empirical model, there is the possibility of separating components or elements for closer study or manipulation.

3.2 Hull model

As seen in Figure 12, page 34, a hull is necessary for any study or investigation; in this study, roll damping for a vessel. Both the physical experiment and the numerical calculation will use the same hull as the foundation.

The line drawings are used as a numeric model for theoretical calculations, and the 3D printed model to do the physical tests, is an older traditional Norwegian fishing vessel that is short in length and has wide width that gives the vessel an "oval" shape. These vessels are typically produced in a Fiberglass Reinforced Polyester (FRP) to manufacture a series of identical hulls.

Hull digitalization

The hull designed in this investigation exists as a line drawing (PDF) in 2D. Converting the line drawing to 3D is essential for creating a physical model or using the 3D drawing for numerical calculations. For this reason, the information in the drawing is converted to 3D through a two-step digitization process, see Figure 13:

1. Transferring of line drawing coordinates to computer readable coordinates for computer programs.
   Combination of the coordinates points into a 3D, a model with surfaces.

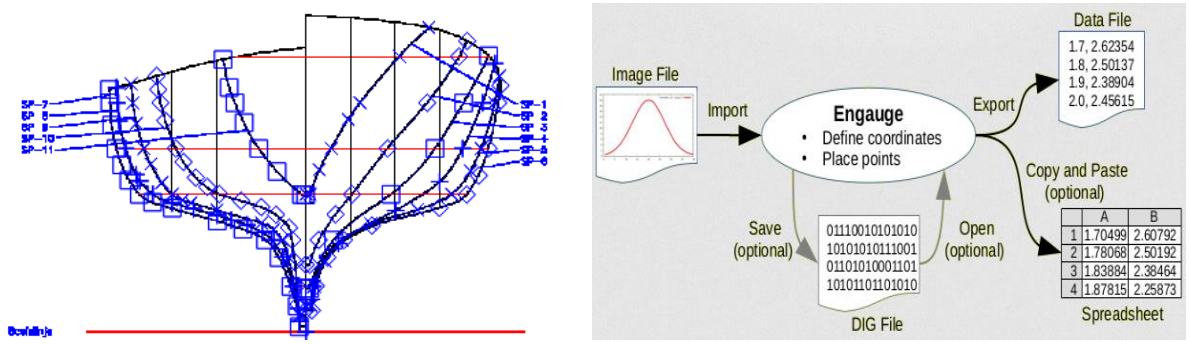

a) The line drawing of vessel.

b) Illustrating conversion process (Mitchell, 2020)

Figure 13: From PDF to 3D coordinates.

Engauge Digitizer was used to read the transferred coordinates and convert and import these to a new file readable by Excel were the coordinates from the frame(s) will be sorted in before exported to DELFTShip. The coordinates for each point for each frame, vertical and horizontal, are presented based on the known distance of the vessel frame as measured from the line drawing, see Figure 14, page 37.

# x, Nullpunkt	
12058,93, "-0,004"	

# x, Spant 1	# x, Spant 2
12062,6, "1075,34"	12058,49, "528,99"
12096,1, "1076,61"	12095,15, "529,41"
12166,62, "1254,93"	12126,23, "633,05"
12274,3, "1439,17"	12171,31, "722,47"
12437,84, "1697,97"	12287,57, "894,51"
12518,04, "1799,62"	12450,67, "1081,73"
12661,42, "1960,58"	12756,71, "1439,65"
12852,96, "2161,35"	13091,64, "1800,11"
12980,29, "2282,92"	13194,71, "1928,45"
13105,35, "2389,24"	13292,79, "13292,79"
	13364,7, "2163,52"
	13432,5, "2285,47"

1. *Raw data from Engauge exported unsorted*

x	z
12058,93	-0,004
12062,6	1075,34
12096,1	1076,61
12096,1	1254,93
12274,3	1439,17
12437,84	1697,97
12518,04	1799,62
12661,42	1960,58
12852,96	2161,35
12980,29	2282,92
13105,35	2389,24

2. *Sorted raw data of one section.*

Figure 14: Data from Engauge exported to Excel.

These points (Figure 14) with coordinates can later define the vessel hull in 3D by creating a surface between the points and present a virtual 3D model of the vessel. The hull in DELFTShip was exported as a geometry file to a 3D printer to become a physical model, and be used in numerical calculation to estimate A(ω).

Moreover, DELFTShip derives all hydrostatic data derived from geometry, such as; displacement, metacentric height, buoyancy, flotation centre, etc. These values is valid for the physical model and will be used to find the Center of Gravity (CoG) by conducting an inclination test.

The sorted coordinates appears in DELFTship, as point(s) that visualize frame as seen in the line drawings; from here, it is necessary to connect the points using a triangular or squares pattern. The triangles and squares define surface that DELFTShip adapts a polygon mesh to from the skin of the vessel. This allows DELFTShip to calculate a Hydrostatic Table for the vessel.

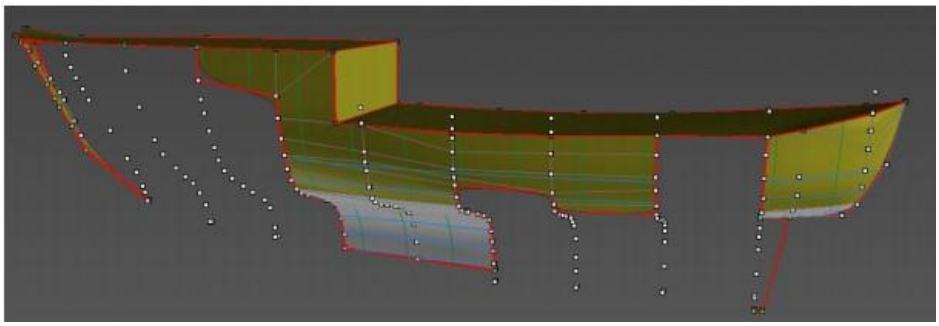

Figure 15: DELFTShip - work in progress, Picture: from DELFTShip.

Figure 15 shows an intermediate stage while modelling of the hull, and how coordinates from Engauge are converted into 3D model by the (white) points that make the vessel model's contour, the light grey lines show triangles and square routes creating the surface and the red lines following the model indicates a watertight area. When working in these programs, the norm is to design only one side of the vessel and mirror the model. Figure 16 shows the complete 3D model, where the left side is the plotted side and the mirrored right side.
It is important to remember that this is only for the outer hull; for 3D printing, there must be added a thickness to the skin. The outer hull itself, as described in DELFTShip, can be used in numerical calculations.

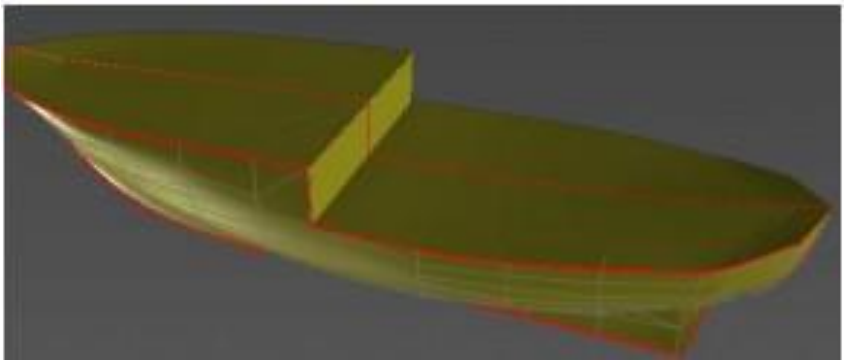

Figure 16: Mirrored model, Picture: from DELFTShip.

The next stage is to export the DELFTship file for 3D printing or numerical analysis.

3.3 Physical Model Track

The exported model file from DELFTShip as described in Chapter 0 was sent to UiT, Narvik. Here the file was processed into a virtual hull with instructions for the machine to 3D print the hull. The 3D printer at UiT, Narvik, has a working space of 50x50x50 [cm], limiting the sizes of models to be printed. For this study, the vessel is approximately 9 [m], the decision became to have a model scale of 1:10, and were printed in three pieces and mounted together with metal splinters and glue, Figure 17, page 40. Moreover, the printed model received a hull thickness of 1 [cm], with deck height (Z axes) inside of 1000 [mm] above the origin set at the aft corner of the keel. Furthermore, as 3D printers can make arbitrary parts needed, bilge keels were printed, with specifications to fit the hull in at a specific place: h =1.0 [m] and 2.5 [m] forward, and the bilge keel has a height of 20 [cm] in full scale, placement for bilge keels can be seen in Figure 17a, page 40. Based on studies, observation, and conversation with a ship engineer at Selfa Arctic (Hokland, 2020), this was chosen as placement of the bilge keel. It is worth mentioning that the bilge keel placement may be suboptimal with regards to damping functionality since the placement is influenced by the fishermen's considerations to avoid conflict between fishing lines and nets with the bilge keel. (Putra, Iskandar, & Novita, 2018).

The test procedure and work with the physical model also provides with needed input for the numerical model, such as;

1. What cases to simulate for comparison
2. Weight distribution in the vessel
3. CoG and definition of water line-height

It was therefore logical to start with the physical experiment, to define necessary physical sizes, situations and cases for further numerical simulation.

Hull model: The model does not have the superstructure or closed deck; however a deck was designed as plate for mounting inside the model to fit weights and sensor. Bilge keels were printed with the possibility to be mounted or removed with screws depending on test with or without the bilge keel, see Figure 17. The figure also shows the hull before coating to show the assembly from parts into the complete model

a) *Before priming and coating, with bilge keel mounted.*

b) *After priming and coating, without bilge keel mounted.*

Figure 17: Finished model from 3D printer, Picture: Own archive.

The last stage was to prime and coat the model to ensure the model is watertight in the joints and between plastic layers. Furthermore, a smooth coating was applied to minimize friction and give the model a smooth surface during the model tests. The main dimensions of the model and full scale vessel is listed in Table 3, page 41.

Table 3: Main dimensions for vessel and model.

Definitions	Model	Vessel
$L_{o.a.}$	94 [cm]	9.4 [m]
L_{pp}	80 [cm]	8.04 [m]
Width	32 [cm]	3.2 [m]
Height to "deck"	17.8 [cm]	1.78 [m]
Depth (used in tests)	13.1 [cm]	1.31 [m]
Weight (Total)	8.15 [kg]	7.52 [t]

Experiment setup: One of the concerns regarding the water tank at UiT is the size; the tank is relatively small compared to more professional tanks, which can be over 200 [m] long and 25 [m] wide depending on the purpose of the thank is, see Table 1, page 14.

Table 4: Main dimensions of water tank.

L	4.05 [m]
L_{inside}	3.95 [m]
B	1.61 [m]
B_{inside}	1.50 [m]
Depth	2.5 [m]

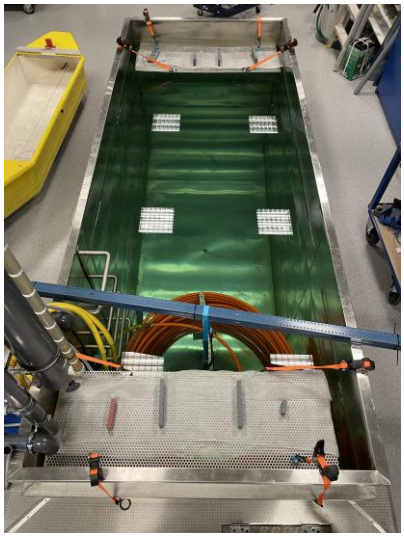

Figure 18: Water tank at UiT, Tromsø, Picture: Own archive.

As seen in Figure 18, the water tank at UiT, Tromsø, has straight aluminum walls. In addition to the small size tank, the straight aluminum walls will make the waves reflect and take a longer time for waves to be absorbed; this will cause disturbance when measuring the roll motion as the radiated waves reflected off the walls will quickly return to the experiment area.

The orange coil seen in pictures lies deep, so there is no interference from the coil with the results. Moreover, the model was placed across the tank; as waves radiate from the hull, since the waves predominantly radiate from the ship sides and must travel a longer distance before being reflected. Wave breaking equipment was inserted in the tank to help absorb the radiated waves; this way, each roll test last longer before reflected wave energy influenced results, obtaining cleaner measurements.

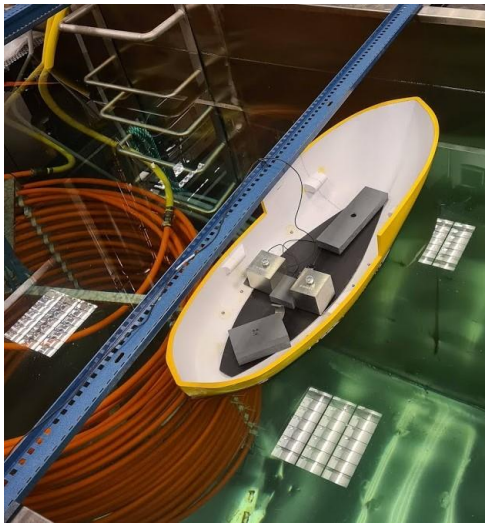

Figure 19: Showing positioning of model and the aluminum rod holding the cord, Picture: Own archive.

A blue aluminum bar (Figure 19) was placed across the tank for holding the electrical cord attached to the instrumentation, allowing it hang freely and not influence the model motion. Furthermore, the model was floating freely without any mooring lines attached, which caused the model to change heading slightly during tests. However, the heading change was small and came after several roll iterations, so the effect of heading change was believed to be negligible.

Wave breaking equipment: As mentioned previously and seen in Figure 20, the wave damping equipment in the form of perforated plate, and layers of fine mesh netting lying on the plate's top was installed in the tank. Four loading straps hold the plate and make it possible to adjust the perforated plate's depth and angle to get the best possible effect.

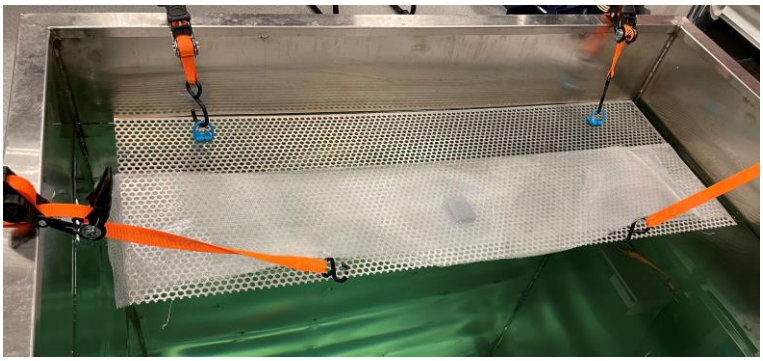

Figure 20: Wave breaking equipment used in water tank at UiT, Tromsoe, Picture: Own archive.

There are many different ways to make the waves be absorbed- die out. It all depends on the sizes of models, water tanks, and what test-result are of interest.

Each of these systems has advantages and disadvantages, making it sometimes necessary to combine techniques. The wave damping equipment lay on top of the water plane, with a small angel down towards the water plane to illustrate a beach. The beach system and use of perforated plates and fine wire screen is described as popular and effective by (Ouellet & Datta, 1986).

Instruments and experiment sequence

Due to the size of the vessel model and that UiT does not have a professional test tank with belonging measuring equipment, there was some concern about measuring the model motion in the water tank. There are usually larger sized models and sensitive measuring equipment connected to the model in professional and large water tanks, i.e., Trondheim (see Table 1 p.14).

Normal-sized Motion Reference Unit (MRU) for use on-board vessels weight about 2.0 [kg] with a diameter of 105 [mm] and height of 140 [mm] (Kongsberg, 2021). The size of these MRU's can cause a problem regarding weight and a placement issue, particularly of the used model-size. The solution was to use a Miniature Attitude Heading Reference System (Figure 21 b)), a small and light MRU with high-performance sensor technology (LORD, 2014), (see Appendix II).

a) Normal-sized MRU in bracket (Kongsberg, 2021)

b) Microstrain MRU, model 3DM-GX-15 used on vessel model, Picture: Own archive.

Figure 21: Compering of Motion Reference Units.

The data acquisition software SensorConnect from MicroStrain was used to record data from the MRU. SensorConnect was used to set up the MRU and set it to transmit the rotation angles and rotation rates to SensorConnect, the physical connection was completed with an RS232 interface to the computer, and a lightweight cable connected to the MRU and was configured to sample the motions at 100 [Hz]. SensorConnect keeps a database of all recorded data which can be exported in time slices to various formats. The data was exported time-stamped to a regular CSV file which was readable by Matlab. In Matlab, the recorded data was sorted into test sequences, making it possible to remove unneeded data and focus on one specific time sequence if wanted. Furthermore, with the high resolution MRU from (LORD,

2014), the quality of measurements was satisfying. The MRU is based on Kalman-filter technology and transmits filtered data, therefore there was no need for a noise filtering of the data in Matlab.

Experiment matrix

Test repetitions are essential when doing research about the motion of vessels and obtaining satisfying results. Each heeling condition, with and without bilge keel, was performed with twenty repetitions (Table 5) by manually applying a force at the reeling of the model while observing the readout of the MRU heel angle and releasing the model. There was some variation in the initial heeling angle, although, even if the heeling angle is not 100 [%], the displacement does not change as it would with extra weight for making the model heel and quickly remove the weight, and with 20 repetitions, the average should be good enough to get satisfying results.

Table 5: Number of repetitions.

Heeling condition	Repetitions
0.2 radians with bilge keel	20
0.2 radians without bilge keel	20
0.1 radians with bilge keel	20
0.1 radians without bilge keel	20
Total	**80**

3.4 Finding Center of Gravity

There are different methods one can use to find CoG on smaller actual size vessels and especially models. Due to the model size, scientific experiments rather than a standard heeling test could be performed.

(Aasjord & Enerhaug, 2013) Suggested finding the CoG by attaching the vessel, in this study the model, to a wire or rope and swinging the vessel back and forth in a relatively fixed axis, making the model act as a pendulum. An idealized pendulum has all mass is centered in one point and suspended in a wire massless. In the context of this vessel, the pendulum's length is the distance from the suspension point to the location of the centre of gravity. When the pendulum is at rest, the centre of gravity is vertical below the axis. When the pendulum swings, the centre of gravity moves in an arc of a circle. The longer the wire is, the more accurate the result should be. When an object, which is heavier than the rope, is suspended to that rope, the rope's weight is negligible, assuming the object is much heavier than the rope.

Oscillations for small decreases, with a good approximation for the mathematical pendulum, the swing time T is given by the Equation (3.1).

$$T = 2\pi\sqrt{\frac{l}{g}} \tag{3.1}$$

l = Length of wire

g = Gravity acceleration $\rightarrow$ 9.81 [m/s2]

(SNL, 2021)

By neglecting the rope's weight, it should be possible to calculate the distance from the pivot point to the CoG of the model. Figure 22 shows the model being used as a pendulum in order to find VCG and LCG.

In theory, this is a reasonable estimation method, although it did not work well in the conducted test. The result ended in a CoG over the railing on the aft part of the model. The uncertainties may come from the measurements from the pendulum suspending point and to the CoG of the model, which can come from the lightweight of the model vs rope's weight. However, this is unlikely but possible since the model is only 2 [kg], and the rope has some weight on its own.

Moreover, there were problems with getting the model to oscillate in fixed axes, and this can come from the suspension point in top, the lightweight of the model or friction making the model spin.

a) Vertical CoG. *b) Longditudal CoG.*

Figure 22: Finding Center of Gravity, Picture: Own archive.

The standard method for finding the CoG is to conduct an inclination test, which was done with the model. The heel test is carried out by knowing the ship's weight and moving known weights to port and starboard in a specific order and distance, see Figure 23, page 48. Using the same computer setup as described in **Experiment setup** makes it possible to measure the heel angles and to calculate the distance from GoC to the metacenter. The metacenter height is known from the hydrostatic report produced by DELFTShip.

a) Weights placement and shifting.

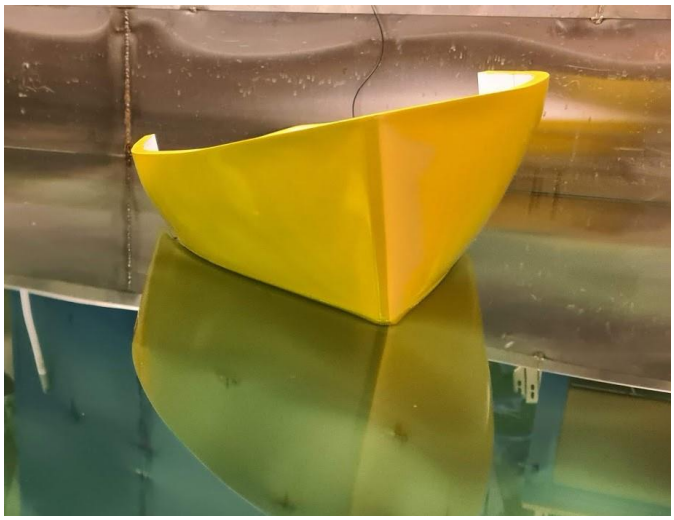

b) Heeling test.

Figure 23: Model with equipment during heeling test, Picture: Own archive.

In heel tests for an actual vessel with a computer setup, there will be a pendulum as a secondary measurement to ensure the measurement from the computer setup is correct. By using trigonometry with the pendulum result, the calculation of GM is possible.

Due to the size and material used in this experiment, the model is light and was weighed down, see Table 6, page 49. The same weights used for weighting down the model was used for heeling the model. The weights were therefore also used to define the waterline of the model during model tests and numerical calculations.

Table 6: Weight(s) for model.

Component	**Weight [kg]**	**Placement [cm]**
Model	2.52	Distributed all over
Model plate (model inside deck/equipment deck)	0.40	Distributed at z=100mm
Bilge keel x 2	0.06	As fitted, see Figure 17
Sensor	0.05	Center
Weight 1	2.04	From aft: 31.5 From Port: 6.5
Weight 2	2.04	From aft: 31.5 From Starboard (STB) : 6,5
Weight 3	0.450	From aft: 60.3 Center X-axes
Weight 4	0.450	From aft: 14.6 Center X-axes
Weight 5	0.120	From aft: 31,5 Center X-axes
Total	**8.13 ≈ 8.15**	+ 0.02 kg is screw for bilge keel and Velcro for weights
Remarks: all weights are placed on model plate with height (Z-axes) of 10 [cm].		

From the heel test in this condition the GM for light ship where found by calculating the accumulated moment vs. tan(ϕ).

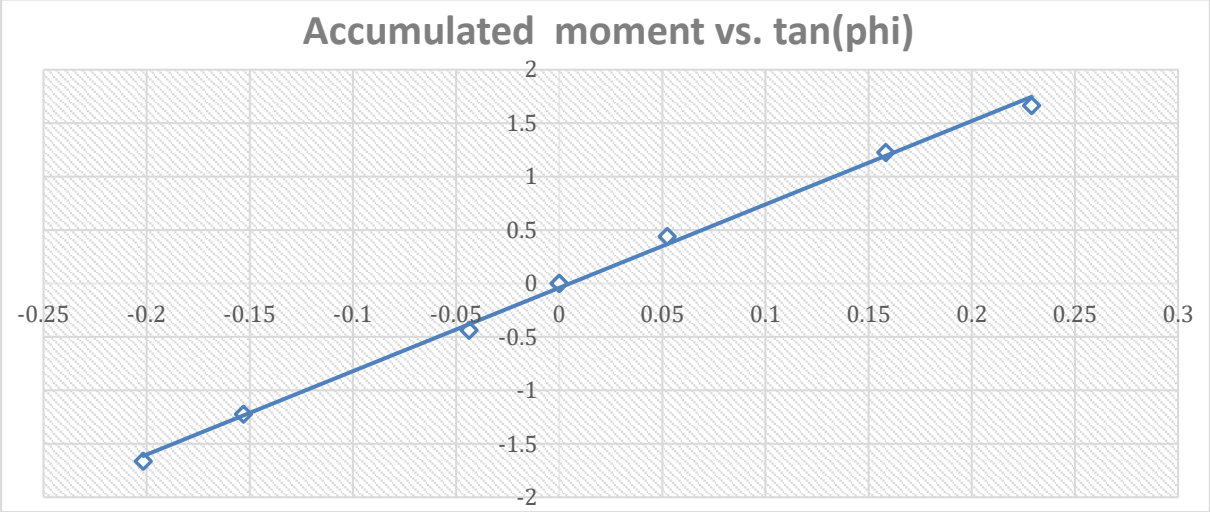

Figure 24: Accumulated moment.

Figure 24 shows the results from the heel test. As seen, the points are on a relatively straight line, indicating that the test's conduction is satisfactory. Moreover, the metacenter height from the DELFTShip report, is used for calculating the vertical moment for the hull during the inclination test; furthermore, use a momentum balance to calculate distance for the centre of gravity (CoG). The distance from CoG to the water plane (OG) will be used in the numerical calculation.

CoG light ship	
Light ship weight	3.05
Vertical moment during test	11.13104
Vertical moment subtraction for weights	-6.681
Vertical moment subtraction for tanks	0
Vertical moment added for weights	0
Sum vertical moment	4.450036
CoG light ship	1.459028

	Corrected CoG		
	VCG'	1.459028	
GM =			0.957228676
VCG			1.365771324

Figure 25: Shows the GM for light ship.

Figure 25 shows a section of the calculation method used to find CoG; the process uses known weights and leverage arm. For a full review, see Appendix I.

3.5 Numeric Model Track

The numerical model will be run in a mathematical computer program for simulation and finding the roll motion and roll decay coefficient. By reducing Equation (2.2) to a set of two 1.order ODE (Ordinary Differential Equation) the equations that can easily be used in Matlab for simulation in time, with, e.g. RKF45[6] function as long as mass, damping and stiffness are known, at least possible to estimate or calculate. With the RKF45 function and the possibility to decompose each equation for the damping contribution, the roll damping experiment, or investigation, can be compared with the result from the practical test.

$$\frac{d}{dt}\phi = \dot{\phi} \tag{3.2}$$

$$\frac{d}{dt}\dot{\phi} = \frac{\sum Moment}{I} \tag{3.3}$$

The damping moment of ships is related to a multiplicity of factors such as hull shape, loading condition, bilge keel, rolling frequency, and range of rolling angle. For small roll angles, the damping moment is directly proportional to the angular roll velocity. But with increasing roll angle, nonlinear damping will become significant. Due to substantial viscous effects, computing the roll damping moment using potential theory is problematic (Ibrahim & Grace, 2009). (Himeno, 1981) came up with a detailed description of the equivalent damping coefficient and expressed various contributions regarding hull friction, eddy damping wave damping, lift force and bilge keel damping.

The following sources can determine the viscous damping:

- Hull friction damping moment, C_F
- The moment resulting from separation and eddies, C_E.
- Lift damping moment due to angle of attack as the vessel rolls, C_L.
- Appendixes: Bilge-keel damping, C_{BK} and skeg keel, C_{SK}

[6] RKF45 is an algorithm in numerical analysis for the numerical solution of ordinary differential equations (Mahooti, 2021).

Decomposing due to bilge keels can be sorted into listed components:

- Bilge keels moment due to normal force, C_{BKN}.
- Moment due to interaction between hull and bilge keel, C_{BKH}.
- Modification to wave-making due to the presence of bilge keels, C_{BKW}.

The damping components C_L and C_W are linear, C_{BKW}, C_F,C_E, C_{BKN}, and C_{BKH} are nonlinear and depending on the amplitude. The expression of linear and nonlinear damping moments is as follows:

$$C_{lin} = C_L + C_W \tag{3.4}$$

$$C_{nonlin} = C_F + C_E + C_{BKN} + C_{BKHW} \tag{3.5}$$

The roll damping cannot be counted as linear when roll amplitude is larger than a few degrees, e.g. 5 [°]. When the roll angle increases, the damping also increases; one approach for solving this is adding the quadratic component into the equation.

$$(I_{xx} + A(\omega))\ddot{\phi}_4 + C_{lin}\dot{\phi}_4 + C_{nonlin}|\dot{\phi}_4|\dot{\phi}_4 + K\phi_4 = 0 \tag{3.6}$$

Moreover, in ship stability regarding vessel motion, added mass is the inertia added to the vessel; because the accelerating vessel must move some volume of water as it moves through it. The open-source program Nemoh is a numerical solver for the computation of first-order hydrodynamic coefficients such as added mass, radiation, damping and excitation forces in the frequency domain. (Babarit & Delhommeau, 2015). The program has been developed for over 30 years at École Centrale de Nantes in France and released as an open-source in January 2014. Nemoh uses linear free surface potential flow theory, with the assumptions of an inviscid fluid, incompressible and irrational flow. Green's second identity and the appropriate Green function is applied. The resulting linear Boundary Element Method (BEM) for the free surface flow around a body is of first order with assumptions of small motions around mean position and linearized free surface equations. Nemoh uses the Panel method in order to solve the linear BEM. Furthermore, Nemoh can be operated in Matlab or on the command line.

The process of running NEMOH starts with hull from DELFTShip. NEMOH uses the same model as DELFTShip, by exporting the geometry file from DELFTShip as a STL.file. The STL.file creates a list of points, or coordinates, with associated couplings between these coordinates, which creates triangles. With NEMOH's accompanying program, *MeshMagic*

that converts the STL file into a geometry file for NEMOH and sets the initial draught for the vessel. As NEMOH bases on the panel method, the STL format is highly suitable. Along with the STL input, placement CoG input found from heel test explained in Chapter 0, NEMOH can solve A(ω) and B(ω) from a selection of frequencies (ω). A(ω) can be input for Equation (2.3), and B(ω) will be used as the linear added mass in roll and for the linear wave damping coefficient.

As seen in Equation (2.3), the mass, here consisting of the Inertia in roll, along with the additional mass contribution A(ω) is needed. The rigid body inertia in roll is unknown. It is possible to measure inertia, although, in this study, the inertia estimated numerically, based on knowledge of the geometry of the hull and the weight of the hull which is measured.

The NEMOH preprocessor, Mesh-magic[7] contributed to the numerical estimation of inertia in roll, by distributing the known mass evenly throughout the model. The distribution of mass became a 10cm (full scale) thickness over the vessel's hull. After estimating I_{xx} for the hull, adding the inertias for weight used for maintaining the correct waterline to the hull is necessary.

Table 7: Calculation of additionally weights distribution.

Steiners Theorem; $I_Z = I_{Xi} + A_i d_i$^2				KG 1.46 [m]		Deck 1 [m]			
Weight [kg]	Id	L [m]	B [m]	H [m]	Lx [m]	Bx [m]	Hx [m]	A [m]	I_{zi} [kg*m^2]
2.04E+03	I_{x1}	0.6	0.6	0.6		0.65	0.16	0.669403	1.04E+03
2.04E+03	I_{x2}	0.6	0.6	0.6		0.65	0.16	0.669403	1.04E+03
450	I_{x3}	2.22	0.6	0.2	0		0.36	0.36	7.33E+01
450	I_{x4}	1.11	0.6	0.4	0		0.26	0.26	4.99E+01
120	I_{x5}	0.68	0.6	0.2	0		0.36	0.36	1.96E+01
									3271.916
						Vessel			3588
						Total			6859.916

The inertia of the weights were estimated using the Steiners Theorem, which considers the distribution of the inertias from the axis of rotation, see Table 7.

[7] MeshMagic: https://lheea.github.io/meshmagick/

The weights used for maintaining the correct waterline is identical to the weights used in the inclining experiment and placed with port/starboard symmetry, see Figure 19, page 42.

Even after the codes used in this study have been checked several times as described in ITTC and checked against the original codes from (Himeno, 1981), some deviations from (ITTC, 2017) were needed to get comparable results between physical experiment and simulation.

- The Eddy damping: $Cr \geq 0$. Solution as (Kawahara, Maekawa, & Ikeda, 2012)
- Skeg damping: The leverage arms estimated to impact with regards to length a and S, see Figure 9, page 32. Moreover, how the skeg is defined; what should count as skeg damping and what should count as hull damping? The traditional Norwegian fisheries vessel has a smoot hull with non-obvious transitions from hull to skeg.
- Bilge keel: was calculated on sections and a percentage was used to modify the force to account for the bilge keel only covering parts of the sections at the start and end of the bilge keel. .

As mentioned throughout the thesis, the simulation part of the study has been in Matlab. In this chapter, the approach to estimating the roll motion and damping will be presented and explanation of the "program flow" where the different definitions, calculation and estimation for creating the vessel in Matlab. All codes used is specified from (ITTC, 2017) and checked with the original code published by (Himeno, 1981). Furthermore, attached are the reproduced and used Mathlab codes as Appendix IV.

The use of Matlab is for two purposes; one is to analyze the experiment data from the physical test, secondly, to simulate the vessel, both with the same conditions. The purpose is to study the damping effect with and without bilge keel on a traditional Norwegian fisheries vessel and comparing how the ITTC formulas perform vs. experiments.

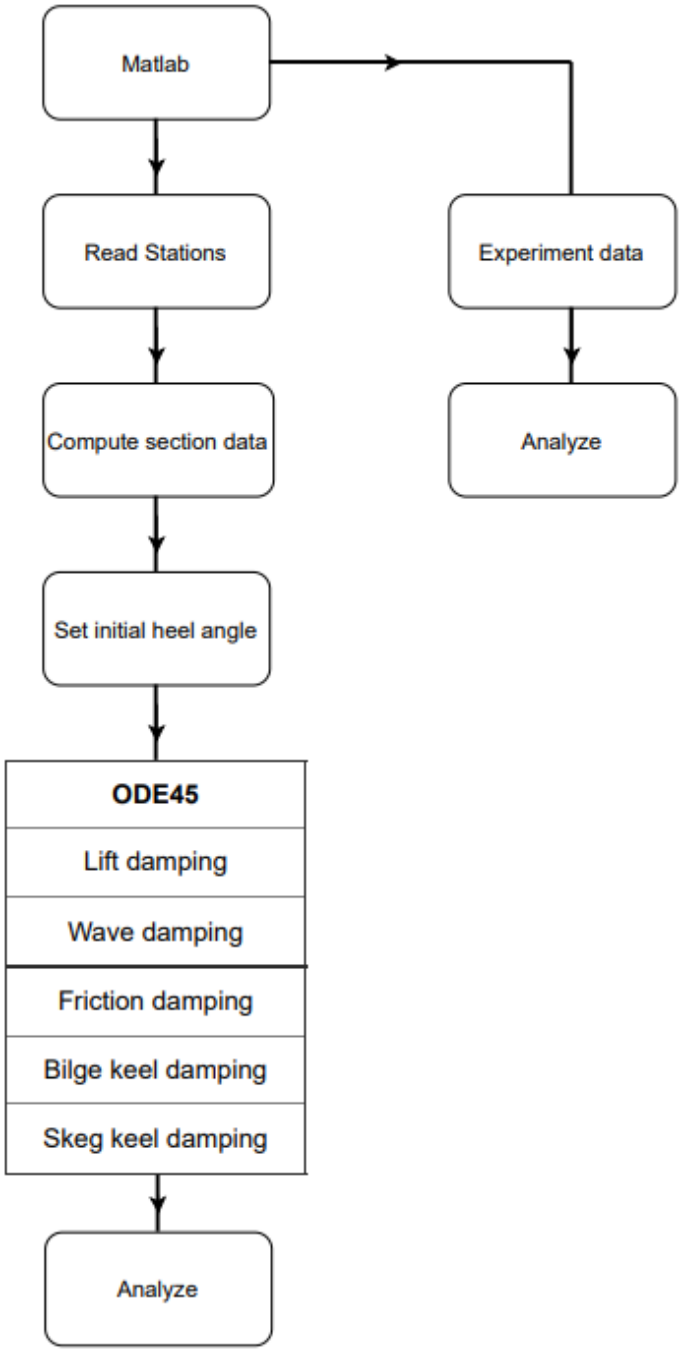

Figure 26 Flow chart of approach with Matlab.

The program starts by reading station from the DELFTShip file and creates a set of arrays that define the vessel's sections.

The compute section data (CSD) use the sections arrays and the vessel's initial parameters to describe the hull form and are divided into several functions. Each Matlab function, of course, has its particular function. E.g. how the hull shape is to be defined, how damping coefficients are determined, definition of areas for bilge keel and skeg keel and force components throughout the hull form, based on the procedures established in (ITTC, 2017).

When CSD is complete, the initial heel angle is the next step. The initial heel angle is incorporated in CSD to illustrated that changes in the heel angle are the only part needed to alternate results.

Matlab's standard solver for ODE is the function ODE45. This function implements a Runge-Kutta (RKF) method with a variable time step for efficient calculation.

The Ode45 process needs the heel angle and heel velocity derivative every time the heel angle changes. Therefore, each damping component is computed at each time step to calculate the derivative of the heel angle velocity. The derivative of the heel angle is the heel velocity.

Some coefficients are amplitude-depended and need a simulation that uses a step-by-step method to find the current motion amplitude. This thesis uses a combination of roll period and max value of the angle during each roll period. Each roll period is simulated in sequence. Meaning; when a rolling period is simulated, the maximum angle of the last roll period is used as the motion amplitude. Each roll period is simulated with the last roll velocity and position as the initial state and the start time of the simulation is changed to the last time stamp in the previous roll period. At the start of the simulation the initial angle is used as the amplitude of the motion.

It is worth mentioning that the simulation can take some seconds for each result due to the time aspect. Matlab simulates that the vessel is in a heel condition and is then released and rolls back and forth until it is in stable equilibrium.

Simulations can also be used to show the reverse case with a load shifting from zeros heel. Input arguments in the simulation will be a moment equal to a displacement of common cargo unit. For the case of a small fisheries vessel a a 75 [%] fully loaded fish container is presumed to shift from the midship to the rail. Common container dimensions for a fishing vessel used in this study have the dimensions LxBxH = 1 x 1 x 1 [m], which means 75 [%] will be equal to 750 [kg]. From midship to rail, the distance is 1.6 [m], and the width of the container is 1 [m], meaning the length the container is shifting will be equal to 1.1 [m]. The simulation is to demonstrate the overshoot angel the vessel will experience during a sudden shift of cargo. The simulation use the same code as the heel decay tests with an initial heel angle and heel velocity of zero and an external moment of 750 [kg] * 1.1 [m]

3.6 Comparison of results

The decay tests with the model is performed 20 times for case to suppress and minimize the effect of noise and random disturbance, such as reflected waves from the sides without wave damping installed. Additionally, since the experiment is carried out by manually heeling the model and releasing it, repeating the same experiment increases the reliability of the outcome, when the outcome is similar for several trials it is an indication of a successful series of experiments. The simulation replicate the decay tests and will be analyzed in the same was as the experiment to compare the characteristic parameters of the decay moment:

- Amplitude
- Frequency
- Logarithmic decrement

By examining the decay of the motion or reduction of rolling angle amplitude over time, estimation of relative damping coefficient is possible.

Since Matlab estimates for the full-scale vessel, it is necessary to Froude-scale the simulation before comparing results with the experiment. Because it is the roll angle and velocity is measured in the experiment, there is only a need to scale the time factor, since the Froude scale factor for angles and angular velocities is 1.

When comparing the results, some elements are essential to be aware of;

- The vessel's eigen frequency must be the same between the experiment and the simulation; with the appropriate scaling applied
    - The eigen frequency gives a clue if the mass and stiffness are defined correct between the model test and numeric calculation.
- Logarithmic decrement
    - Shows if the damping ratio for the simulation vs experiment is equal. This will show if the procedure to calculate damping in ITTC is able to reproduce the damping on a smaller vessel with suboptimal bilge keel placement and skeg.

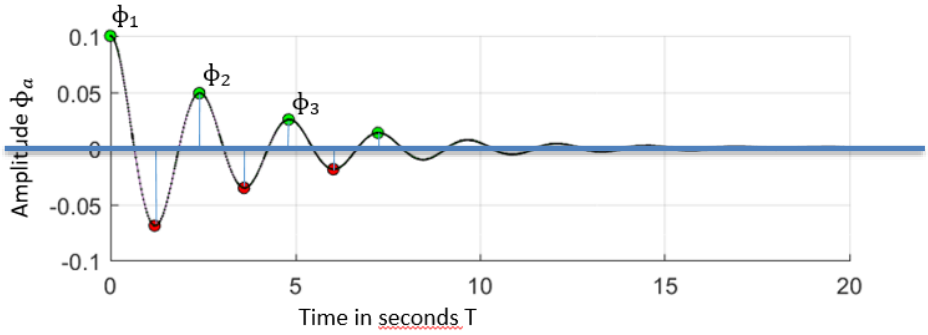

Figure 27: Definition of subsequent amplitudes when calculating the logarithmic decrement

The damping ratio can then be found from the roll motion time-series from the logarithmic decrement of two consequent amplitudes. In this thesis the definition of the logarithmic decrement from (Aarsæther, Kristiansen, Su, & Lugni, 2015) shown in Equation (3.7) is used.

$$Decrement, \qquad \xi_{44} = \frac{log\left(\Phi_a^{(i-1)}/\Phi_a^{(i)}\right)}{T^{(i)} - T^{(i-1)}} \tag{3.7}$$

The method of determining the logarithmic decrement becomes less precise as the damping ratio increases past about 0.5, and it does not apply for a damping ratio greater than 1.0 because the system is overdamped, since it will not have peaks in the response. However, a classical vessel is underdamped, so this is a suitable method for analyzing the results.

Measured data from the experiment were collected as explained in Chapter 0 and loaded into Excel for sorting. Furthermore, the data were loaded into Matlab for simulation and presented as graphs (see example Figure 27). From the graph, it is possible to find the damping factor using "find peaks" in Matlab for both top peaks and bottom peaks and with the combination of Equation (3.7). The calculation of the damping ratio is by using top and bottom peaks separately to prevent any "non-zeros" equilibrium angle from the experiments. If the equilibrium angle is, e.g. higher than zero, the value between the first and second green peak in Figure 27 and the value between the first green and red peak will give a "bouncing" result.

4 Results

This thesis and study of roll motion for smaller traditional Norwegian fishing vessels was created by comparing physical experiment and numerical calculations. Both physical experiment and numerical calculation have performed with the same factors:

- Heeled to 0.2 [rad] and released, with and without bilge keel
- Heeled to 0.1 [rad] and released, with and without bilge keel

The conduction of these tests is to estimate the characteristics of the hull damping with and without bilge keels with the logarithmic decrement.

Moreover, simulation of a container suddenly shifting is also conducted to investigate the overshoot and in the interest of finding a final heel angle after such sudden shifting of load.

Finally, a simulation of damping without a skeg keel, with and without bilge keel is presented to investigate the hulls damping effect on its own.

The data result from this study and investigation will be separately presented regarding the physical experiment and the numerical simulation(s) – presentation of the logarithmic decrement for the origin of the study will be the final result

All plots are shown in model scale, simulation results are Froude scaled with 1:10

The mean motion frequencies of the simulation and experiment are shown in Table 8.

Table 8: Mean roll frequency in model scale calculated form experiment and simulation data.

		0.1 rad	0.2 rad
No bilge keel	Simulation	0.76	0.76
	Experiment	0.72	0.72
Bilge keel	Simulation	0.76	0.76
	Experiment	0.71	0.72

4.1 Experiments

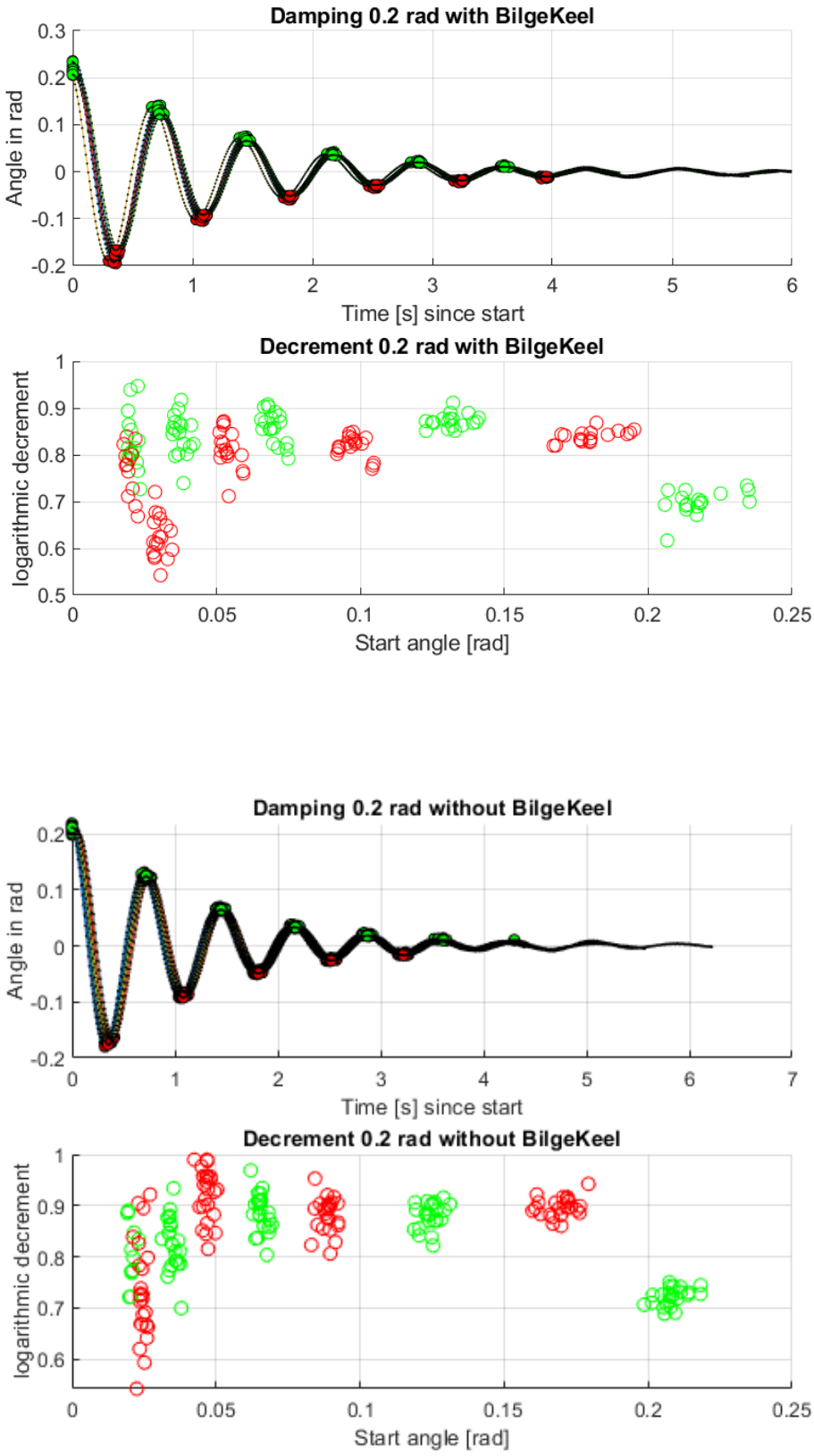

Figure 28: Experimental data, 0.2 [rad] with and without bilge keel.

As seen in Figure 28, there is not much difference with or without the bilge keel with 0.2 [rad]. The amplitude have relatively the same value, the curves has the same frequency, and the settling time is the same. However, the logarithmic decrement is more concentrated at the beginning of the heel period without the bilge keel and slightly more scattered towards the end regarding the value (y-axes) of the logarithmic decrement than with the bilge keel. Moreover, the logarithmic decrement also has a higher value throughout the total rolling period without the bilge keel, especially at 0.05 [rad]. In the end, at the smaller response amplitudes, the measurements blend into one another, making the result hard to analyze.

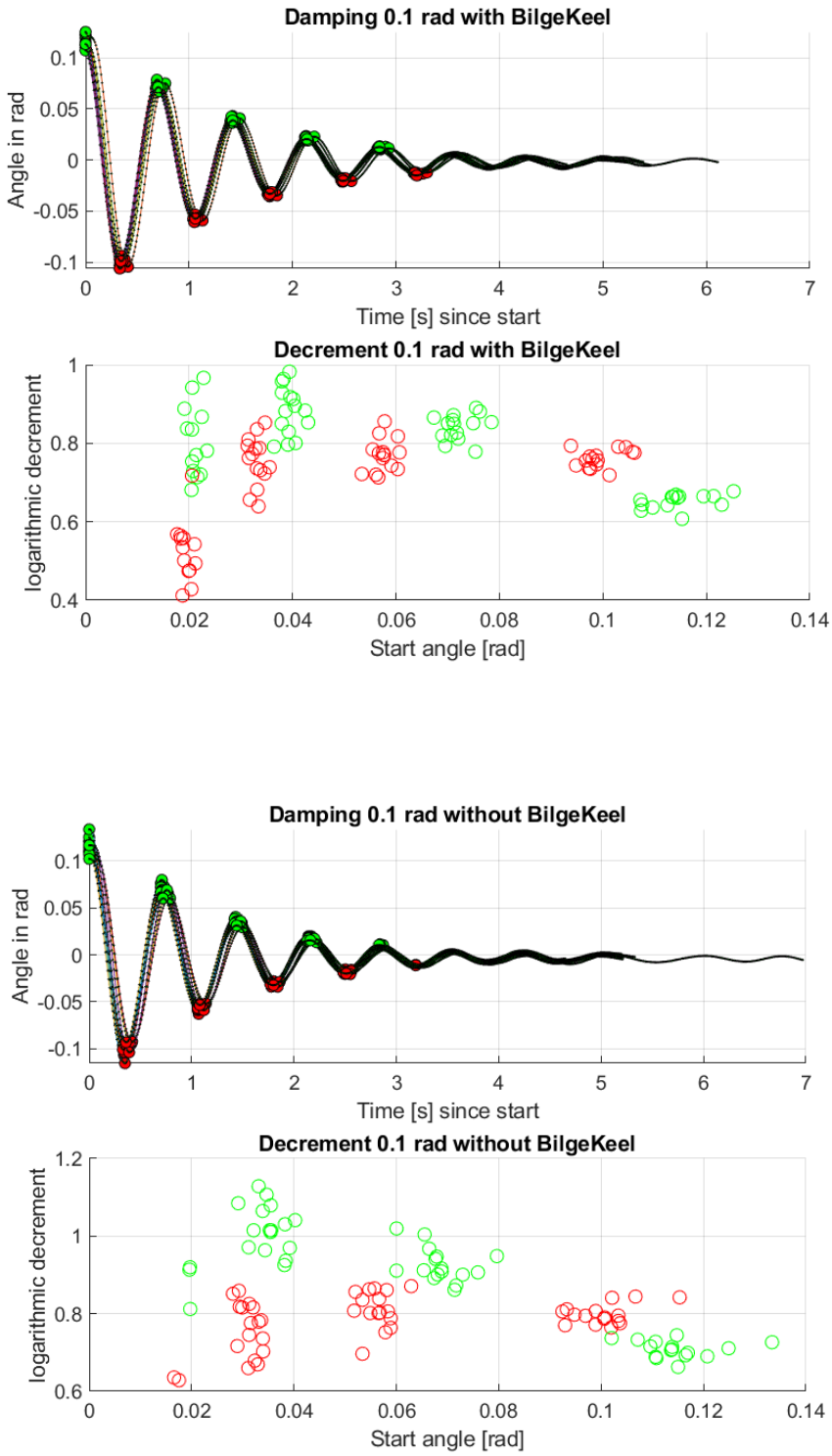

Figure 29: Experimental data, 0.1 [rad] with and without bilge keel.

As seen in Figure 29, there is not much difference with or without the bilge keel with 0.1 [rad]. The amplitude have relatively the same value, the response has the same frequency, and the settling time is the same. However, with the bilge keel, the logarithmic decrement is more concentrated throughout the total rolling period, although, without the bilge keel, the logarithmic decrement has a higher value. Moreover, at 0.02 [rad] (the end of roll motion), only a couple of measurements regarding the logarithmic decrement without the bilge keel is registered vs with bilge keel, where relatively all sequences are registered.

4.2 Numeric simulations

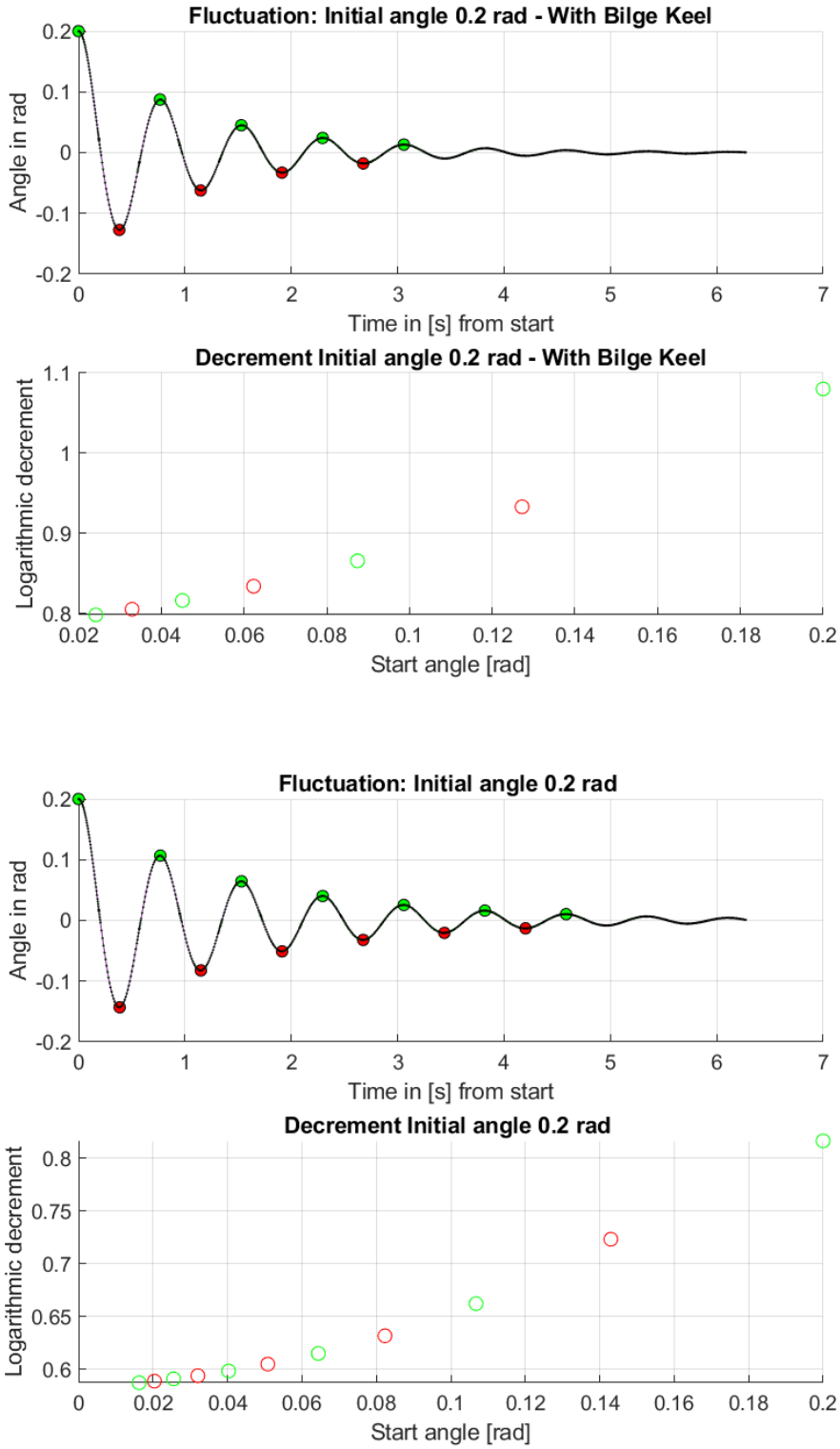

Figure 30: Simulated data, 0.2 [rad] with and without bilge keel.

As seen in Figure 30, there is a slight difference in the amplitude regarding with or without bilge keel; without the bilge keel is higher. Moreover, the settling time is longer without the bilge keel; the last measurement with bilge keel is just over 3 [s], while without, it is just over 4.5 [s], although the frequency is relatively the same. Furthermore, the logarithmic decrement has a much higher value in the beginning with the bilge keel and also moves down much faster than without bilge keel.

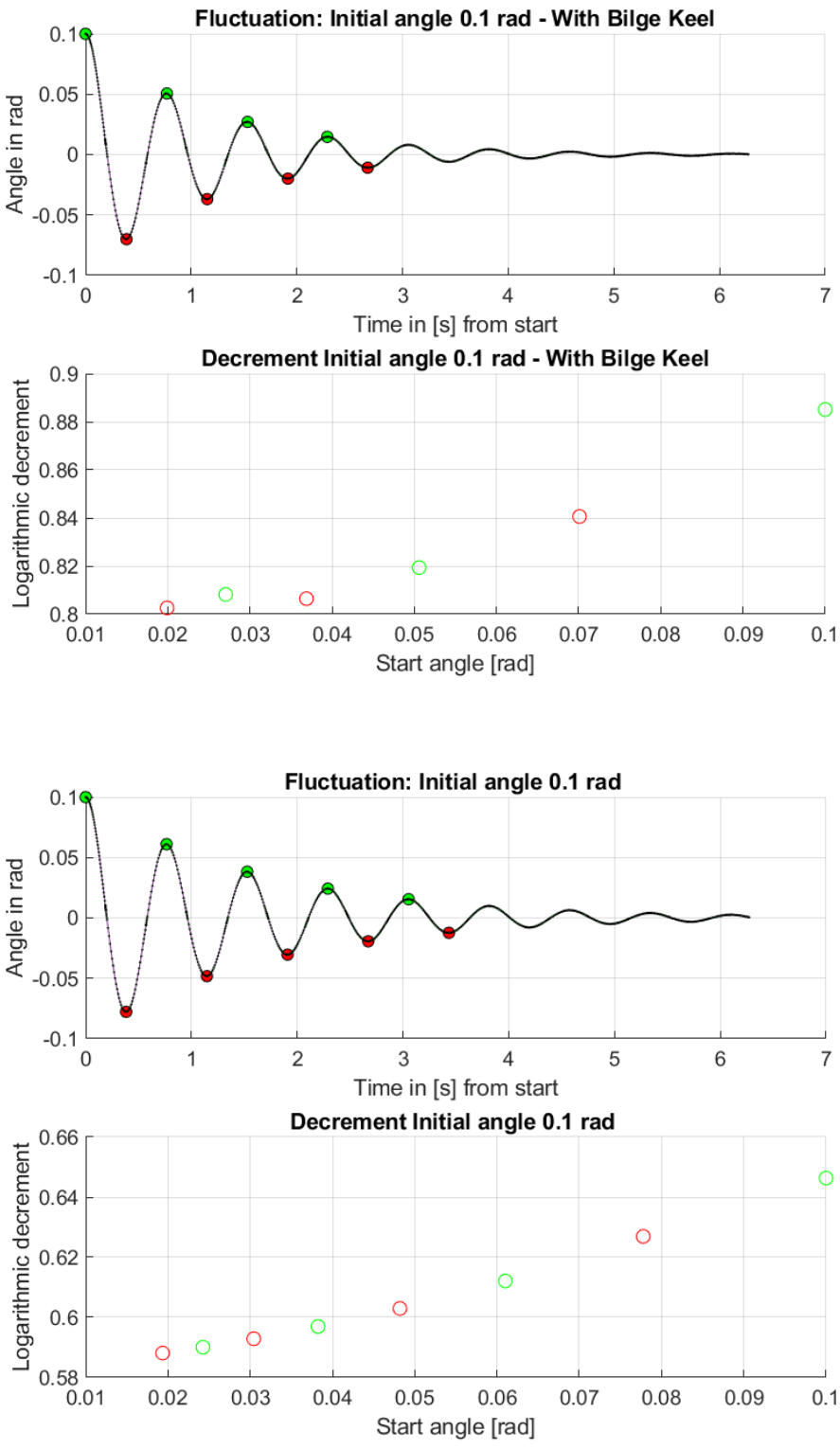

Figure 31 Simulated data, 0.1 [rad] with and without bilge keel.

As seen in Figure 30, there is a slight difference in the amplitude regarding with or without bilge keel; without the bilge keel is higher. Moreover, the settling time is longer without the bilge keel; the last measurement with bilge keel is just over 2.5 [s], while without, it is about 3.5 [s], although the frequency is relatively the same. Furthermore, the logarithmic decrement has a much higher value in the beginning with the bilge keel and also soothes down much faster than without bilge keel. Furthermore, at the end of the roll period (0.03 [rad]), the logarithmic decrement jumps slightly.

4.3 Result container shifting

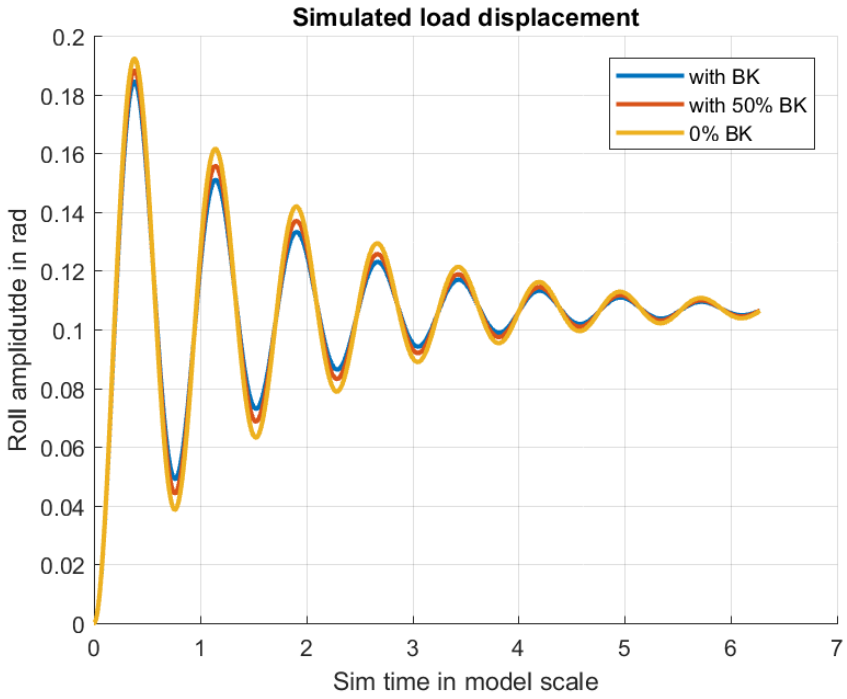

Figure 32: Simulation data, sudden shifting of load.

As seen in Figure 32, the highest heel from the simulation of a sudden shifting of the load is below the heel angle used in this study, even without bilge keel, and the vessel will settle in approximately 0.11 [rad] ≈ 6 [deg.]. The maximum heel angle is about 0.19 [rad] ≈ 11 [deg.], and there is little difference with and without bilge keels. The simulation was repeated with 50% bilge keel effect to test the effect if one side of the bilge keels was in influenced by the presence of the skeg. The small effect may be influenced by the bilge-keel dependence on a motion amplitude, which is zero for the first roll period with the implementation of ITTC damping in this thesis. The relative damping ratio ξ can be estimated from the percentage overshoot as presented in Chapter 2.2.2 by using Equation (2.15). With the values presented the PO becomes 73% and the resulting \eta is calculated as 0.1. This shows that the roll motion is underdamped as shown in Figure 32. The damping ratio can be estimated from the response of shifting cargo.

4.4 Comparing experiment vs simulation

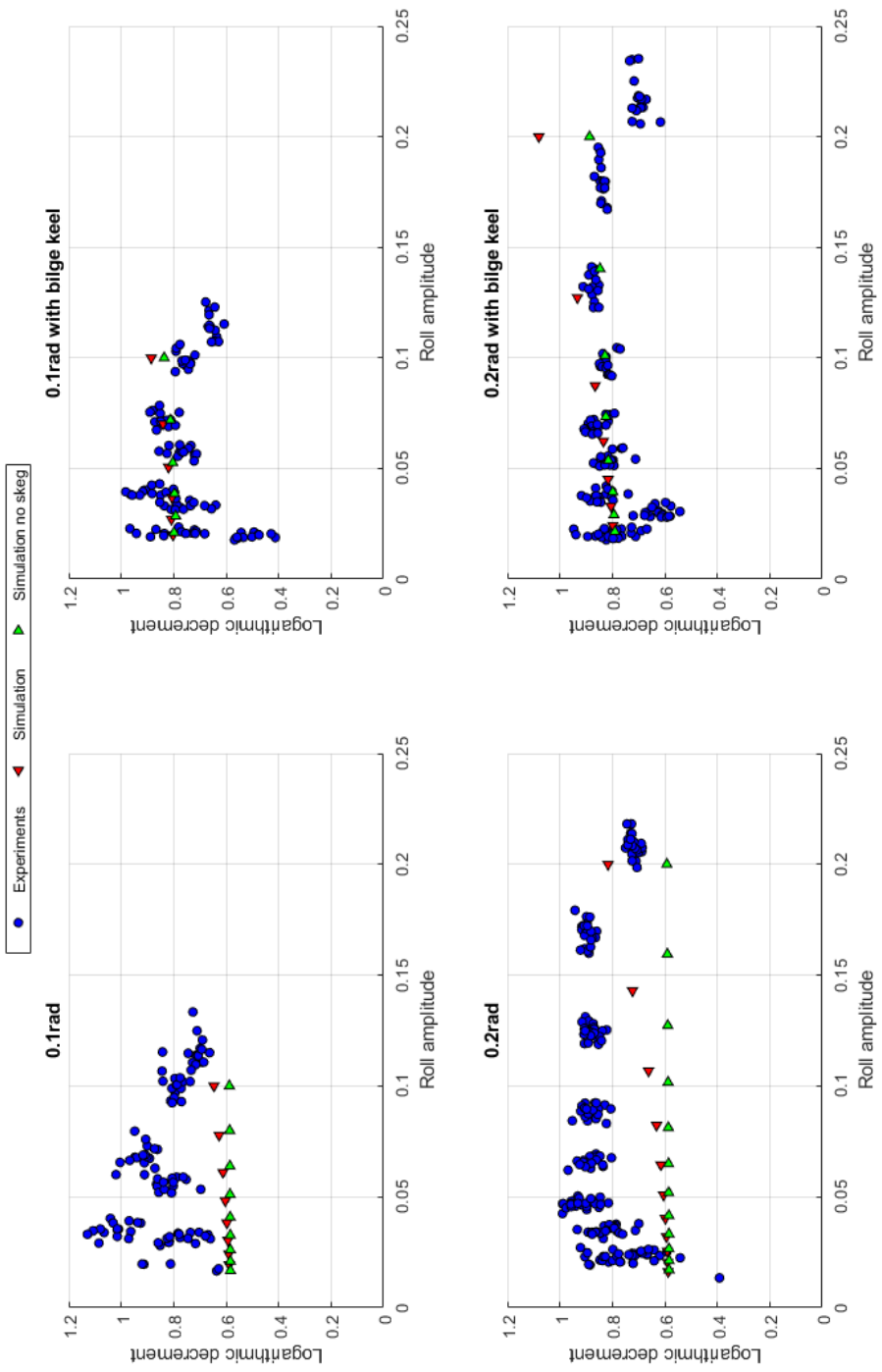

Figure 33: Comparing all four conditions.

As seen in Figure 33, page 70, the logarithmic decrement is similar when comparing the experiment and simulation at a heel angle of 0.1 [rad] with bilge keel.
Without the bilge keel, the logarithmic decrement for the experiment is slightly more significant at 0.1 [rad] when released from 0.2 [rad] than when released from 0.1 [rad], although at ca 0.06 [rad], the value is equal. However, without bilge keel, the logarithmic decrement is higher for the experiment vs simulation.

The logarithmic decrement at 0.1 [rad] with bilge keel is more concentrated than without bilge keel. Without bilge keel, the logarithmic decrement is higher at the end than with bilge keel.

The logarithmic decrement at 0.1 [rad] with and without bilge keel and 0.2 [rad] with and without bilge keel, the value regarding the experiment is relatively the same; however, the logarithmic decrement is more concentrated with bilge keel for both heel conditions than without the bilge keel.

A notable result is that the decrement "curves" in the opposite direction regarding experiment and simulation, mostly when heeling 0.2 [rad]. It is also worth mentioning that there is a simulation without a skeg keel to see the effect.

5 Discussion

Experiment

According to ITTC, the effect of the bilge keels is dependent on motion amplitude. The similarity regarding the experiments test results 0.1 [rad] and 0.2 [rad], with and without the bilge keel, can occur due to the size and placement of the bilge keel. One theory is that the bilge keel ends up in the "shadow" area of the skeg keel as the vessel rolls, so the bilge keel does not contribute as much to the viscous forces. A shadow area can result from either the skeg keel being too high, the bilge keel being too low or placed at a lesser efficient location.

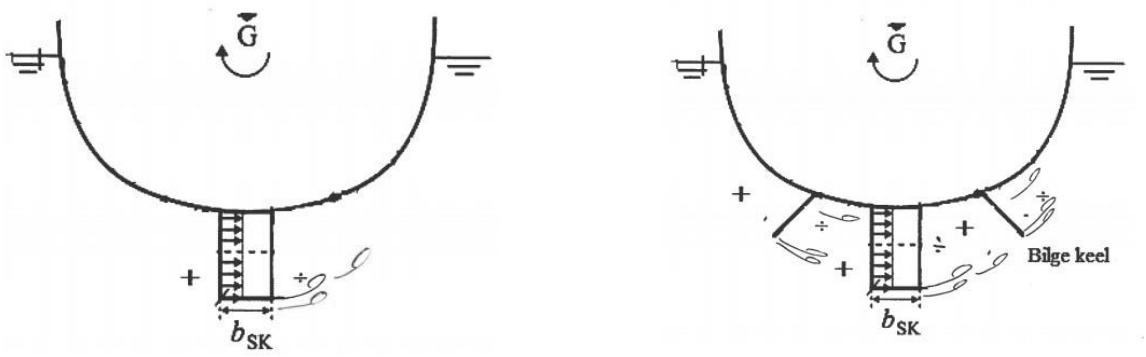

a) Flow around Skeg keel alone.

b) Flow around bilge keel on both sides of Skeg

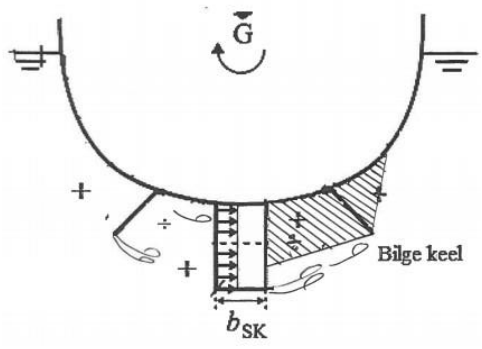

c) Shaded area illustrates shadow area for bilge keel.

Figure 34: Illustration of flow and pressure created around Skeg and Bilge keel. High and low pressure areas are indicated with "+" and "-"respectively.

As the vessel rolls, the water that flows around the skeg keel will not flow around the bilge keel, as illustrated in Figure 34 (c), which may influence the effectiveness of the bilge keels.

Simulation

The simulation result is as expected, higher amplitude without the bilge keel, longer settling time without the bilge keel, and the logarithmic decrement value is higher with bilge keel than without bilge keel.

Comparing experiment and simulation

The amplitude difference between the experiments and the simulation can come from the accuracy difference when heeled. The simulation starts from precisely the given heel, e.g. 0.2 [rad]. In contrast, the experimental tests were manually given a heel while looking at the readings from the MRU on a computer, making the model heel slightly more before the model is released.

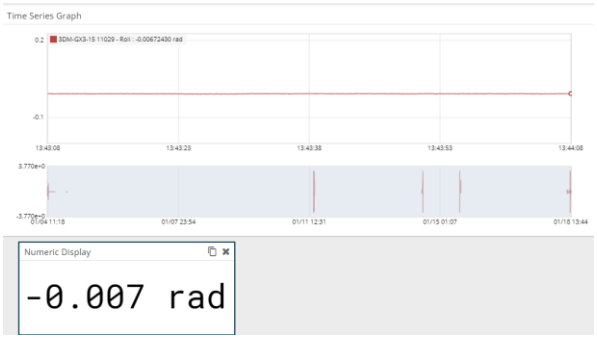

Figure 35: Heel measurement before experimental test start. Picture: Own archive.

Moreover, the model had a slight heel of - 0.007 [rad] at the beginning of the testing. The small initial heel is due to the placement of weights. The bottom plate and the weights were mounted onto the model with velcro since it was impracticable to fabricate fixed attachment points. If there had been a bigger model or known weights needed before printing the model, there might be possible to have fabricated fixed attachment points.

One of the theories for the decrement curving the opposite direction may be the effect from the bilge keel regarding the pressure distribution along the hull, length ‘a’ and ‘S’. Figure 9 illustrates the pressure decreases gradually form the skeg along the distance ‘a’ and are easier to estimate. Furthermore, the divided ‘S’ length, where one half (S/2) is constant, and the other half (S/2) gradually decreases. The definition of where the constant force ends and where the gradually decreasing pressure takes over may cause interference regarding over, - and under pressure. There is also the case of overlapping low and high pressure regions when combining the skeg and bilge keel components in the ITTC procedure.

The low and high pressure regions are indicated with ‘+’ and ‘-‘ in Figure 34 (b), page 72 and there is both a ‘+’ and ‘-‘ forward and aft of the skeg. The assumed pressure distribution from the skeg in the form of the ‘a’ and ‘S’ regions, may easily overlap with the assumed low/high pressure areas from the bilge keels. This may explain why the logarithmic decrement for larger angles are smaller than for intermediate angles in the experiments, and smaller overall than in calculations, as these pressure regions will become larger and may cancel out.

Furthermore, the skeg keel depends on the Kc number, determining if the forces acting are drag or inertia. Another theory may be among the definition of the skeg keel. On larges sea-going vessels, the skeg is more "straight and squared", built as an appendix to the stern, while on the vessel used for this study, the skeg keel is more streamlined and smoother as a part of the hull.

Container shifting

The final heel angle for container shifting is equal for all cases. The maximum value in the first roll period is almost twice the size of the final value. Even though the simulation shows that it will be safe with cargo shifting without the bilge keel, there will be a possibility for the vessel to capsize if it is not secured against water entry at the maximum heel angle. The simulation illustrates the response with a single 750 [kg] container shifting from centre to rail, 1.1 [m]. There is little influence of the bilge-keels on the response in the simulation model with similar results for 100%, 50% and 0% bilge keel damping. While the results of the experiments show over prediction of bilge keel damping by the numeric code. There are no unforeseen loads onboard the vessel changing position simultaneously as the container shifts or equipment positioned at the heel side. In this scenario the impact from a small external force in extreme heel position, such as further shifting of cargo, could lead to an increased heel and loss of stability, as the heel just over 0.2 [rad] leads to water onto the deck. The heel during the experiments had maximum heel of 0.2 [rad] due to the open deck, and the prevention of water intake. From the results of the experiment and the percentage overshoot the damping ration has been found to be only 10% of the critical damping, confirming that roll is underdamped.

6 Conclusion

The basis of this study is the similarity in roll motion and the logarithmic decrement between a 3D printed physical model and a numerical model, which bases on the prediction formulas and method recommended by ITTC. Both have the same line drawing and characteristics from an older traditional Norwegian fishing vessel as a foundation. The physical model has an attachable bilge keel to investigate the damping effect with and without bilge keel. Investigated tests are;

- Given heel of 0.1 and 0.2 [rad] and released with zero forwarding speed, with and without bilge keel.

Implementation of 20 repetitions of each condition has been done regarding the experiment to suppress and minimize noise and random disturbance from reflective waves. One simulation regarding the numerical model since the result won't change.

- Sudden shifting of cargo to investigate overshoot angle.

A simulation of cargo shifting, corresponding to a fishing container with about 750 [kg] fish, from midship to the rail.

The results show good similarity regarding the logarithmic decrement with bilge keel in both heel situations. Without bilge keel, the logarithmic decrement has a somewhat higher effect in both heel situations. In a heel > 0.17 [rad], the logarithmic decrement curves in the opposite direction at the beginning, before assembling at 0.15 [rows]. Furthermore, the simulation shows that the vessel will withstand an influenced force from a container shifting and settle in ca 1.1 [rad].

7 Further work

Further work will be to keep on a study on the hydrodynamic effect on vessels. As a start, it can be interesting to investigate the interference between the bilge keel and skeg keel and the shadow area for the bilge keels that this thesis suggest will develop. The dimension between skeg keel and bilge keel could also be an interesting topic together with roll amplitude. The model used in this thesis did not support roll angles in excess of 0.2 [rad], so it was not possible to increase the roll amplitude to see if the interference effect increased further with amplitude.

Furthermore, the angle of the heel caused by a sudden shifting of load can be an appealing topic regarding maximum heel angle and resting angle, and the effect this will have regarding other equipment or similar, which can lead to further heel or worse. Example of study:

- How will roll damping appendages affect the ability to withstand sudden shifts of cargo?

Will it help resist and withstand a higher heel angle, making fishers safer, or will it lead to an increase of time for the vessel to straighten, e.g. water stays longer on deck and reduces stability.

Some of the segments in mentioned topics can be studied using the already existing model. For some cases and new equipment may be needed. If, e.g. production of new sets of bilge keels are needed, UiT, Narvik already have the model in their system, so printing new bilge keels requires new placement and, if needed or wanted, a new size bilge keel.

References

Arntsen, R., Røds, J. F., Haugseggen, Ø., & Nilsen, S. M. (2016). *Utvikling av hydrostatiske data for lab-skip.* Tromsø: UiT - The arctic University of Norway, on behalf of authors. Retrieved February 15, 2018

Babarit, A., & Delhommeau, G. (2015, September). Retrieved February 24, 2021, from Theoretical and numerical aspects of the open source BEM solver NEMOH. In Proc. of the 11th European Wave and Tidal Energy Conference (EWTEC2015), Nantes, France.

Baniela, S. I. (2008, October 02). Roll Motion of a Ship and the Roll Stabilising Effect of Bilge Keels. *The Journal of Navigation, 61*(4), 667-686. doi:https://doi.org/10.1017/S0373463308004931

Bautu, A., & Bautu, E. (2020, October 15). *Particle Swarms in Statistic Physics*. Retrieved from ResearchGate: https://www.researchgate.net/publication/221787772_Particle_Swarms_in_Statistical_Physics

Bell, K. (2008, April 18). *USFWS National Digital Library*. Retrieved from digital.media.fws.org: https://digitalmedia.fws.gov/digital/collection/natdiglib/id/71/rec/2

DELFTship. (2021, January 01). *DELFTship Maritime Software*. (Hellopixels) Hentet April 25, 2021 fra DELFTship Maritime Software web site: https://www.delftship.net/

Faltinsen, O. M. (1990). *Sea loads on ships and offshore structures.* (I. Dyer, R. T. Eatock, J. N. Newman, & W. G. Price, Red.) Cambridge: The press syndicate of the Unversity of Cambridge. Hentet February 01, 2017

Haugslett, Å. (2015, February 05). Skipsmotstand & modellprøving. *Hydrodynamics at UiT, The Arctic University of Norway*. Tromsoe, Troms, Norway: UiT, The Arctic University of Norway. Retrieved June 07, 2018

Havarikommisjon, S. (2020). *RAPPORT OM FORLIS AV FISKEFARTØYET ANDREAS ØST AV NORD-FUGLØY 18. FEBRUAR 2018.* Gouvermantle, Accident investigation.

Lillestrøm: Statens Havarikommisjon. Hentet October 22, 2020 fra https://havarikommisjonen.no/Sjofart/Avgitte-rapporter/2020-06

Havarikommisjon, S. (2021). *RAPPORT OM FORLIS MED FISKEFARTØYET FAY LEYU/9827619 NORDØST AV HONNINGSVÅG 28. DESEMBER 2019* . Lillestrøm: Statens Havarikommisjon. Hentet March 01, 2021 fra https://havarikommisjonen.no/Sjofart/Avgitte-rapporter/2021-01

Havarikommisjonen, S. F. (2010). *Forlis av fiskefartøyet Lill-Anne, LM6753.* Statens Havarikommisjon for Transport. Lillestrøm: Statens Havarikommisjon for Transport. Retrieved February 25, 2021, from https://havarikommisjonen.no/Sjofart/Avgitte-rapporter/2010-08

Heller, V. (2012). Development of wave devices from initial conseption to commersial demonstration . *Elsevier*, 1-32. Retrieved May 27, 2021, from https://reader.elsevier.com/reader/sd/pii/B9780080878720008040?token=8AF1E562EFF2A1D6F2FB1776D28F343A09697C809272B2BE97BA8DFE8AC40A69D2EAE563E6BBE0EB02B2752499C941BF&originRegion=eu-west-1&originCreation=20210527094402

Himeno, Y. (1981). *Prediction of roll damping - State of the art.* Review and verrification with use of computer, University of Michigan, Department of Naval Architecture and Marine engineering. Retrieved March 23, 2021

Hokland, Ø. (2020, October 12). Ship engineer, Selfa Arctic AS. (G. Kristiansen, Interviewer)

Ibrahim, R. A., & Grace, I. M. (2009, June 11). Modeling of Ship Roll Dynamics and Its Coupling with Heave and Pitch. *Mathematical Problems in Engineering*, 32. doi:10.1155/2010/934714

Ikeda , Y., Himeno, Y., & Tanaka, N. (1978). *Components of roll damping of ship at forward speed.* Universtity of Osaka Prefecture, Department of Naval Architecture. Journal of The Naval Architects, Japan. Retrieved March 23, 2021

Ikeda , Y., Komatsu, K., Himeno, Y., & Tanaka, N. (1976). *On roll damping - Effect of hull surface created by bilge keels.* Univeristy of Osaka Prefecture, Department of Naval

Architecture. Journal of The Kansai Society of Naval Architects, Japan. Retrieved March 23, 2021

Ikeda, Y., Himeno, Y., & Tanaka , N. (1977). *On roll damping force of ship - Effect of friction of hull and normal force of bilge keel.* University of Osaka Prefecture, Department of Naval Arcitecture. Journal of The Kansai Society of Naval Architects, Japan. Retrieved March 23, 2021

Ikeda, Y., Himeno, Y., & Tanaka, N. (1977). *On eddy making component of roll damping force on naked hull.* Univerity of Osaka Prefecture, Department of Naval Architecture. Journal of The Society of Naval Architects, Japan. Retrieved March 23, 2021

ITTC. (2017, May). Numerical Estiamtion of Roll Damping. *ITTC - Recomended Procedures and Guidelines*, 1-32. Retrieved April 20, 2020, from https://www.ittc.info/media/8151/75-02-07-045.pdf

ITTC, A. (2020, October 13). *ittc*. Retrieved from ittc.info: https://ittc.info/

Kawahara, Y., Maekawa, K., & Ikeda, Y. (2012). A Simple Prediction Formula of Roll Damping of Conventional Cargo Ships on the Basis of Ikeda's Method and Its Limitation. *Journal of Shipping and Ocean Engineering*, 201-210. Retrieved March 23, 2021, from https://citeseerx.ist.psu.edu/viewdoc/download?doi=10.1.1.494.1730&rep=rep1&type=pdf

Kawahara, Y., Maekawa, K., & Ikeda, Y. (2012). A Simple Prediction Formula of Roll Damping of Conventional Cargo Ships on the Basis of Ikeda's Method and Its Limitation . *Journal of Shipping and Ocean Engineering*, 201-210. Hentet March 23, 2021 fra file:///C:/Users/gkr018/Downloads/A%20Simple%20Prediction%20Formula%20of%20Roll%20Damping%20of%20Conventional%20Cargo%20Ships%20on%20the%20Basis%20of%20Ikeda%E2%80%99s%20Method%20and%20Its%20Limitation%20(2).pdf

Kongsberg. (2021). *Kongsberg maritime.* Hentet April 15, 2021 fra www.Kongsberg.com: https://www.kongsberg.com/no/maritime/products/vessel-reference-systems/motion-and-heading-sensors/mru/#technicalInformation

Lofoten, D. (2021, February 15). *Vågan*. Retrieved from https://lofoten.info/Visitlofoten: https://lofoten.info/en/vaagan/?Article=473

LORD, M. (2014). *Sensing System.* Hentet December 16, 2020 fra www.microstrain.com: http://files.microstrain.com/3DM-GX3-25-Attitude-Heading-Reference-System-Data-Sheet.pdf

Mahooti, M. (2021, May 10). *MathWorks.* Hentet May 10, 2021 fra MathWorks Central File Exchange: https://se.mathworks.com/matlabcentral/fileexchange/73881-runge-kutta-fehlberg-rkf45

Marin Design, A. (2016). Laila. *Finnish new build.* Marin Design, Kolvereid, Norway. Hentet August 09, 2021 fra https://www.marindesign.no/fartoy/laila/

McLean, D. J. (2019, March 27). *wikipedia.org*. Retrieved from Wikipedia.org/wiki/lift_force: https://en.wikipedia.org/wiki/Lift_(force)#/media/File:Airfoil_lift_and_drag.svg

Minsaas, A., Baarholm, R., & Steen , S. (2010). *Ocean Space Center - Fremtidens marintekniske kunnskapssenter.* Trondheim: Marintek - Norsk Marinteknisk Forskningsinstitutt AS.

Mitchell, M. (2020, October 15). *http://markummitchell.github.io/*. Retrieved from http://markummitchell.github.io/engauge-digitizer/

Norwegian Maritime Authority . (2020, October 27). *New regulations.* Retrieved from www.Sdir.no: https://www.sdir.no/globalassets/global-2/om-sdir/publikasjoner/brosjyrer/nytt_regelverk_for_fiskebaater_under_15_meter.pdf?t=1569410923517

Norwegian Maritime Authority. (2020, October 23). *Accidents 1981-2019.* Retrieved from www.sdir.no: https://www.sdir.no/sjofart/ulykker-og-sikkerhet/ulykkesstatistikk/#Ta_kontakt_ved_behov_for_andre_rapporter

Ouellet , Y., & Datta, I. (1986). A survey of wave absorbers. *Journal of Hydraulic Research, 24*, 265-280. doi:10.1080/00221688609499305

Pecher, A., & Kofoed, J. P. (2016). Handbook of Ocean Wave Energy. I J. H. Todalshaug, D. R. Manhar, B. Raton, & N. I. Xiros (Red.), *Hydrodynamics of WECs* (Vol. VII, ss. 139-158). Trondheim, Norway: Springer Open. doi:10.1007/978-3-319-39889-1

Putra, P. K., Iskandar, B. H., & Novita, Y. N. (2018). Using Length of Bilge Keel to Length of Waterline Ratio to Reduce Ship Rolling Motion. *Engineering, Technology & Applied Science Research, 8*, 2731-2734. doi:http://dx.doi.org/10.48084/etasr.1861

Rodrigues, J. M., & Soares , C. G. (2015). • A generalized adaptive mesh pressure integration technique applied to progressive flooding of floating bodies in still water. *Ocean Engineering*, 140-151.

Ruponen, P. (2014). Adaptive time step in simulation of progressive flooding. *Ocean Engineering* (p. 10). Elsevier. Retrieved April 20, 2020, from https://www.sciencedirect.com/science/article/pii/S0029801813004514?via%3Dihub

Ruponen, P., Kurvinen, P., Saisto, I., & Harras, I. (2010, Oct-Dec). EXPERIMENTAL AND NUMERICAL STUDY ON PROGRESSIVE FLOODING IN FULL-SCALE . *Trans RINA, 152*, 197-208. doi:10.3940/rina.2010.a4.195

Ruponen, P., Manderbacka, T., & Lindroth, D. (2017). On the calculation of the righting lever curve for a damage ship. *Ocean Engineering*, 313-324.

Sintef. (2020, January). Simulation tool for port maneuvering . *Port operations*. Trondheim, Trøndelag, Norway: Sintef. Retrieved April 06, 2021, from https://www.sintef.no/prosjekter/2019/havneoperasjoner/

SNL. (2021, January 05). *Store Norske Leksikon*. Retrieved from www.snl.no: https://snl.no/pendel_-_fysikk

Söder, C.-J., Rosén, A., & Huss, M. (2017, November 29). Ikeda revisited. *Journal of Marine Science and Technology*, 306-316. Retrieved April 20, 2020, from https://link.springer.com/article/10.1007%2Fs00773-017-0497-z

The Norwegian Safety Investigation Authority. (2020). *Capsizing of fishing vessel Andreas, east of Nord-Fugløy 18. February 2018.* Lillestrøm: The Norwegian Safety Investigation Authority.

Veer, R. v. (2000). Experimental and numerical investigation on progressive flooding and sloshing in complex compartment geometries. *International Conference on Stability of Ships and Ocean Vehicles. Volume A*, pp. 305-321. Tasmania, Australia: Proceedings of the 7th International Conference on Stability of Ships and Ocean Vehicles. Retrieved January 10, 2021, from http://resolver.tudelft.nl/uuid:8ad31041-2b13-4c04-9cbe-612cf475d34a

Wilhemsen, S. (2018, March 30). *Marinetraffic.com/no/reiert*. Retrieved March 09, 2021, from www.marinetraffic.com: https://www.marinetraffic.com/no/photos/picture/ships/3029174/257924700/shipid:4947835/imo:0/mmsi:257924700/vessel:REIERT

Winter, R. d. (2018). *Designing Ships using Constrained Multi-Objective Efficient Global Optimization.* Leiden, Netherland: Leiden University.

Aarsæther, K. G., Kristiansen, D., Su, B., & Lugni, C. (2015). Modelling of Roll Damping Effects for a Fishing Vessel With Forward Speed. *ASME 2015 34th International Conference on Ocean, offshore and Arctic Engineering* (pp. 1-10). St. John's, Newfoundland, Canada: Researchgate.

Aasjord, H. L., & Enerhaug, B. (2013). *Stabilitet og stabilitetsmarginer for mindre fiskefartøy*. Trondheim: SINTEF Fiskeri og Havbruk AS.

Aasjord, H. L., & Enerhaug, B. (2013). *Stabilitet og stabilitetsmarginer for mindre fiskefartøy*. SINTEF, Fiskeeri og havbruk AS. Trondheim: SINTEF. Retrieved November 22, 2020

Appendix I – calculating GM light ship

Vessel	UiT-2021-KG	Date		Place			All weights in tons
				Veather			All distances in meters

Condition	Ta	Tm STB	Tm Por	Tf	Displacement (ton)	KB	BM	KM
	1.314	0	0	1.314	8.15	1.018	1.305	2.323

	Vekt A		Vekt B		Vekt C		Vekt D		Sum	Penndel lenght		
	2.04		0.45							2.1		
Weight moved	Arm A	Mom A	Arm B	Mom B	Arm C	Mom C	Arm D	Mom D		Rash	Angel	tan(phi)
1	0.6	1.224		0		0	0	0	1.224		9	0.158384
2	0	0	0.975	0.4388	0	0	0	0	0.43875		3	0.052408
3	0.6	1.224	0.975	0.4388		0	0	0	1.66275		12.9	0.229031
4	-0.6	-1.224		0		0	0	0	-1.224		-8.7	-0.15302
5		0	-0.975	-0.439	0	0	0	0	-0.4388		-2.5	-0.04366
6	-0.6	-1.224	-0.975	-0.439		0	0	0	-1.6628		-11.4	-0.20164
7		0		0	0		0	0	0		0	0
8		0		0	0		0	0	0		0	0

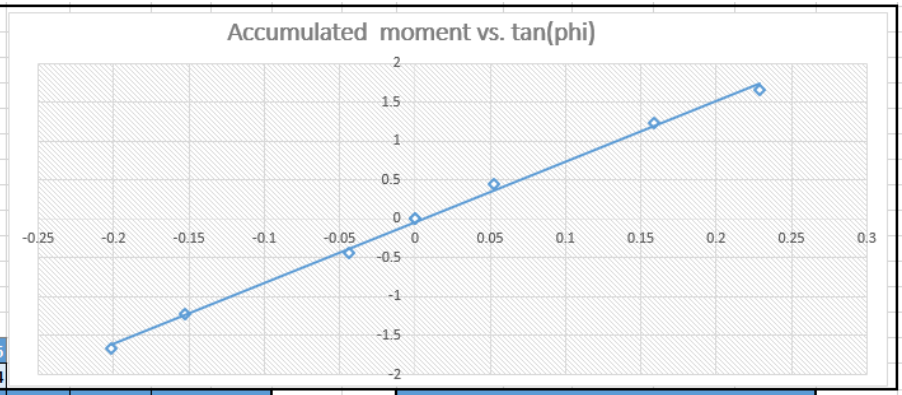

GM =	0.957228676
VCG	1.365771324

Weights onboard	Name	VCG	Weight	Vert mom
1	Ballast	0	0	0
2			0	

Weights onshore	Name	VCG	Weight	Vert mom
1	Vekt A	1.365	2.04	2.7846
2	Vekt B	1.365	2.04	2.7846
3	Vekt C	1.09	0.45	0.4905
4	Vekt D	1.09	0.45	0.4905
5	Vekt E	1.09	0.12	0.1308

Tank content	Name	VCG	Weight	Vert mom
1	Diesel		0	
2	Fresh w.		0	
3	Hydrolic		0	

CoG light ship	
Light ship weight	3.05
Vertical moment during test	11.13104
Vertical moment subtraction for weights	-6.681
Vertical moment subtraction for tanks	0
Vertical moment added for weights	0
Sum vertical moment	4.450036
CoG light ship	1.459028

Corrected CoG	
VCG'	1.459028

Appendix II – MRU Data scheme

LORD PRODUCT DATASHEET

3DM-GX3® -15

Miniature Inertial Measurement Unit And Vertical Gyro

The **3DM-GX3®** -15 is a high-performance, miniature Inertial Measurement Unit and Vertical Gyro, utilizing MEMS sensor technology. It combines a triaxial accelerometer, triaxial gyro, temperature sensors, and an on-board processor running a sophisticated sensor fusion algorithm to provide static and dynamic orientation, and inertial measurements.

Features & Benefits

Best in Class

- precise inertial measurements
- high-speed sample rate & flexible data outputs
- high performance under vibration and high g

Easiest to Use

- smallest, lightest industrial IMU available
- simple integration supported by SDK and comprehensive API

Cost Effective

- reduced cost and rapid time to market for customer's applications
- aggressive volume discount schedule

Applications

Accurate orientation and positioning under dynamic conditions such as:

- Inertial Aiding of GPS
- Unmanned Vehicle Navigation
- Platform Stabilization, Artificial Horizon
- Antenna and Camera Pointing
- Health and Usage Monitoring of Vehicles
- Reconnaissance, Surveillance, and Target Acquisition
- Robotic Control
- Personnel Tracking

System Overview

The 3DM-GX3® -15 offers a range of fully calibrated inertialmeasurements including acceleration, angular rate, deltaTheta, anddeltaVelocity vectors. It can also output computed orientationestimates including Euler angles (pitch and roll), rotation matrix andquaternion. All quantities are fully temperature compensated and aremathematically aligned to an orthogonal coordinate system. Theangular rate quantities are further corrected for g-sensitivity and scalefactor non-linearity to third order. The 3DM-GX3® -15 architecture hasbeen carefully designed to substantially eliminate common sources oferror such as sensitivity to supply voltage variations. On-board coningand sculling compensation allows for use of lower data output rateswhile maintaining performance of a fast internal sampling rate. For those users, integrators or OEMs who develop their own orientation and navigation applications, the 3DM-GX3® -15 is shipped with a complete Data Communications Protocol guide that provides access to the powerful LORD **MicroStrain®** Inertial Packet Protocol (MIP). Applications of your own design can readily be developed in any coding language and on any computing platform including microprocessors

The 3DM-GX3® -15 is initially sold as a starter kit consisting of anIMU module, RS-232 or USB communication and power cable,software CD, user manual, and quick start guide.

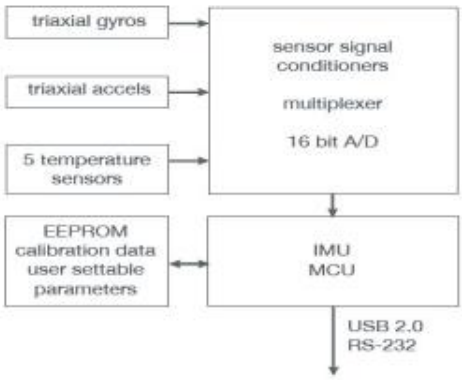

LORD MicroStrain®
SENSING SYSTEMS

3DM-GX3® -15 Miniature Inertial Measurement Unit And Vertical Gyro

Specifications

IMU Specifications

Attitude and Heading	
Attitude heading range	360° about all 3 axes
Accelerometer range	±5 g standard
Gyroscope range	±300°/sec standard
Static accuracy	±0.5° pitch and roll typical for static test conditions
Dynamic accuracy	±2.0° pitch and roll for dynamic (cyclic) test conditions and for arbitrary angles
Long term drift	pitch and roll drift eliminated by complementary filter architecture
Repeatability	0.2°
Resolution	<0.1°
Data output rate	up to 1000 Hz
Filtering	sensors sampled at 30 kHz, digitally filtered (user adjustable) and scaled into physical units; coning and sculling integrals computed at 1 kHz
Output modes	acceleration, angular rate, deltaTheta, deltaVelocity, Euler angles, quaternion, rotation matrix
General	
A/D resolution	16 bits SAR oversampled to 17 bits
Interface options	USB 2.0 or RS232
Baud rate	115,200 bps to 921,600 bps
Power supply voltage	+3.2 to +16 volts DC
Power consumption	80 mA @ 5 volts with USB
Connector	micro-DB9
Operating temperature	-40° C to +70° C
Dimensions	44 mm x 24 mm x 11 mm - excluding mounting tabs, width across tabs 37 mm
Weight	18 grams
ROHS	compliant
Shock limit	500 g
Software utility	CD in starter kit (XP/Vista/Win7 Win8 compatible)
Software development kit (SDK)	complete data communications protocol and sample code

Sensor Specifications

	Accels	Gyros
Measurement range	±5 g	±300°/sec
Non-linearity	±0.1 % fs	±0.03 % fs
In-run bias stability	±0.04 mg	18°/hr
Initial bias error	±0.002 g	±0.25°/sec
Scale factor stability	±0.05 %	±0.05 %
Noise density	80 µg/√Hz	0.03°/sec/√Hz
Alignment error	±0.05°	±0.05°
User adjustable bandwidth	225 Hz max	440 Hz max
Sampling rate	30 kHz	30 kHz
Options		
Accelerometer range	±1.7 g, ±16 g, ±50 g	
Gyroscope range	±50°/sec, ±600°/sec, ±1200°/sec	

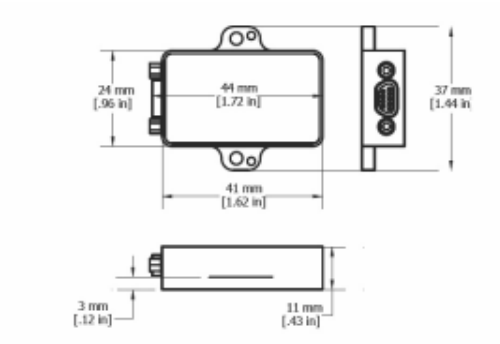

8400-0043 Rev. 001

LORD Corporation
MicroStrain® Sensing Systems
459 Hurricane Lane,
Suite 102
Williston, VT 05495 USA
www.microstrain.com
ph: 800-449-3878
fax: 802-863-4093
sales@microstrain.com
Patent Pending

Appendix III - Result without Skeg and Bilge Keel

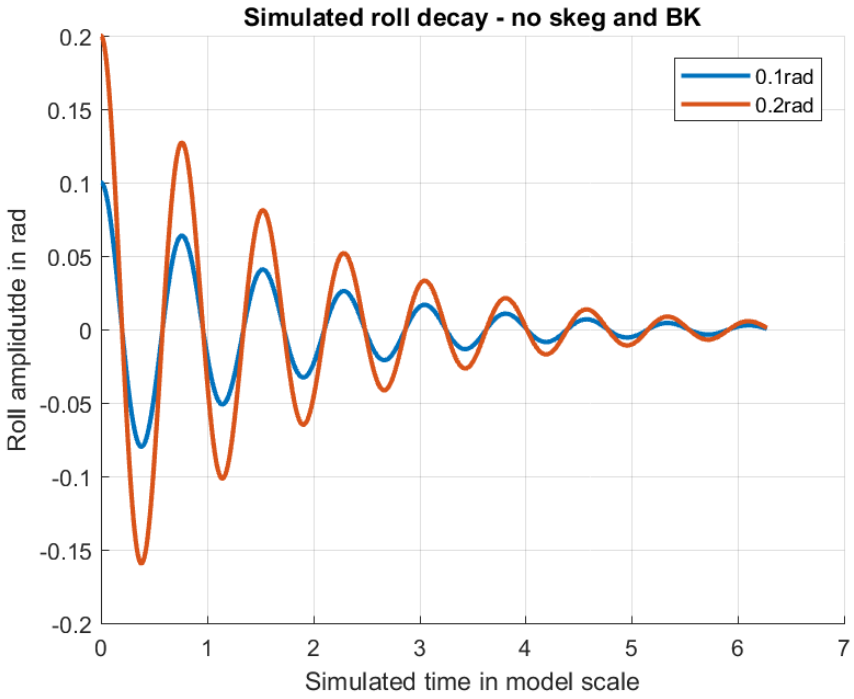

Figure 36: Result without Skeg and Bilge Keel.

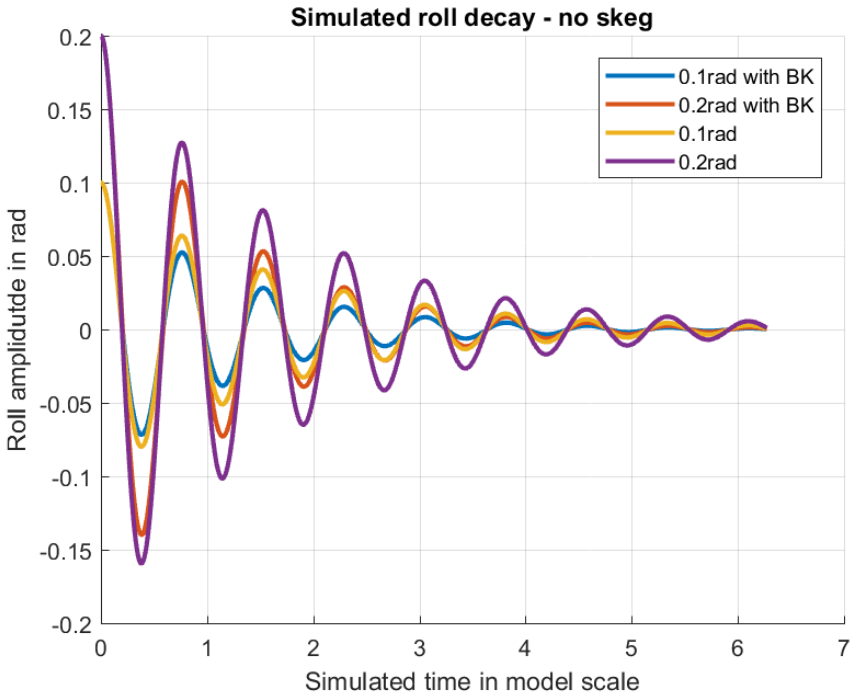

Figure 37: Result without Skeg and with Bilge Keel.

Appendix IV – Matlab code

```
function s = readDelftStation( fname, cutoff )
    if ~exist('cutoff','var')
        % third parameter does not exist, so default it to something
         cutoff = NaN;
    end
    f = fopen(fname);
    s = {};
    while 1
       s_ = readStation(f);
       if isempty(s_)
           break
       else
           if s_(1,2) ~= 0 && s_(end,2)==0
               s_ = flip(s_);
           end

           if ~isnan(cutoff)
               ix_keep = s_(:,3)<=cutoff;
               y = interp1( s_(3:end,3),s_(3:end,2),cutoff);
               s_ = s_(ix_keep,:);
               if ~isempty(s_)
                 s_ = [s_;s_(1,1),y,cutoff;s_(1,1),0,cutoff];
               end
           end

           s{end+1} = s_;
       end

    end

end

function s = readStation(f)
    station_line = fgetl(f);
    if station_line < 0
        s = [];
        return
    end
    tok = split(station_line,":");
    x = str2double(tok{end});
    discard = fgetl(f);
    discard = fgetl(f);
    s = [];
    l=fgetl(f);
    while l(1) ~= '-'
        l = replace(l,'(knuckle)','');
        tok = split(l," ");
        tok = tok(~cellfun('isempty',tok));
        y = str2double(tok{1});
        z = str2double(tok{2});
        s = [s; x,y,z];
        l=fgetl(f);
    end
    discard = fgetl(f);
end
```

```
function A = polygonArea( x, y )
    A = 0;
    if isempty(x)
        return
    end

    if ~( x(1) == x(end) && y(1) == y(end))
       x(end+1)=x(1);
       y(end+1)=y(1);
    end

    for i = 1:length(x)-1
        A = A + 0.5*(x(i)*y(i+1)-x(i+1)*y(i));
    end
    A =abs(A);
end

%%%%%%%%%%%%%%%%%%%%%%END%%%%%%%%%%%%%%%%%%%%%%
```

```
function Xdot = rollDecay2(T,X,amp,vann,skipsdata,seksjonsdata,BKscale,SKscale,↙
T_start,M)
    roll_angle = X(1);
    roll_velocity= X(2);
    ny = vann.ny;
    rho = vann.rho;
    w0 = sqrt(skipsdata.K/skipsdata.Mass);

    LD = liftDamping(rho,skipsdata.V,skipsdata.L,skipsdata.T,skipsdata.B,skipsdata.Cm,↙
skipsdata.OG);
    WD = waveDamping( w0 );
    FD = frictionDamping(rho,skipsdata.V,amp,w0,ny,2*pi*w0,skipsdata.Cb,skipsdata.B,↙
skipsdata.OG,skipsdata.L,skipsdata.T);
    ED = eddyDamping(rho,seksjonsdata.deltaL,seksjonsdata.Bs,seksjonsdata.Ts,↙
seksjonsdata.A,seksjonsdata.a1,seksjonsdata.a3,seksjonsdata.M,seksjonsdata.H0,↙
skipsdata.OG);
    BD = BKscale*bilgeKellDamping(rho,seksjonsdata.deltaL,amp,seksjonsdata.sigma,↙
seksjonsdata.Bs,seksjonsdata.Ts,skipsdata.OG,seksjonsdata.H0,seksjonsdata.bBK,↙
seksjonsdata.lBK);
    SD = SKscale*skegKeelDamping2(rho,seksjonsdata.deltaL,amp,seksjonsdata.seksjoner,↙
skipsdata.OG,seksjonsdata.ix_skeg);

    D2 = -(LD + FD + ED + BD + SD); % kvadratisk demping
    D1 = -(WD); % Lineær demping
    Mext = 0;% Eksternt moment

    if T > T_start
         Mext = M;
    end

    Xdot = zeros(2,1);
    Xdot(1) = roll_velocity;

    % summere krefter
    sumF = D2*abs(roll_velocity)*roll_velocity + D1*roll_velocity -skipsdata.↙
K*roll_angle + Mext;

    Xdot(2) = sumF/skipsdata.Mass; % M = I*(phi_dot_dot)
end

function dL = liftDamping(rho,V,L,d,B,Cm,OG)
    if Cm <= 0.92 % Cm = Midship coefficient
        kappa = 0;
    elseif Cm>0.92 && Cm <= 0.97
        kappa = 0.1;
    else % Cm >= 0.97 && Cm < 0.99
        kappa = 0.3;
    end
    Kn  = 2*pi*d/L+ kappa*(4.1*B/L-0.045); % Representerer løftehellingen som ofte↙
brukes i manøvrering av skip

    l0 = 0.3*d; % Tilsvarer angrepsvinkelen til løftelegemet ved hjelp av andre↙
definisjoner (Se Thesis kap. 2.5)
    lr = 0.5*d; % Avstand fra vannlinje til senter av løftekraft
```

```
    dL = 0.5*rho*V*L*d*Kn*l0*lr*(1-1.4*OG/lr+0.7*OG/(l0*lr)); % Denne er avhengig av↙
hastighet og siden fartøyet ligger i ro blir denne = 0
end

function dW = waveDamping( w )
    data =[ 0,0;
            0.100000000,    6.2609E-07;
            0.200000000,    0.000227884;
            0.300000000,    0.004973497;
            0.400000000,    0.03901065;
            0.500000000,    0.1798444;
            0.559322034,    0.3910207;
            0.618644068,    0.7884855;
            0.677966102,    1.488001;
            0.737288136,    2.66036
            0.796610169,    4.540946;
            0.855932203,    7.44838
            0.915254237,    11.80002;
            0.974576271,    18.13638;
            1.033898305,    27.13793;
            1.093220339,    39.6351
            1.152542373,    56.63719;
            1.211864407,    79.33257;
            1.271186441,    109.0948;
            1.330508475,    147.4746;
            1.389830508,    196.1717;
            1.449152542,    256.9912;
            1.508474576,    331.7888;
            1.56779661,     422.3604;
            1.627118644,    530.3492;
            1.686440678,    657.1035;
            1.745762712,    803.5392;
            1.805084746,    970.0105;
            1.86440678,     1156.196;
            1.923728814,    1361.031;
            1.983050847,    1582.701;
            2.042372881,    1818.708;
            2.101694915,    2065.975;
            2.161016949,    2321.031;
            2.220338983,    2580.208;
            2.279661017,    2839.845;
            2.338983051,    3096.489;
            2.398305085,    3347.037;
            2.457627119,    3588.846;
            2.516949153,    3819.775;
            2.576271186,    4038.176;
            2.63559322,     4242.893;
            2.694915254,    4433.179;
            2.754237288,    4608.638;
            2.813559322,    4769.157;
            2.872881356,    4914.843;
            2.93220339,     5045.977;
            2.991525424,    5162.971;
            3.050847458,    5266.365;
            3.110169492,    5356.769;
```

```
            3.169491525,    5434.893;
            3.228813559,    5501.512;
            3.288135593,    5557.448;
            3.347457627,    5603.558;
            3.406779661,    5640.697;
            3.466101695,    5669.705;
            3.525423729,    5691.384;
            3.584745763,    5706.462;
            3.644067797,    5715.622;
            3.703389831,    5719.437;
            3.762711864,    5718.413;
            3.822033898,    5712.962;
            3.881355932,    5703.432;
            3.940677966,    5690.07
            4.000000000,    5673.086;
            4.253333333,    5562.775;
            4.506666667,    5395.999;
            4.760000000,    5173.961;
            5.013333333,    4875.263;
            5.266666667,    4353.354;
            5.520000000,    10536.07;
            5.773333333,    4723.363;
            6.026666667,    4877.942;
            6.280000000,    4044.741;
        ];
    dW = interp1(data(1:end-4,1),data(1:end-4,2),w,'linear');
end

function dF = frictionDamping(rho,V,amp,w,ny,Tr,Cb,B,OG,L,d)

    if abs(amp) < 1e-4
        dF = 0;
        return;
    end

    % Re = 0.512*r^2*amp^2*w/ny; % Reynold's number
    Rf = (1/pi)*( (0.887+0.145*Cb)*(1.7+Cb*B)-2*OG ); % 3D ship hull estimation
    Cf = 1.328*(3.22*Rf^2*amp^2/(Tr*ny))^-0.5; % Frictional coeffisient
    Sf = L*(1.7*d+Cb*B); % 3D ship hull estimation
    B44f0 = 0.5*rho*Sf*Rf^3*Cf; % Damping coeffisient at zero forward speed
    B44f = B44f0*(1+4.1*(V/(w*L))); % For forward speed, B44f0 is intergrated from↙
B'44f0
    dF = B44f;
end
% En funksjon tilhørende EddyDemping, Skrogformfaktor
function rmax = Rmax(M,a1,a3,psi)
    rmax = M*sqrt( ((1+a1)*sin(psi)-a3*sin(psi))^2+((1-a1)*cos(psi)+a3*cos(3*psi))^2↙
);
end

function dE = eddyDamping(rho,deltaL,Bs,Ts,A_in,a1_in,a3_in,M_in,H0_in,OG)
    dE = 0;
    num_section = length(Bs);
    for section = 1:num_section % Number of sections
    % Definerer gyldige seksjonsdata for matrisene til skroget
```

```
        d = Ts(section); % Dybde
        b = Bs(section); % Bredde
        A = A_in(section); %Areal under vann
        a1 = a1_in(section); %Lewis form parameter
        a3 = a3_in(section); %Lewis form parameter
        M =  M_in(section);
        H0 = H0_in(section);


        if ~( A == 0 || b == 0 || d == 0 )
            sigma = A/(b*d);

            if( OG>d*sigma)
                OG = d*sigma*0.9999;
            end

            sigmadot = (sigma-(OG/d))/(1-(OG/d)); % Area cofficient (Areal under vann/Bredde*dypgang forhold)
            Hdot0 = H0/(1-(OG/d)); % Bredde/dypgang-forhold, inklluderer OG -> avstand vannlinje-Tyngdepunkt

            % Utregning av Lewis form factor
            % utregning hentet fra Himeno 1981 (kode i appendix)
            H0_ = Hdot0;
            E = (H0_-1.0)/(H0_+1.0);
            E2 = E*E;
            AA = 4.0*sigmadot*1.0e-2/pi +E2;
            O = -AA/(AA+3.0);
            O2 = sqrt(O*O - (AA-1.0)/(AA+3.0));
            A3 = O+O2;
            A1 = E*(1.0+A3);
            MM = b/(2*(1+A1+A3));

            a1 = A1;
            a3= a3;
            M = MM;

            psi1 = 0;
            psi2 = 0.5*acos(a1*(1+a3)/(4*a3));
            rmax_psi1 = Rmax(M,a1,a3,psi1);
            rmax_psi2 = Rmax(M,a1,a3,psi2);
            % Løkke nedenfor definere hvordan verdi psi skal ha for videre
            % bruk i definering av skrogform
            if rmax_psi1>=rmax_psi2
               rmax=rmax_psi1;
               psi = psi1;
            else
               rmax=rmax_psi2;
               psi = psi2;
            end

            r = 2*d*sqrt(H0*(sigma-1)/(pi-4));

            A0 = (-2*a3*cos(5*psi))+(a1*(1-a3)*cos(3*psi))+(((6-3*a1)*a3^2)+((3*a1-a1^2)*a3)*a3+a1^2)*cos(psi); % Beskrevielse/definering av skrogform
```

```
            B0 = (-2*a3*sin(5*psi))+(a1*(1-a3)*sin(3*psi))+(((6+3*a1)*a3^2)+↙
((3*a1+a1^2)*a3)*a3+a1^2)*sin(psi); % Beskrevielse/definering av skrogform

            H = 1+a1^2+(9*a3^2)+(2*a1*(1-3*a3)*cos(2*psi))-((6*a3*cos(4*psi))); % Del↙
av beskrivelse av skrogform

            f1 = 0.5*(1+tanh(20*(sigma-0.7))); % Del av beskrivelse av skrogform
            f2 = 0.5*(1-cos(pi*sigma))-1.5*(1-(exp(-5*(1-sigma))))*sin(pi*sigma)^2; %↙
Del av beskrivelse av skrogform
            f3 = 1+4*exp(-1.65e5*(1-sigma)^2); % Del av beskrivelse av skrogform

            % Løkken ndedenfor definerer hvordan radius til Bilgekeel skal beregnes
            if (H0<=1)&&(r/d>=Hdot0)
                r = b/2;
            end
            if (H0>1)&&(r/d>1)
                r = d;
            end

            gamma = ( sqrt(pi)*f3*(rmax+2*M/H)*sqrt(A0^2+B0^2) ) / (2*d*(1-OG/d)*sqrt↙
(Hdot0*sigmadot)); % En del av utykket for Cp, ved bruk av skrogformdefinisjon
            Cp = 0.5*(0.87*exp(-gamma)-4*exp(-0.187*gamma)+3); % Trykkoffisient
            Cr =  ((1-f1*r/d)*(1-OG/d)       +f2*(H0-f1*r/d)^2)*Cp*(rmax/d)^2; %↙
Trykkoffisient
            Cr_ = ((1-f1*r/d)*(1-OG/d-f1*r/d)+f2*(H0-f1*r/d)^2)*Cp*(rmax/d)^2; %↙
Trykkoffisient

            if Cr < 0
                Cr = 0;
            end
            %Moment = Cr*(0.5*rho*d^4*L*phidot*abs(phidot)); %phi = roll angular↙
velocity [phi(m) = ((phi(n)-1)+phi(n))/2], M = eddy making component for roll damping

            Bdot44e0 = rho/2*d^4*Cr;
            if isnan(Bdot44e0)
                error("Not-a-number error");
            end
            dE = dE + Bdot44e0*deltaL; % Dempingen
        end
    end
end

function dBK =  bilgeKellDamping(rho,deltaL,phi_a,sigma_in,Bs_in,Ts_in,OG,H0_in,↙
bBK_in,lBK_in)
    dBK = 0;
    if phi_a == 0
        return
    end

    % Definerer gyldige seksjonsdata for matrisene til skroget
    num_section = length(Ts_in);
    for i = 1:num_section
        d = Ts_in(i);
        b = Bs_in(i);
        H0 = H0_in(i);
```

```
        sigma = sigma_in(i);
        bBK = bBK_in(i); % Bredde BilgeKeel
        lBK = lBK_in(i); % Lengde BilgeKeel

        R1 = 2*d*sqrt((H0*(sigma-1))/(pi-4)); %R kjøl radius
        Rd = d;
        Rb = b/2;
        R =R1;

        if d <= 0 || bBK==0
            continue
        end
        % Løkke definerer radius til kjølen
        if H0>=1 && (R1/d)>1
            R = Rd;
        elseif (H0<=1) && ((R1/d)>H0)
            R = Rb;
        end

        f = 1+0.3*exp(-160*(1-sigma)); % Korreksjonsfaktor for å ta hensyn til økning
av strømningshastigheten rundt kjløle n
        Lrxbk = d*sqrt( (H0-0.2929*R/d)^2 +(1-OG/d-0.2929*R/d)^2 );  %Lrxbk = Lengde
fra rull akse til tuppen of BK

        S0 = 0.3*( (pi*f*Lrxbk*phi_a))+1.95*bBK; %

        m1 = R/d; % Formfaktor
        m2 = OG/d; % Formfaktor
        m3 = 1-m1-m2; % Formfaktor
        m4 = H0-m1; % Formfaktor
        m5 = (((0.414*H0)+(0.0651*m1^2)-(m1*(0.382*H0+0.0106))))/((H0-0.215*m1)*(1-
0215*m1)); % Formfaktor
        m6 = (((0.414*H0)+(0.0651*m1^2)-(m1*(0.382+0.0106*H0))))/((H0-0.215*m1)*(1-
0215*m1)); % Formfaktor

        %for m7 - Formfaktor
        if S0>0.25*pi*R
            m7 = (S0/d)-0.25*pi*m1;
        elseif S0<=0.25*pi*R
            m7 = 0;
        end

        %for m8 - Formfaktor
        if S0>0.25*pi*R
            m8 = m7+0.414*m1;
        elseif S0<=0.25*pi*R
            m8 = m7+1.414*m1*(1-cos(S0/R));
        end


         BB = m4^3/3 / (H0-0.215*m1) + (1-m1)^2 * (2*m3-m2)/6/(1-0.215*m1)+m1*
(m3*m5+m4*m6); % Formfaktor

         B0 = (m2^2/(3*(H0-0.215*m1)))+(((1-m1)^2*(2*m3-m2))/(6*(1-0.215*m1)))+m1*
(m3*m5+m4*m6); % Formfaktor
```

```
        A0 = (m3+m4)*m8-m7^2; % Formfaktor

        Cd = 22.5*((bBK)/(pi*Lrxbk*phi_a*f))+2.4;  %Cd = Drag coeffisient, Cd = Cp+ -↙
Cp-
        Cp_positiv = 1.2; % Trykkoffisient
        Cp_negativ = Cp_positiv-Cd; % Trykkoffisient
        intCpLpdG = d^2*((-A0*Cp_negativ)+(B0*Cp_positiv)); % "Utledet" Integral til↙
bruk i B44bkH0, se formel 2.22 i Thesis

        B44bkN0 = 0.5*rho*Lrxbk^3*f*bBK*Cd; % seksjonsdelt lineær koeffisient for↙
slingrekjølens normale kraftkomponent fra
        % rulledempingen uten hastighet fremover
        B44bkH0 = 0.5*rho*Lrxbk^2*f^2*intCpLpdG; % seksjonsdelt lineær koeffisient↙
for slingrekjølens skrogtrykk fra
        % rulledempingen uten hastighet fremover

        B44bk = B44bkN0 + B44bkH0;
        dBK = dBK + B44bk*deltaL*lBK; % Dempingen
    end
end


 function dSK =  skegKeelDamping2(rho,deltaL,phi_a,seksjoner,OG,ix_skeg)
    dSK = 0;

    if phi_a == 0
        return
    end

    P_G = [0,1.31+OG];

    for sec = 1:length(seksjoner) % Definerer gyldige seksjonsdata for matrisene til↙
skroget
        seksjondata = seksjoner{sec};
        if ~isempty( seksjondata )
            %plot3 (seksjondata(:,1), seksjondata(:,2),seksjondata(:,3),'b-' )
            ix = ix_skeg(sec);
            if ix == 0
                continue;
            end
            %plot3 (seksjondata(:,1), seksjondata(:,2),seksjondata(:,3),'b-' )
            ix = ix_skeg(sec);
            if ix == 0
                continue;
            end

            %plot3 (seksjondata(:,1), seksjondata(:,2),seksjondata(:,3),'r-o' )
            %plot3 (seksjondata(ix,1), seksjondata(ix,2),seksjondata(ix,3),'co' )

            % ========================
            %
            %  |             |
            %--O <-a -  - - -+- -
            %   \*          /
            %    \*       //  <-- S
```

```
            %     ***ix *==
            %        | |
            %        | |
            %        |_|
            %        ^
            %        |-- start=2
            %
            %
            % ========================
            Bsk = 2*seksjondata(2,2); % Bredde på Skegkeel
            Lsk = seksjondata(ix,3)-seksjondata(1,3); % Høyde på Skegkeel

            Ke = pi*phi_a*(P_G(2)-seksjondata(1,3))/Lsk; % Keulegan-Carpenter nummer
            a = sum( sqrt(diff( seksjondata(ix:end-1,2)).^2+ diff(seksjondata(ix:end-1,3)).^2 )  ); % Lengde på Cp+ siden av skroget, avtar gradvis over lengden
            S = 1.65*Ke^(2/3)*Lsk; % Total lengde på Cp- siden av skroget, S/2 er konstant, og resterende S/2 avtar gradvis -> se ITTC, s. 11
            % Lengden a og S er avstand fra hvor Skegget slutter (toppen av skegget) til hvor skroget blir for krummet til å noen effekt

           if 0 <= Ke && Ke <= 2
                Cd0 = 2.425*Ke;
            elseif Ke >= 2
                Cd0 = -0.3*Ke+5.45;
            end
            Cd = Cd0*exp(-0.38*Bsk/Lsk); % Drag coeffisient (Cp_positiv-Cp_negativ)

            Cp_positiv = 1.2; % Trykkoffisient forran skegg
            Cp_negativ = Cp_positiv - Cd; % Trykkoffisient bak skegg


            bidragTrykk_skeg = 0; % Trykkbidrag skegg
            bidragSug_skeg = 0; % Sugbidrag skegg
            bidragTrykk_hud = 0; % Trykkbidrag skroget ( Fra hvor skegget slutter (toppen av skegget) til hvor skroget blir for krummet til å noen effekt )
            bidragSug_hud = 0; % Sugbidrag Skroget (Fra hvor skegget slutter (toppen av skegget) til hvor skroget blir for krummet til å noen effekt )

            % løkke fra kant av kjøl: punkt 2, til "skegpunkt": ix-1
            % for hvert par av punkter regner "trykk" + moment rundt OG
            for ii = 2:ix-1
                ys_n = seksjondata(ii:ii+1,2); %
                zs_n = seksjondata(ii:ii+1,3);%
                ys_p = -ys_n; %
                zs_p = zs_n; %

                dl = sqrt( diff(ys_n).^2 + diff(zs_n).^2 ); % Definerer hvor langt
                s_n = [diff(ys_n),diff(zs_n)]; % vektor langs linjestykke
                N_n = [-s_n(2),s_n(1)]; % vektor normalt på linjestykke
                N_n = N_n/norm(N_n); %

                midpunkt_n = [ mean(ys_n),mean(zs_n) ]; %
                arm_n = P_G-midpunkt_n; %

                s_p = [diff(ys_p),diff(zs_p)]; % Vektor langs linjestykke
```

```
                N_p = [s_p(2),-s_p(1)]; % Vektor normalt på linjestykke
                N_p = N_p/norm(N_p); %

                midpunkt_p = [ mean(ys_p),mean(zs_p) ]; % Gjennomsnitt av vektor(er)↙
normalt på linjestykket
                arm_p = P_G-midpunkt_p; %


                moment_trykk = cross( [0,arm_p], [0,N_p]*Cp_positiv*dl); %
                moment_sug =  cross( [0,arm_n], [0,N_n]*Cp_negativ*dl); %

                bidragTrykk_skeg = bidragTrykk_skeg + moment_trykk(1); %
                bidragSug_skeg = bidragSug_skeg + moment_sug(1); %

            end

            bidragSkeg = bidragTrykk_skeg + bidragSug_skeg;


            % løkke fra "skegpunkt": ix, til vannlinje (end-1)
            % beregne 'a'
            a = 0; % teller for å beregne 'a'
            %  'form' for 'a' langs punkter på seksjon fra 1 ved ix til 0 ved↙
vannlinje
            a_shape = zeros( 1,size(seksjondata,1)-1-ix);
            for ii = ix:size(seksjondata,1)-2
                ys = seksjondata(ii:ii+1,2);
                zs = seksjondata(ii:ii+1,3);

                dl = sqrt( diff(ys).^2 + diff(zs).^2 );
                a_shape(ii-ix+1) = a;
                a = a + dl;
            end
            % normaliserer a_shape slik at den blir i området [1,0],
            % hekter på manglende verdi siden løkken går til nest siste
            % punkt før vannlinje (der er a = 0)
            a_shape = [(a-a_shape)/a,0];

            % for hvert par av punkter regner "trykk" + moment rundt OG
            for ii = ix:size(seksjondata,1)-2
                ys_p = -seksjondata(ii:ii+1,2);
                zs_p = seksjondata(ii:ii+1,3);

                dl = sqrt( diff(ys_p).^2 + diff(zs_p).^2 );

                s_p = [diff(ys_p),diff(zs_p)]; % vektor langs linjestykke
                N_p = [s_p(2),-s_p(1)]; % vektor normalt på linjestykke
                N_p = N_p/norm(N_p);

                midpunkt_p = [ mean(ys_p),mean(zs_p) ];
                arm_p = P_G-midpunkt_p;

                basis_trykk = a_shape(ii+1-ix+1);
                skraa_trykk = a_shape(ii-ix+1)-a_shape(ii+1-ix+1);
```

```
                basis = Cp_positiv*basis_trykk*dl;
                skraa = Cp_positiv*skraa_trykk*dl*0.5;
                total = basis + skraa;

                moment = cross( [0,arm_p], [0,N_p]*total);

                bidragTrykk_hud = bidragTrykk_hud + moment(1);

            end

            % løkke fra "skegpunkt": ix, til vannlinje (end-1)
            % beregne 'S' området
            if S > a
                Smax=a ;
            else
                Smax=S;
            end

            if S/2 > a
                S = a/2;
            end

            % beregner hvor punktet mellom S/2 (flat trykk) og S/2 (skrått trykk) er
            arc = 0;
            ix_p1new = 0;
            ix_p2new = 0;
            for ii = ix:size(seksjondata,1)-2
                ys = seksjondata(ii:ii+1,2);
                zs = seksjondata(ii:ii+1,3);

               dl = sqrt( diff(ys).^2 + diff(zs).^2 );
               if (arc+dl) >= Smax && ix_p2new==0
                   fraction = (Smax-arc)/dl;
                   P1 = seksjondata(ii,:);
                   P2 = seksjondata(ii+1,:);
                   P2_new = P1 + fraction*(P2-P1);
                   ix_p2new = ii;
               elseif (arc+dl) > S/2 && ix_p1new == 0
                   fraction = ((S/2)-arc)/dl;
                   P1 = seksjondata(ii,:);
                   P2 = seksjondata(ii+1,:);
                   P1_new = P1 + fraction*(P2-P1);
                   ix_p1new = ii;

                end
                arc = arc + dl;
            end

            %Setter inn punktet på distanse S/2 fra 'ix' og på S fra 'ix'
            seksjondata = [seksjondata(1:ix_p1new,:); P1_new; seksjondata(ix_p1new+1:↙
ix_p2new,:);P2_new;seksjondata(ix_p2new,:)];
            seksjondata = unique(seksjondata,'rows','stable');
            ix_p1new = find( ( (seksjondata(:,2)==P1_new(2)) + (seksjondata(:,3)↙
==P1_new(3)) )==2,1);
            ix_p2new = find( ( (seksjondata(:,2)==P2_new(2)) + (seksjondata(:,3)↙
```

```
==P2_new(3)) )==2,1);


            % regner trykk og moment for S=0 -> S/2 (konstant trykk)
            for ii = ix:ix_p1new
                 ys_n = seksjondata(ii:ii+1,2);
                 zs_n = seksjondata(ii:ii+1,3);

                 dl = sqrt( diff(ys_n).^2 + diff(zs_n).^2 );
                 s_n = [diff(ys_n),diff(zs_n)]; % Vektor langs linjestykke
                 N_n = [-s_n(2),s_n(1)]; % Vektor normalt på linjestykke
                 N_n = N_n/norm(N_n);

                 midpunkt_n = [ mean(ys_n),mean(zs_n) ];
                 arm_n = P_G-midpunkt_n;

                total = Cp_negativ*dl;
                moment = cross( [0,arm_n], [0,N_n]*total);
                bidragSug_hud = bidragSug_hud + moment(1);
            end

            % regner trykk og moment for S=S/2 -> Smax (skrått trykk)
            arc = S/2;
            for ii = ix_p1new:ix_p2new-1
                 ys_n = seksjondata(ii:ii+1,2);
                 zs_n = seksjondata(ii:ii+1,3);

                 dl = sqrt( diff(ys_n).^2 + diff(zs_n).^2 );
                 s_n = [diff(ys_n),diff(zs_n)]; % vektor langs linjestykke
                 N_n = [-s_n(2),s_n(1)]; % vektor normalt på linjestykke
                 N_n = N_n/norm(N_n);

                 midpunkt_n = [ mean(ys_n),mean(zs_n) ];
                 arm_n = P_G-midpunkt_n;


                base = (Smax-(arc+dl))/(Smax-S/2);
                top =  (Smax-arc)/(Smax-S/2) - base;

                total = Cp_negativ*(base+0.5*top)*dl;
                moment = cross( [0,arm_n], [0,N_n]*total);
                bidragSug_hud = bidragSug_hud + moment(1);
                arc = arc + dl;
            end

            % Summerer alle bidrag
            demping = 1/2*rho*(P_G(2)-seksjondata(1,3)).^2*deltaL*( -bidragSkeg +↙
bidragTrykk_hud + bidragSug_hud);
            dSK = dSK+demping;
         end
     end
 end

  %%%%%%%%%%%%%%%%%%%%%%END%%%%%%%%%%%%%%%%%%%%%%%%%%%%%
```

```
    modelscale = 10;

    % Parametre for fartÃ¸yet
    Ixx = 6859; % Beregnet i regneark Fullskala, Appendix I i Thesis
    Aw = 4500; % Hentet fra NEMOH rundt w = 0.7 (rimelig konstant)
               % - A(w) fra nemoh - added mass ved frekvens w
    GM = 0.957; % fra krengeprÃ¸ve
    depl = 8.258e3; % fra Meshmagick
    g = 9.81; % Gravitasjonskraften/hastigheten

    Mass = Ixx+Aw;
    K = GM*depl*g; % Stivhet til fartÃ¸y
    %fprintf('Full  scale - w0 = sqrt(K/Ixx)=%f  => T=%f\n',sqrt(K/Mass),2*pi/sqrt↙
(K/Mass) )
    %fprintf('Model scale - w0 = sqrt(K/Ixx)=%f  => T=%f\n',sqrt(K/Mass)/sqrt(10),↙
2*pi/sqrt(K/Mass)/sqrt(10) )

    V = 0; % Forover hastighet
    L = 8.5; % Lpp
    B = 3.2; % Bredde
    d = 1.31; % Dypgang
    Cm = 0.34;% Midskipskoeffisient
    OG = 0.15; % KG = 1.46 , T = 1.31 OG = 1.46-1.31 = 0.15
    Cb = 0.22; % Blokk koffisient

    vann = struct();
    vann.ny = 1e-6;
    vann.rho = 1000;

    skipsdata = struct();
    skipsdata.Mass = Mass;
    skipsdata.GM = GM;
    skipsdata.DsiplacementM3 = depl;
    skipsdata.K = K;
    skipsdata.V = V;
    skipsdata.L = L;
    skipsdata.B = B;
    skipsdata.T = d;
    skipsdata.Cm = Cm;
    skipsdata.Cb = Cb;
    skipsdata.OG = OG;

    seksjonsdata = struct();

     % (Seksjoner) er DelftShip-filen til fartÃ¸yet,
     % blir lest inn med dypgang 1.31 m
     seksjonsdata.seksjoner = readDelftStation( 'Viksund31_GK_KGA_shell.txt',1.31);
     seksjonsdata.num_sec = length(seksjonsdata.seksjoner);   % Lager/definerer 0-↙
matriser fra skrogets Delftship-fil
     seksjonsdata.Xs = zeros(seksjonsdata.num_sec,1);         % Lengde skrog
     seksjonsdata.Bs = zeros(seksjonsdata.num_sec,1);         % Bedde skrog
     seksjonsdata.Ts = zeros(seksjonsdata.num_sec,1);         % Dypgang skrog
     seksjonsdata.A = zeros(seksjonsdata.num_sec,1);          % Areal, defineres ved↙
hjelp av a1 og a2
     seksjonsdata.a1 = zeros(seksjonsdata.num_sec,1);         % Lewis form parameter
```

```
     seksjonsdata.a3 = zeros(seksjonsdata.num_sec,1);          % Lewis form parameter
     seksjonsdata.M = zeros(seksjonsdata.num_sec,1);           %
     seksjonsdata.H0 = zeros(seksjonsdata.num_sec,1);          % Bredde/dypgang-forhold
     seksjonsdata.sigma = zeros(seksjonsdata.num_sec,1);       % Area cofficient (Areal↙
under vann/Bredde*dypgang forhold)
     seksjonsdata.bBK = zeros(seksjonsdata.num_sec,1);         % Bredde/hÃ¸yde pÃ¥↙
slingrekjÃ¸l
     seksjonsdata.lBK = zeros(seksjonsdata.num_sec,1);         % Andel av seksjon↙
dekket av slingrekjÃ¸l [0,1]

     for sec = 1:length(seksjonsdata.seksjoner) % Finner verdiene i 0-matrisene
         % Benevnelsene nedenfor betyr det samme som ovenfor (Tidligere)
         seksjon = seksjonsdata.seksjoner{sec}; % Definerer gyldige seksjonsdata for↙
matrisene til skroget
         if ~isempty( seksjon )
             seksjonsdata.Xs(sec) = seksjon(1,1); %
             seksjonsdata.Bs(sec) = 2*max(seksjon(:,2)); % Ganger med 2 siden man tar
             %utgangspunkt i Halve fartÃ¸yet
             seksjonsdata.Ts(sec) = max(seksjon(:,3))-min(seksjon(:,3)); %
             seksjonsdata.A(sec) = 2*polygonArea(seksjon(:,2),seksjon(:,3)); %
             %Finner arealet av skrog ved hjelp av polygonfunskjon ganger
             % med 2 siden tar utgangspunkt i Halve fartÃ¸yet

             seksjonsdata.sigma(sec) = seksjonsdata.A(sec)/(seksjonsdata.Bs(sec)↙
*seksjonsdata.Ts(sec)); %
             seksjonsdata.a1(sec) = (seksjonsdata.Bs(sec)-seksjonsdata.Ts(sec))/2; %
             seksjonsdata.a3(sec) = (-(seksjonsdata.Bs(sec)+seksjonsdata.Ts(sec))+sqrt↙
(abs((seksjonsdata.Bs(sec)+seksjonsdata.Ts(sec))^2+(8*(seksjonsdata.Bs(sec)↙
*seksjonsdata.Ts(sec)-(4*seksjonsdata.A(sec))/pi)))))/4; %
             seksjonsdata.M(sec) = seksjonsdata.Bs(sec)/(2*(1+seksjonsdata.a1(sec)↙
+seksjonsdata.a3(sec))); %

             seksjonsdata.H0(sec) = seksjonsdata.Bs(sec)/(2*seksjonsdata.Ts(sec));
         end
     end
    % Finner dypgang
    test = find(seksjonsdata.Ts>0);
    seksjonsdata.Lwet = (seksjonsdata.seksjoner{ test(end) }(1,1) -  seksjonsdata.↙
seksjoner{ test(1) }(1,1)); %
    seksjonsdata.deltaL = seksjonsdata.Lwet/(test(end)-test(1)); %

    % Definerer hvor lengden BilgeKeel starter (fra akter) og stopper pÃ¥
    % Finner seksjoner hvor BilgeKeel skal starte og stoppe
    % StÃ¸rrelsen pÃ¥ BilgeKeel
    % Grenser for  hvor bidraget fra BilgeKeel skal gjelde
    % Bidraget fra BilgeKeel
    bk_x_from = 1.4;
    bk_x_to = 4.72;
    seksjonsgrense_plus = seksjonsdata.Xs+seksjonsdata.deltaL/2;
    seksjonsgrense_min  = seksjonsdata.Xs-seksjonsdata.deltaL/2;
    bk_ix_start = find( seksjonsgrense_plus> bk_x_from,1);
    bk_ix_to = find( seksjonsgrense_plus> bk_x_to,1);
    seksjonsdata.bBK(bk_ix_start:bk_ix_to)=0.2;
    seksjonsdata.lBK(bk_ix_start:bk_ix_to)=1;
```

```
    grense_start = seksjonsgrense_min(bk_ix_start);
    grense_to = seksjonsgrense_min(bk_ix_to);

    andel_start = (bk_x_from-grense_start)/seksjonsdata.deltaL;
    andel_to = (bk_x_to-grense_to)/seksjonsdata.deltaL;

    seksjonsdata.lBK(bk_ix_start) = andel_start;
    seksjonsdata.lBK(bk_ix_to) = andel_to;

    seksjonsdata.ix_skeg = zeros( 19,1); %Definerer SkegKeel hilke seksjoner av↙
SkegKeel
    % som skal beregnes og hvor 'hÃ¸yt opp' pÃ¥ fartÃ¸yet skegget skal gjelde
    seksjonsdata.ix_skeg(2) = 0;
    seksjonsdata.ix_skeg(3) = 12;
    seksjonsdata.ix_skeg(4) = 9;
    seksjonsdata.ix_skeg(5) = 9;
    seksjonsdata.ix_skeg(6) = 7;
    seksjonsdata.ix_skeg(7) = 7;


%BKscale = 1;
%amp = 0.0;
%[TOUT,YOUT] = ode45(@(t,y) rollDecay2(t,y,vann,skipsdata,seksjonsdata,BKscale,↙
T_start,M), 0:0.1:10, [amp,0]);
%hold on
%plot(TOUT/sqrt(modelscale),YOUT(:,1),'linewidth',2,'DisplayName','with BK')
%grid('on')

figure();
title('Simulated roll decay')
hold('on')
grid('on')
xlabel('Simulated time in model scale')
ylabel('Roll amplitude in rad')

SKscale = 1;

BKscale = 1;
T_start_load = 1;
M_load = 0;
amp = 0.1;
[T,Y] = simRollAmp(amp,amp,vann,skipsdata,seksjonsdata,BKscale,SKscale,T_start_load,↙
M_load);
plot(T/sqrt(modelscale),Y(:,1),'linewidth',2,'DisplayName','0.1rad with BK')
T_01bk = T;
Y_01bk = Y;

BKscale = 1;
T_start_load = 1;
M_load = 0;
amp = 0.2;
[T,Y] = simRollAmp(amp,amp,vann,skipsdata,seksjonsdata,BKscale,SKscale,T_start_load,↙
M_load);
plot(T/sqrt(modelscale),Y(:,1),'linewidth',2,'DisplayName','0.2rad with BK')
T_02bk = T;
```

```
Y_02bk = Y;


BKscale = 0;
T_start_load = 1;
M_load = 0;
amp = 0.1;
[T,Y] = simRollAmp(amp,amp,vann,skipsdata,seksjonsdata,BKscale,SKscale,T_start_load,↙
M_load);
plot(T/sqrt(modelscale),Y(:,1),'linewidth',2,'DisplayName','0.1rad')
T_01 = T;
Y_01 = Y;


BKscale = 0;
T_start_load = 1;
M_load = 0;
amp = 0.2;
[T,Y] = simRollAmp(amp,amp,vann,skipsdata,seksjonsdata,BKscale,SKscale,T_start_load,↙
M_load);
plot(T/sqrt(modelscale),Y(:,1),'linewidth',2,'DisplayName','0.2rad')
T_02 = T;
Y_02 = Y;
legend('0.1rad with BK','0.2rad with BK','0.1rad','0.2rad');

saveas( gcf(), 'Simulated fluctuation.png' );


[phi_sim_01, dekr_sim_01] = plotRollDecaySim(T_01/sqrt(modelscale),Y_01,'Initial angle↙
0.1 rad ');
saveas( gcf(), 'Simulated fluctuation 01rad.png' );
[phi_sim_02, dekr_sim_02] = plotRollDecaySim(T_02/sqrt(modelscale),Y_02,'Initial angle↙
0.2 rad ');
saveas( gcf(), 'Simulated fluctuation 02rad.png' );
[phi_sim_01bk, dekr_sim_01bk] =plotRollDecaySim(T_01bk/sqrt(modelscale),↙
Y_01bk,'Initial angle 0.1 rad - With Bilge Keel');
saveas( gcf(), 'Simulated fluctuation 01rad_BK.png' );
[phi_sim_02bk, dekr_sim_02bk] =plotRollDecaySim(T_02bk/sqrt(modelscale),↙
Y_02bk,'Initial angle 0.2 rad - With Bilge Keel');
saveas( gcf(), 'Simulated fluctuation 02rad_BK.png' );




figure()
title('Simulated roll decay - no skeg')
hold('on')
grid('on')
xlabel('Simulated time in model scale')
ylabel('Roll amplidutde in rad')
SKscale = 0;
BKscale = 1;
T_start_load = 1;
M_load = 0;
amp = 0.1;
```

```
[T,Y] = simRollAmp(amp,amp,vann,skipsdata,seksjonsdata,BKscale,SKscale,T_start_load,↙
M_load);
plot(T/sqrt(modelscale),Y(:,1),'linewidth',2,'DisplayName','0.1rad with BK')
T_01bk_noskeg = T;
Y_01bk_noskeg = Y;


BKscale = 1;
T_start_load = 1;
M_load = 0;
amp = 0.2;
[T,Y] = simRollAmp(amp,amp,vann,skipsdata,seksjonsdata,BKscale,SKscale,T_start_load,↙
M_load);
plot(T/sqrt(modelscale),Y(:,1),'linewidth',2,'DisplayName','0.2rad with BK')
T_02bk_noskeg = T;
Y_02bk_noskeg = Y;


BKscale = 0;
T_start_load = 1;
M_load = 0;
amp = 0.1;
[T,Y] = simRollAmp(amp,amp,vann,skipsdata,seksjonsdata,BKscale,SKscale,T_start_load,↙
M_load);
plot(T/sqrt(modelscale),Y(:,1),'linewidth',2,'DisplayName','0.1rad')
T_01_noskeg = T;
Y_01_noskeg = Y;


BKscale = 0;
T_start_load = 1;
M_load = 0;
amp = 0.2;
[T,Y] =simRollAmp(amp,amp,vann,skipsdata,seksjonsdata,BKscale,SKscale,T_start_load,↙
M_load);
plot(T/sqrt(modelscale),Y(:,1),'linewidth',2,'DisplayName','0.2rad')
T_02_noskeg = T;
Y_02_noskeg = Y;
legend('0.1rad with BK','0.2rad with BK','0.1rad','0.2rad');

saveas( gcf(), 'Simulated fluctuation no skeg.png' );



[phi_sim_01_noskeg, dekr_sim_01_noskeg] = plotRollDecaySim(T_01_noskeg/sqrt↙
(modelscale),Y_01_noskeg,'Initial angle 0.1 rad ');
saveas( gcf(), 'Simulated fluctuation 01rad_noskeg.png' );
[phi_sim_02_noskeg, dekr_sim_02_noskeg] = plotRollDecaySim(T_02_noskeg/sqrt↙
(modelscale),Y_02_noskeg,'Initial angle 0.2 rad ');
saveas( gcf(), 'Simulated fluctuation 02rad_noskeg.png' );
[phi_sim_01bk_noskeg, dekr_sim_01bk_noskeg] = plotRollDecaySim(T_01bk_noskeg/sqrt↙
(modelscale),Y_01bk_noskeg,'Initial angle 0.1 rad - With Bilge Keel');
saveas( gcf(), 'Simulated fluctuation 01rad_BK_noskeg.png' );
[phi_sim_02bk_noskeg, dekr_sim_02bk_noskeg] = plotRollDecaySim(T_02bk_noskeg/sqrt↙
(modelscale),Y_02bk_noskeg,'Initial angle 0.2 rad - With Bilge Keel');
```

```
saveas( gcf(), 'Simulated fluctuation 02rad_BK_noskeg.png' );



figure()
title('Simulated roll decay - no skeg and BK')
hold('on')
grid('on')
xlabel('Simulated time in model scale')
ylabel('Roll amplidutde in rad')
SKscale = 0;
BKscale = 0;
T_start_load = 1;
M_load = 0;
amp = 0.1;


T_start_load = 1;
M_load = 0;
amp = 0.1;
[T,Y] = simRollAmp(amp,amp,vann,skipsdata,seksjonsdata,BKscale,SKscale,T_start_load,↙
M_load);
plot(T/sqrt(modelscale),Y(:,1),'linewidth',2,'DisplayName','0.1rad')
T_01_noskeg_nobk = T;
Y_01_noskeg_nobk = Y;


T_start_load = 1;
M_load = 0;
amp = 0.2;
[T,Y] =simRollAmp(amp,amp,vann,skipsdata,seksjonsdata,BKscale,SKscale,T_start_load,↙
M_load);
plot(T/sqrt(modelscale),Y(:,1),'linewidth',2,'DisplayName','0.2rad')
T_02_noskeg_nobk = T;
Y_02_noskeg_nobk = Y;
legend('0.1rad','0.2rad');

saveas( gcf(), 'Simulated fluctuation no skeg and BK.png' );


[phi_sim_01_noskeg_nobk, dekr_sim_01_noskeg_nobk] = plotRollDecaySim↙
(T_01_noskeg_nobk/sqrt(modelscale),Y_01_noskeg_nobk,'Initial angle 0.1 rad ');
saveas( gcf(), 'Simulated fluctuation 01rad_noskeg.png' );
[phi_sim_02_noskeg_nobk, dekr_sim_02_noskeg_nobk] = plotRollDecaySim↙
(T_02_noskeg_nobk/sqrt(modelscale),Y_02_noskeg_nobk,'Initial angle 0.2 rad ');
saveas( gcf(), 'Simulated fluctuation 02rad_noskeg.png' );



figure();
title('Simulated load displacement')
hold('on')
grid('on')
xlabel('Sim time in model scale')
ylabel('Roll amplidutde in rad')
```

```
vekt_container = 0.71*1.06*1.35*900*0.75 + 82;
F = vekt_container*9.81;
arm = 1.1;
M = F*arm;

SKScale = 1;
BKscale = 1;
T_start_load = 0;
M_load = M;
amp = 0.0;
[T,Y] =simRollAmp(amp,0.18,vann,skipsdata,seksjonsdata,BKscale,SKscale, T_start_load,↙
M_load);
plot(T/sqrt(modelscale),Y(:,1),'linewidth',2,'DisplayName','with BK')
T_load_100bk = T;
Y_load_100bk = Y;

BKscale = 0.5;
T_start_load = 0;
M_load = M;
amp = 0.0;
[T,Y] =simRollAmp(amp,0.18,vann,skipsdata,seksjonsdata,BKscale,SKscale,T_start_load,↙
M_load);
plot(T/sqrt(modelscale),Y(:,1),'linewidth',2,'DisplayName','with 50% BK')
T_load_50bk = T;
Y_load_50bk = Y;

BKscale = 0.0;
T_start_load = 0;
M_load = M;
amp = 0.0;
[T,Y] =simRollAmp(amp,0.18,vann,skipsdata,seksjonsdata,BKscale,SKscale,T_start_load,↙
M_load);
plot(T/sqrt(modelscale),Y(:,1),'linewidth',2,'DisplayName','0% BK')
T_load_00bk = T;
Y_load_00bk = Y;

legend('with BK','with 50% BK','0% BK');

saveas( gcf(), 'Simulated load shifting.png' );

%%%%%%%%%END%%%%%%%%%%%%%
```

```
function [ang, dekr] = plotRollDecayData(index,Total,text)
    figure()
    subplot(211)
    hold('on') % ikke visk ut plott - plott pÃ¥ toppen av forrige graf
    grid('on')
    title(['Damping ', text])
    xlabel('Time [s] since start')
    ylabel('Angle in rad')

   subplot(212)
   hold('on') % ikke visk ut plott - plott pÃ¥ toppen av forrige graf
   grid('on')
   title(['Decrement ' , text])
   xlabel('Start angle [rad]')
   ylabel('logarithmic decrement')

    ang = [];
    dekr = [];
    for i = 1:size(index,1)
       subplot(211)

       fprintf('ForsÃ¸k gÃ¥r fra index %i til %i\n',index(i,1),index(i,2));
       t_start = Total(1,index(i,1)); %hent ut start tidspunkt
       t_end   = Total(1,index(i,2)); %hent ut slutttidspunkt
       fprintf('ForsÃ¸k gÃ¥r fra tid %f[s] til %f[s]\n',t_start,t_end);

       slice = index(i,1):index(i,2); % hent ut radnummer for data
       data = Total(:,slice); % hent ut data for dette forsÃ¸ket
       data(1,:) = data(1,:) - t_start;
       data(2,:) = data(2,:)  - -0.007; % korrigering for konstant krengevinkel

       % i 'data' har vi nÃ¥ kun dette forsÃ¸kket fra T=0 finner
       % pekverdiene i data
       [PKS1,LOCS1] = findpeaks(data(2,:),data(1,:));
        PKS1 = [data(2,1),PKS1];
        LOCS1 = [data(1,1),LOCS1];

       % finner bunnene
       [PKS2,LOCS2] = findpeaks(-data(2,:),data(1,:));

       ix1 = PKS1>0.025;
       ix2 = PKS2>0.025;

       PKS1 = PKS1(ix1);
       LOCS1 = LOCS1(ix1);

       PKS2 = PKS2(ix2);
       LOCS2 = LOCS2(ix2);

       %PKS = [PKS1,-PKS2];
       %LOCS = [LOCS1,LOCS2];
       %peak_data = [LOCS; PKS];

       plot(data(1,:),data(2,:),'-', 'LineWidth',↙
0.1,'MarkerEdgeColor','k','MarkerFaceColor','g', 'MarkerSize',0.75);
```

```
        plot(LOCS1,PKS1,'o', 'LineWidth',↙
0.1,'MarkerEdgeColor','k','MarkerFaceColor','g', 'MarkerSize',5);
        plot(LOCS2,-PKS2,'o', 'LineWidth',↙
0.1,'MarkerEdgeColor','k','MarkerFaceColor','r', 'MarkerSize',5);
        plot(data(1,:),data(2,:),'-o', 'LineWidth',↙
0.1,'MarkerEdgeColor','k','MarkerFaceColor','g', 'MarkerSize',0.75);

        subplot(212)

        startvinkel1 = PKS1(1:length(PKS1)-1);
        vinkeldifferanse1 = diff(PKS1);
        dekrement1 = abs( vinkeldifferanse1 ./ startvinkel1 );

        startvinkel2 = PKS2(1:length(PKS2)-1);
        vinkeldifferanse2 = diff(PKS2);
        dekrement2 = abs( vinkeldifferanse2 ./ startvinkel2 );

        plot( abs(startvinkel1), log(dekrement1), 'go');
        plot( abs(startvinkel2), log(dekrement2), 'ro');


        ang = [ang,abs(startvinkel1),abs(startvinkel2)];
        dekr = [dekr, log(dekrement1), log(dekrement2)];
        %pause;
    end

end

%%%%%%%%%%%%%%%%%%%%%%%%END%%%%%%%%%%%%%%%%%%%%%%%%
```

```
function [ang, dekr] = plotRollDecaySim(TOUT,YOUT,text)
    figure()
    subplot(211)
    hold('on') % ikke visk ut plott - plott pÃ¥ toppen av forrige graf
    grid('on')
    title(['Fluctuation: ', text])
    xlabel('Time in [s] from start')
    ylabel('Angle in rad')

   subplot(212)
   hold('on') % ikke visk ut plott - plott pÃ¥ toppen av forrige graf
   grid('on')
   title(['Decrement ' , text])
   xlabel('Start angle [rad]')
   ylabel('Logarithmic decrement')


   subplot(211)

   data =  [TOUT';YOUT'];

   % i 'data' har vi nÃ¥ kun dette forsÃ¸kket fra T=0 finner
   % pekverdiene i data
   [PKS1,LOCS1] = findpeaks(data(2,:),data(1,:));
    PKS1 = [data(2,1),PKS1];
    LOCS1 = [data(1,1),LOCS1];

   % finner bunnene
   [PKS2,LOCS2] = findpeaks(-data(2,:),data(1,:));

   ix1 = PKS1>0.0125;
   ix2 = PKS2>0.0125;

   PKS1 = PKS1(ix1);
   LOCS1 = LOCS1(ix1);

   PKS2 = PKS2(ix2);
   LOCS2 = LOCS2(ix2);

   %PKS = [PKS1,-PKS2];
   %LOCS = [LOCS1,LOCS2];
   %peak_data = [LOCS; PKS];

   plot(data(1,:),data(2,:),'-', 'LineWidth',↙
0.1,'MarkerEdgeColor','k','MarkerFaceColor','g', 'MarkerSize',0.75);
   plot(LOCS1,PKS1,'o', 'LineWidth',0.1,'MarkerEdgeColor','k','MarkerFaceColor','g',↙
'MarkerSize',5);
   plot(LOCS2,-PKS2,'o', 'LineWidth',0.1,'MarkerEdgeColor','k','MarkerFaceColor','r',↙
'MarkerSize',5);
   plot(data(1,:),data(2,:),'-o', 'LineWidth',↙
0.1,'MarkerEdgeColor','k','MarkerFaceColor','g', 'MarkerSize',0.75);

   subplot(212)

   startvinkel1 = PKS1(1:length(PKS1)-1);
```

```
    vinkeldifferanse1 = diff(PKS1);
    dekrement1 = abs( vinkeldifferanse1 ./ startvinkel1 );

    startvinkel2 = PKS2(1:length(PKS2)-1);
    vinkeldifferanse2 = diff(PKS2);
    dekrement2 = abs( vinkeldifferanse2 ./ startvinkel2 );

    plot( abs(startvinkel1), log(dekrement1), 'go');
    plot( abs(startvinkel2), log(dekrement2), 'ro');

    ang = [abs(startvinkel1),abs(startvinkel2)];
    dekr = [ log(dekrement1), log(dekrement2)];

end

%%%%%%%%%%%%%%%%%%%%%%%END%%%%%%%%%%%%%%%%%%%%%%%
```